Dissecting the Mechanism of a Toxic Ribonuclease

By

Marcia Carmen Haigis

A dissertation submitted in partial fulfillment

of the requirements for the degree of

Doctor of Philosophy

(Biochemistry)

at the

University of Wisconsin–Madison

2002

Committee's Page. This page is not to be hand-written except for the signatures

A dissertation entitled

Dissecting the Mechanism of a Toxic Ribonuclease

submitted to the Graduate School of the
University of Wisconsin-Madison
in partial fulfillment of the requirements for the
degree of Doctor of Philosophy

by

Marcia C. Haigis

Date of Final Oral Examination: January 21, 2002

Month & Year Degree to be awarded: **December** **May** 2002 **August**

****

Approval Signatures of Dissertation Committee

Ronald T. Raines

Robert Beckwith

Ann Axtell

Signature, Dean of Graduate School

Martin Cadwallader/EH

Committee's Page. This page is not to be hand-written except for the signatures

For Kevin

and my parents

ACKNOWLEDGEMENTS

I am grateful to former and present members of the Raines lab for providing a creative and energetic scientific environment. I thank my advisor, Dr. Ronald T. Raines for his support. He allowed me the freedom to pursue projects that excited me, and never wavered in his belief in my scientific ability. His enthusiasm for diverse areas of science and breadth of knowledge provides an excellent example. I must thank Drs. Tony Klink, Pete Leland, and Bradley Kelemen for their instruction and guidance when I began my graduate work. The constant friendship and scientific knowledge of Dr. Chiwook Park have been invaluable. The experiments in Chapter 5 would not be possible without the work of Dr. Eric Haag. Erin Kurten, a talented undergraduate, has contributed to the data in Chapters 3 and 4. I must thank Carla Bender and Dr. J. Petrini for teaching me about stem cells. I thank Kim Dickson for our many discussions. I thank Richele Abel, Dr. Brian Miller, Betsy Kersteen, and Kenneth Woycechowsky for their scientific input, laughter, and encouragement.

My family and friends have been a precious source of support and love. I thank my Mom, Dad, and my siblings, Mark and Tracy, for their belief in me. Most importantly, I thank Kevin Haigis, my husband; he has been a true partner, and is someone I can always depend on. He has made both emotional and concrete contributions to this thesis. His faith and encouragement in me have allowed me to come this far. I admire him as a wonderful person and as a great scientist.

ABSTRACT

Select members of the bovine pancreatic ribonuclease (RNase A) superfamily are toxic to tumor cells. RNase A, itself, is not normally cytotoxic, but Onconase® (ONC), an amphibian homologue, is a potent cytotoxin. This thesis examines the molecular basis of ribonuclease-mediated cytotoxicity. The steps for ribonuclease cytotoxicity are: (1) cell-surface binding, (2) internalization, (3) translocation to the cytosol, and (4) degradation of cellular RNA. ONC and RNase A bind the surface of mammalian cells and are readily internalized in a dose-dependent manner. This internalization is mediated by acidic vesicles that are not dependent on the activity of dynamin. Internalized ribonucleases translocate to the cytosol from a pre-ER compartment. Sequence-specific lysosome-targeted degradation does not limit the toxicity of RNase A variants.

Ribonucleases must evade the cytosolic ribonuclease inhibitor protein (RI) to be cytotoxic. A variant of G88R RNase A, K7A/G88R RNase A, binds RI with lowered affinity and has enhanced cytotoxicity. The role of RI as an intracellular modulator of ribonuclease cytotoxicity was investigated directly by varying its level within mammalian cells. RI limits the potency of toxic RNase A variants but has no effect on the cytotoxicity of ONC, indicating that ONC is not regulated by RI. The toxicity of ONC and RNase A variants correlates with the growth rate of cells.

The biology of pancreatic ribonucleases and RI was explored by genetic methods. RI is a modular protein that has evolved rapidly by exon duplication. Pancreatic ribonuclease (*Rib1*) and ribonuclease inhibitor (*Rnh*) genes are present in the mouse genome as a single

functional copy. Targeting constructs were used to disrupt the *Rib1* and *Rnh* alleles in mouse embryonic stem cells. These cells will be used to create animals that do not produce Rib1 or Rnh protein, and will provide the first insight into their *in vivo* functions.

TABLE OF CONTENTS

LIST OF TABLES

LIST OF FIGURES

ABBREVIATIONS

ANG.....Angiogenin

ATCC.....American Type Culture Collection

BODIPY® 507/545 IA..... .....N-(4,4-difluoro-1,3,5,7-tetramethyl-4-bora-3a, 4a-diaza-s-indacene-2-yl)iodoacetamide

BODIPY® FL IA.....N-(4,4-difluoro-5,7-dimethyl-4-bora-3a, 4a-diaza-s-indacene-3-propionyl)-N′-iodoacetamide

BS-RNase.....bovine seminal ribonuclease

DMEM.....Dulbecco's modified Eagle medium

DTNB..... 5,5′-dithiobis(2-nitrobenzoic acid)

DTT.....dithiothreitol

ECP.....eosinophil cationic protein

EDN.....eosinophil-derived neurotoxin

EDTA..... ethylenediaminetetraacetic acid

6-FAM.....6-carboxyfluorescein

FBS.....fetal bovine serum

FM™ 1-43.....(N-(3-triethylammoniumpropyl)-4-(4-(dibutylamino)styryl) pyridinium dibromide)

IC_{50}.....concentration that gives 50% inhibition

K_d.....equilibrium dissociation constant

K_i.....equilibrium inhibition constant

LIF.....leukemia inhibitory factor

LRR.....leucine-rich repeat

MEM.....minimum essential medium

MES.....2-[N-morpholino]ethanesulphonic acid

NBCS.....newborn calf serum

NCBI.....National Center for Biotechnology Information

Neo.....neomycin phosphotransferase resistance gene

OG.....2′,7′-difluorofluorescein (Oregon Green™ 488)

ONC.....Onconase®

PAGE.....polyacrylamide gel electrophoresis

PBS.....phosphate-buffered saline

PCR.....polymerase chain reaction

PDB.....Protein Data Bank

*p*I.....isoelectric point

poly(C).....poly(cytidylic acid)

poly(U).....poly(uridylic acid)

RI.....ribonuclease inhibitor

Rib1.....murine pancreatic ribonuclease gene

RNA.....ribonucleic acid

RNase 1.....human pancreatic ribonuclease

RNase A.....bovine pancreatic ribonuclease A

Rnh.....murine ribonuclease inhibitor gene

RPMI.....Roswell Park Medical Institute

SDS.....sodium dodecyl sulfate

6-TAMARA.....6-carboxytetramethylrhodamine

TK.....thymidine kinase

T_m.....temperature at the midpoint of thermal denaturation

Tris.....tris(hydroxymethyl)amine

UV.....ultraviolet

Chapter 1

Introduction

Portions of this chapter are in preparation as: Marcia C. Haigis and Ronald T. Raines (2002) Mechanism of a cytotoxic ribonuclease. *Progress in Nucleic Acid Research and Molecular Biology* (solicited review).

History of bovine pancreatic ribonuclease

Bovine pancreatic ribonuclease (RNase A) was one of the most thoroughly studied enzymes of the 20th century. In 1967, the complete tertiary structure of RNase A was determined (Kartha *et al.*, 1967; Wyckoff *et al.*, 1967); it was the fourth protein to have its structure solved. RNase A was the model protein used during landmark studies of protein folding, enzymology, and structural stability. In 1972, Moore and Stein were given the Nobel prize for connecting the tertiary structure of RNase A with its catalytic activity (Moore & Stein, 1973). That year, Anfinsen was jointly acknowledged for demonstrating that the primary structure of RNase A is responsible for its tertiary fold (Anfinsen, 1973). In 1984, Merrifield received the Nobel prize for the complete chemical synthesis of RNase A on a solid matrix (Merrifield, 1985; Merrifield, 1986).

RNase A is a small, kidney-shaped protein comprised of 124 amino acid residues (Figure 1.1). It contains four disulfide bonds that involve all eight of its cysteine residues. These disulfide bonds hold together elements of secondary structure and are important for the legendary conformational stability of RNase A (Shimotakahara *et al.*, 1997; Volles *et al.*, 1999; Klink *et al.*, 2000; Wedemeyer *et al.*, 2000). The active site is situated in a cationic groove that runs through the middle of the protein. RNA binding in this groove is facilitated by Coulombic interactions. Specifically, RNA binding involves two types of RNase A subsites that enable contacts to: (1) bind the phosphoryl backbone of RNA, and (2) confer base specificity (for reviews, see: Nogués *et al.*, 1995; Cuchillo *et al.*, 1997; Raines, 1998).

RNase A is a highly efficient endonuclease and can catalyze reaction rates at k_{cat}/K_M values up to 10^9 $M^{-1}s^{-1}$ (Park & Raines, 2001). RNase A cleaves the P–$O^{5'}$ bond of RNA after a pyrimidine nucleotide in a two-step mechanism (Figure 1.2) (Findlay *et al.*, 1961). In first step, His12 abstracts a proton from the 2′ hydroxyl of the substrate, promoting the formation of a 2′,3′-cyclic phosphodiester intermediate, and His119 protonates the 5′ oxygen of the leaving group. In the second step, His119 abstracts a proton from a water molecule, which then hydrolyzes the cyclic intermediate to form a 3′ phosphomonoester. In this step, His12 donates a proton to the 2′ oxygen to complete the catalytic cycle. Chemical modification and site-directed mutagenesis studies have identified many of the amino acid residues that are responsible for substrate binding, as well the residues that are important for catalysis (for reviews, see: Parés *et al.*, 1991; Nogues *et al.*, 1995; Cuchillo *et al.*, 1997; Raines, 1998).

Homologues of ribonuclease A

The amino acid sequence is known for more than forty homologues of RNase A, dubbed the RNase A superfamily (for reviews, see: Beintema *et al.*, 1997; Beintema & Kleineidam, 1998). RNase A homologues have been sequenced from diverse mammalian and amphibian species, such as guinea pig, deer, bull frog, two-toed sloth, and swamp buffalo, but not from fish or invertebrates. In addition, multiple homologues can exist in a single species, indicating the frequent occurrence of gene duplications. For example, most mammalian species contain only one copy of the homologue angiogenin (ANG), but the mouse has six copies of the *Ang* gene (Brown *et al.*, 1995; Strydom, 1998). Evolutionary analysis has

revealed that members of the RNase A superfamily are evolving rapidly (for reviews, see Beintema *et al.*, 1997; Beintema & Kleineidam, 1998).

In mammals, the RNase A superfamily can be subdivided into distinct classes: (1) pancreatic-type ribonucleases, (2) eosinophil-derived neurotoxin (EDN), (3) eosinophil cationic protein (ECP), (4) liver ribonuclease, and (5) ANG. Humans produce each of these ribonucleases. Homologues from classes 1, 4, and 5 are secreted from cells, whereas EDN and ECP are found in the regulated secretory granules of eosinophils. An amino acid sequence alignment of several members of the RNase A superfamily is shown in Figure 1.3. The active-site histidine and lysine residues are conserved strictly, as are the disulfide bonds. Yet, not all RNase A homologues are efficient catalysts. For example, ANG has a k_{cat}/K_M value that is 10^4–10^6-fold lower than that of RNase A, suggesting an additional function independent of ribonucleolytic activity (Shapiro *et al.*, 1989).

Ribonuclease Inhibitor

In 1952, Pirotte and Desreux discovered the activity of ribonuclease inhibitor protein (RI) in guinea pig liver extracts (Pirotte & Desreux, 1952). Roth and co-workers observed that this inhibitory activity was inactivated by proteases, heat, *p*-hydroxymercuribenzoate-mediated sulfhydryl modification, and was sensitive to pH changes (reviewed in: Roth, 1962). In addition, the inhibitory activity was isolated to the supernatant fraction of high-speed centrifugation, indicating that it was a cytosolic factor. In the 1970's, techniques were

developed to isolate RI to homogeneity, enabling its biochemical characterization (Blackburn *et al.*, 1977; Blackburn & Moore, 1982).

RI is an acidic (pI~4.7), 50-kDa cytosolic protein (Gribnau *et al.*, 1970). The amino acid sequences of RI from pig, rat, and human, revealed that it is comprised entirely of leucine-rich repeats (LRR) (Hofsteenge *et al.*, 1988; Lee *et al.*, 1988; Kawanomoto *et al.*, 1992). The crystalline structure of RI was solved in 1993 (Kobe & Deisenhofer, 1993); its LRR motifs are arranged in a horseshoe shape, and represent a new protein fold (Figure 1.4) (for reviews, see: Kobe & Deisenhofer, 1995a; Kajava, 1998; Kobe & Kajava, 2001). Human and porcine RI contain 32 and 30 reduced cysteine residues, respectively; oxidation of these thiols is cooperative, and leads to rapid inactivation and degradation of the protein (Blazquez *et al.*, 1996). Variants of RI have been created that have replaced proximal cysteine residues with alanine; and these substitutions cause RI to be less sensitive to oxidation (Kim *et al.*, 1999).

RI binds RNase A in a 1:1 stoichiometry (for reviews, see: Blackburn & Moore, 1982; Lee & Vallee, 1993; Hofsteenge, 1997; Shapiro, 2001). RI is an unusual type of protein inhibitor because it can bind multiple types of ribonucleases (Table 1.1) (Lee & Vallee, 1993; Hofsteenge, 1997; Shapiro, 2001). For example, human RI can bind RNase A, human pancreatic ribonuclease (RNase 1), EDN, and ANG to form complexes with K_d values of 4.4×10^{-14}, 2.0×10^{-13}, 9.4×10^{-16}, and 7.1×10^{-16} M (reviewed by Lee & Vallee, 1993; Hofsteenge, 1997; Shapiro, 2001). These interactions are among the tightest, noncovalent biological interactions known.

The crystalline structure of the porcine RI•RNase A complex was solved in 1995 (Figure 1.4) (Kobe & Deisenhofer, 1995b). The C-terminus of RI forms extensive contacts

with RNase A; >2500Å^2 of surface area is buried at the RI–RNase A interface. As shown in Figure 1.3, many of the amino acid residues of RNase A that are important for RNA binding and catalysis also interact with RI. As such, when bound in a complex with RI, ribonucleases are inactivated, and are no longer free to bind or degrade RNA (Lee & Vallee, 1993). RI is less effective against non-mammalian homologues of RNase A.

Physiological functions of pancreatic ribonuclease and ribonuclease inhibitor

RNase A is a secretory protein that is produced in large quantities in the bovine pancreas both in an unglycosylated (RNase A) and various glycosylated forms. In 1969, Barnard proposed that pancreatic ribonuclease was a requirement for the digestion of dietary RNA in ruminants (Barnard, 1969a). Thus, RNase A would function to degrade ingested RNA, much like trypsin, chymotrypsin, and amylase degrade ingested protein. Curiously, however, levels of pancreatic ribonuclease do not change with fasting or consumption (Barnard, 1969a), in marked contrast to trypsinogen, chymotrypsinogen, and amylase (Snook, 1965).

Evidence in support of a more global role for pancreatic-type ribonucleases can be found in its expression pattern. In humans, mRNA encoding RNase 1 can be found in the pancreas, brain, and mammary gland (Sasso *et al.*, 1999). RNase 1 protein can also be found in the urine and serum (Weickmann & Glitz, 1982). Pancreatic adenocarcinoma cells were found to secrete high levels of RNase 1 into the serum (Peracaula *et al.*, 2000), and RNase 1 is being

investigated as a diagnostic marker for pancreatic cancer (Weickmann *et al.*, 1984; Kobayashi & Kawakubo, 1994).

RI is found in the cytoplasm of cells from nearly all organs, tissues, and glands investigated, although it inhibits secretory ribonucleases (for reviews, see: Lee & Vallee, 1993; Hofsteenge, 1997). Interestingly, RI is not detectable in the plasma, urine, or saliva. (Nadano *et al.*, 1994; Futami *et al.*, 1997). The expression patterns of RI were extensively investigated during the previous three decades, with hope of finding insight into the biological role of RI. Nonetheless, the literature is full of conflicting conclusions. RI expression seems to correlate positively with anabolic activity, such as cell proliferation; increased RI levels have been found in rat liver after treatment with 2-acetamidofluorene to induce tumors (Wojnar & Roth, 1965) and in developing neonatal rats (Suzuki & Takahashi, 1970). Yet, RI levels are not elevated in SV-40–transformed hamster embryo fibroblast cells, stimulated HL-60 cells (Kyner *et al.*, 1979), or many hepatoma cell lines. The labile nature of RI could have compounded the difficulty of correlating RI levels with physiological relevance. A recent study by Alino and co-workers, however, did find that high RI levels decreased angiogenesis and tumor formation in mouse xenographs (Botella-Estrada *et al.*, 2001).

The ubiquitous, but perplexing, tissue distribution of RI, in combination with its ability to bind numerous pancreatic-type ribonucleases, suggests an important biological role. Several hypotheses exist for the physiological role of RI (Beintema *et al.*, 1988; Lee & Vallee, 1993; Hofsteenge, 1997). One hypothesis is that RI functions to inhibit intracellular ribonucleolytic activity. Thus, cells with a low level of RI would have high RNA degradation, while cells

with a high concentration of RI would accumulate RNA. Still, no known cytoplasmic ribonucleases bind RI with high affinity.

A second hypothesis is that RI exists in the cytosol as a safeguard against secreted ribonucleases that would inadvertently become cytoplasmic. Then, RI would function only to protect the cell from auxiliary ribonucleolytic activity. The absence of RI would lead to cell death by RNA degradation.

A third hypothesis is that RI functions to regulate the physiological activity of bound ribonucleases. Pancreatic ribonucleases, once internalized, would be sequestered by RI and released when appropriate. Interestingly, its sensitivity to oxidation provides a mechanism for the regulation of RI by the redox state of the cytosol. As such, RI may be a molecular switch for ribonucleolytic activity during oxidative conditions. Because ribonucleases can be cytotoxic (see next section), oxidation of RI could lead to the death of cells that have suffered oxidative assault.

A fourth hypothesis for the physiological role of RI involves two other RNase A homologues—ECP and EDN. In response to parasitic infections or hypersensitivity reaction, EDN and ECP are released from eosinophils via secretory granules. The interaction of RI with these ribonucleases may provide an additional level of regulation in the body's defense system. These four hypotheses are not mutually exclusive.

Cytotoxic homologues of ribonuclease A

In 1955, RNase A was found to be toxic to carcinomas in mice and rats (Ledoux, 1955a; Ledoux, 1955b). The antitumor activity of RNase A, however, showed poor promise as a therapeutic because high quantities were required (Roth, 1963). In 1973, the antitumor potential of a dimeric homologue, bovine seminal ribonuclease (BS-RNase) was discovered towards Crocker tumor transplants in mice (Matousek, 1973). Further characterization showed that BS-RNase is a poor candidate for a cancer therapy, as it has non-specific toxicity; it is antispermatogenic (Matousek, 1994), hinders embryo development (Matousek, 1975), oocyte maturation (Slavik *et al.*, 2000), and is immunosuppresive (Matousek *et al.*, 1995).

In more recent studies, ribonucleases from *Rana pipiens* (Darzynkiewicz *et al.*, 1988), *Rana catesbeiana* (Nitta *et al.*, 1987; Nitta *et al.*, 1994), and *Rana japonica* were found to contain antitumor activity. Onconase® (ONC) is an RNase A homologue from *Rana pipiens* and is both cytostatic and cytotoxic towards cultured tumor cells (Darzynkiewicz et al., 1988; Ardelt *et al.*, 1991). ONC and has been successful in the treatment of malignant mesothelioma in phase 1 (Mikulski *et al.*, 1993; Mikulski *et al.*, 1995) and phase 2 clinical trials (Mikulski *et al.*, 2002). Side effects of ONC are reversible and include renal toxicity and proteinuria. Phase 3 studies with ONC are in progress.

ONC has 30% amino acid sequence identity with RNase A (Figure 1.3) (Ardelt *et al.*, 1991). The key active-site residues of RNase A, His12, Lys41, and His119, are conserved in ONC. The crystalline structure of ONC has been solved, and RNase A and ONC share

similar secondary and tertiary structure (see Chapter 2) (Wlodawer, 1985; Mosimann *et al.*, 1994). ONC contains four disulfide bonds, three of which are present in RNase A. The divergent disulfide bond in ONC secures its C-terminus, and is responsible for endowing ONC with remarkable thermal stability (Leland *et al.*, 2000; Notomista *et al.*, 2001). The T_m value of ONC is 90 °C, which is 30 °C higher than RNase A (Leland *et al.*, 1998; Notomista *et al.*, 2000).

The active-site cleft in ONC also differs from RNase A. Specifically, the pyroglutamyl residue, Pyr1, of ONC is part of the active site and is thought to be involved with substrate binding (Boix *et al.*, 1996). This structural difference could be responsible for the lower catalytic activity of ONC. ONC demonstrates 10^3–10^5-fold less ribonucleolytic activity than does RNase A (Boix *et al.*, 1996; Leland *et al.*, 1998; Bretscher *et al.*, 2000).

The discovery of ONC in 1988 and its clinical success in subsequent years has intensified the study of other ribonucleases with biological actions (for reviews, see: Schein, 1997; Youle & D'Alessio, 1997; Raines, 1999; Rybak & Newton, 1999; Leland & Raines, 2001). Cell culture experiments have revealed that EDN and ECP have antiviral and cytotoxic potential (Newton *et al.*, 1994; Rosenberg & Dyer, 1995). ONC also demonstrates antiviral activity (Saxena *et al.*, 1996). More recently, RNase 1 was shown to kill Kaposi's sarcoma cells *in vitro* (Griffiths *et al.*, 1997).

The mechanism of ribonuclease-mediated cytotoxicity

The mechanism by which a ribonuclease is cytotoxic can be dissected into four steps: (1) cell-surface binding, (2) ribonuclease internalization, (3) translocation into the cytosol, and (4) evasion of RI and degradation of cellular RNA (Figure 1.5). ONC has low catalytic activity, but is a potent toxin, suggesting that it accomplishes these four steps. In contrast, RNase A is not an efficient toxin. Specifically, RNase A is over $>10^3$-fold less cytotoxic to cells than is ONC (Wu *et al.*, 1993). Why is RNase A a poor cytotoxin, when it has $>10^3$-fold enzymatic activity than does ONC? The answer to this question lies in understanding the molecular basis of ribonuclease-mediated toxicity. A better understanding of this mechanism would allow for the creation of RNase A variants that possess high cytotoxicity. In addition, understanding the basis of toxic action may shed light on factors that govern cell specificity.

The molecular basis for cell-surface binding by ribonucleases is not known. RNase A homologues from *Rana japonica* and *Rana catesbeiana* were isolated originally as lectins that agglutinated tumor cells (Sakakibara *et al.*, 1977; Sakakibara *et al.*, 1979). These ribonucleases are known to bind a specific glycoprotein that is high in sialic acid content (Sakakibara *et al.*, 1979). The crystalline complex of the *Rana catesbeiana* ribonuclease•sialic acid complex showed that two sialic acid molecules bound per ribonuclease and were intimately associated with the active site (Nonaka *et al.*, 1996; Irie *et al.*, 1998). High affinity binding sites (6.2×10^{-8} and 2.5×10^{-7} M) have been reported for ONC–cell-surface binding on 9L glioma cells (Wu *et al.*, 1993), but a specific protein receptor for ONC has not been identified. In addition, BS-RNase binds to the surface of

tumor cells (Matousek, 2001), but not to a specific receptor (Kim *et al.*, 1995b). The cell-surface binding of RNase A or its cytotoxic variants has not been demonstrated. Yet, the non-specific cationization of RNase A does increase its cellular uptake and cytotoxicity (Futami *et al.*, 2001), suggesting that a specific receptor is not involved in cell-surface binding and uptake.

Researchers have exploited the importance of cell-surface binding to enhance ribonuclease cytotoxicity (for reviews, see: Schein, 1997; Rybak & Newton, 1999). For example, epidermal growth factor (EGF) was chemically linked with RNase 1, and this chimera was 10^3-fold more toxic than was RNase 1 alone (Jinno *et al.*, 1996). The EGF–RNase 1-linked protein also displayed specificity and was not toxic to cells lacking the EGF receptor. Youle and co-workers chemically conjugated RNase A to monoclonal antibodies that were specific for transferrin (Newton *et al.*, 1992). This RNase A conjugate was cytotoxic to human leukemia cells at sub-μM concentrations.

After binding to the cell surface, ribonucleases must become internalized by cells and translocate across the plasma membrane to reach the cytosol (Figure 1.5). Two mechanisms exist whereby proteins can be internalized, based on energy-dependent or passive transport. Endocytosis is an energy-dependent process that involves vesicle-mediated internalization of molecules from the cell surface (for a review, see: Marsh, 2001). Endocytosis can be divided into five classes: (1) clathrin-dependent, (2) caveolae, (3) macropinocytosis, (4) phagocytosis, and (5) clathrin- and dynamin-independent. The role of endocytosis in ribonuclease internalization has not been well characterized. The cytotoxicity of ONC is inhibited by the presence of metabolic inhibitors (Wu *et al.*, 1993), implying that energy is

required. Once internalized, it is not known which membrane ribonucleases cross to enter the cytosol.

An alternative mechanism for the internalization of ribonucleases is through direct transport across the plasma membrane. This phenomenon has been documented for some protein domains, such as HIV Tat (Green & Loewenstein, 1988; Prochiantz, 2000). The arginine- and lysine-rich region (residues 47–57) of HIV Tat is sufficient for translocation by an undetermined mechanism, and can occur at 4 °C and in the presence of metabolic inhibitors. The direct translocation across a cell membrane has not been documented for ONC or RNase A. D'Alessio and co-workers did find that the dimeric, form of BS-RNase disrupted negatively charged membranes, whereas the monomeric, non-toxic form did not destabilize membranes (Mancheño *et al.*, 1994).

After internalization, ribonucleases must avoid inhibition by RI to retain catalytic activity (Figure 1.5). ONC and RNase A interact with RI with different affinities. RI binds RNase A with extremely high affinity ($K_i \approx 10^{-13}$ M; Table 1.1). RI has little or no affinity for ONC (Wu *et al.*, 1993; Boix *et al.*, 1996). As a result, ONC is more active in the presence of RI than is RNase A. The substantial difference in binding affinities has proven to be an important factor in the cytotoxicity of ribonucleases. For example, ribonuclease variants that evade RI are cytotoxic (Leland *et al.*, 1998). Gly88 of RNase A forms a tight hydrophobic contact with residues of RI. Replacing Gly88 with an arginine residue (G88R RNase A) disrupts this interaction, decreasing the affinity for RI. G88R RNase A is toxic to human leukemia cells (Leland *et al.*, 1998).

The ribonucleolytic activity, albeit low, of ONC is essential for its cytotoxicity (Wu *et al.*, 1993; Boix *et al.*, 1996; Newton *et al.*, 1997; Newton *et al.*, 1998). Alkylation of the active-site histidine residues in ONC decreases its ribonucleolytic activity by 10^2-fold and abolishes its cytotoxicity (Wu *et al.*, 1993). The N-terminal pyroglutamate of ONC is necessary for its activity. Variants of ONC with an N-terminal methionine residue have low enzyme activity and decreased cytotoxicity (Boix *et al.*, 1996). In addition, ONC appears to degrade tRNA, while RNase A prefers to degrade rRNA (Lin *et al.*, 1994). The role of RNA substrate specificity in ribonuclease toxicity is not known.

Using the cytotoxicity of ONC as a model, mammalian pancreatic ribonuclease variants have been endowed with toxic activity. Youle and co-workers engineered an RNase 1 chimera to enhance cellular targeting and sterically block RI binding by conjugating transferrin to residue 89 (Suzuki *et al.*, 1999). RNase A variants with low catalytic activity are toxic to cells, if the interaction with RI is weakened further (Bretscher *et al.*, 2000). Increasing the conformational stability of G88R RNase A, by the addition of a fifth disulfide bond to tether its C-terminus, also increases its toxicity by 2–3-fold (Klink & Raines, 2000).

In this thesis, I explore the molecular basis of ribonuclease-mediated cytotoxicity. In Chapter 2, I examine the internalization pathway of ONC and RNase A. Chapter 3 is an investigation of the importance of the lysosomal degradation sequence (shown in Figure 1.3) in ribonuclease-mediated cytotoxicity. The contributions of RI affinity and catalytic activity to cytotoxicity are also probed. In Chapter 4, the role of RI is revealed as a modulator of cellular susceptibility. In Chapter 5, the genomic structure and evolution of RI, is presented. Chapter 6 describes the efforts to probe the physiological role of pancreatic ribonuclease, as

well as that of RI.

Table 1.1 Binding constants for ribonuclease inhbitor•ribonuclease complexes[a]

RI	Enzyme	K_d (M)	Ref.
human	RNase A	4.4×10^{-14}	Lee *et al.* (1989)
porcine	RNase A	6.7×10^{-14}	Vicentini *et al.* (1990)
human	Pancreatic ribonuclease, human	2.0×10^{-13}	Boix *et al.* (1996)
human	EDN	9.4×10^{-16}	Shapiro & Vallee (1991)
human	Liver ribonuclease, porcine	4.0×10^{-15}	Hofsteenge *et al.* (1998)
human	ANG, human	7.1×10^{-16}	Lee *et al.* (1989)
human	ANG, bovine	3.4×10^{-15}	Bond *et al.* (1993)
human	ANG, porcine	2.2×10^{-15}	Bond *et al.* (1993)
human	ONC, frog	$\geq 1.0 \times 10^{-6}$	Boix *et al.* (1996)

[a]Adapted from Shapiro (2001).

Figure 1.1 Ribbon diagram of ribonuclease A. Ribbon diagram was created by using the atomic coordinates derived by x-ray diffraction analysis (Kartha *et al.*, 1967). The key active-site residues and disulfide bonds are indicated.

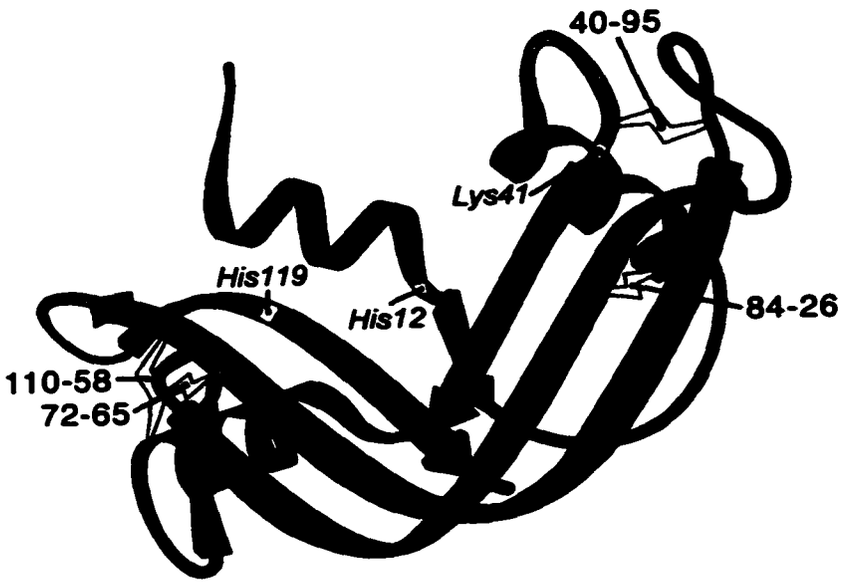
40-95
Lys41
His119
His12
84-26
110-58
72-65

Figure 1.2 Mechanism of ribonuclease A catalysis (Findlay *et al.*, 1961). In the transphosphorylation (step 1) and hydrolysis (step 2) reaction of RNA, "B" is His12 and "A" is His119.

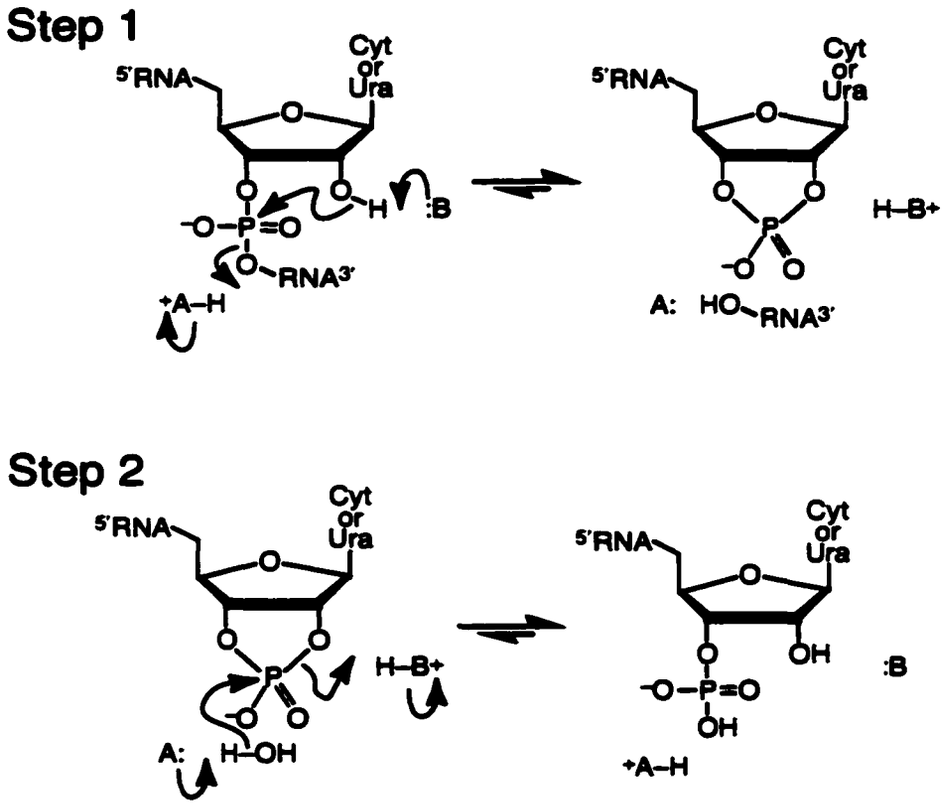
Step 1
5'RNA
Cyt
or
Ura
O
H
:B
-O-P=O
O
RNA3'
+A-H
5'RNA
Cyt
or
Ura
O
H-B+
-O
A: HO
RNA3'
Step 2
5'RNA
Cyt
or
Ura
O
H-B+
-O
A:
H-OH
5'RNA
Cyt
or
Ura
OH
:B
-O-P=O
OH
+A-H

Figure 1.3 Amino acid sequence alignment of homologous ribonucleases. Amino acid sequences were aligned using the PILEUP program (Genetics Computer Group; Madison, WI). Residues are numbered according to RNase A. Amino acid residues that interact with RI, are involved in RNA binding and catalysis, and biologically relevant sequences are indicated.

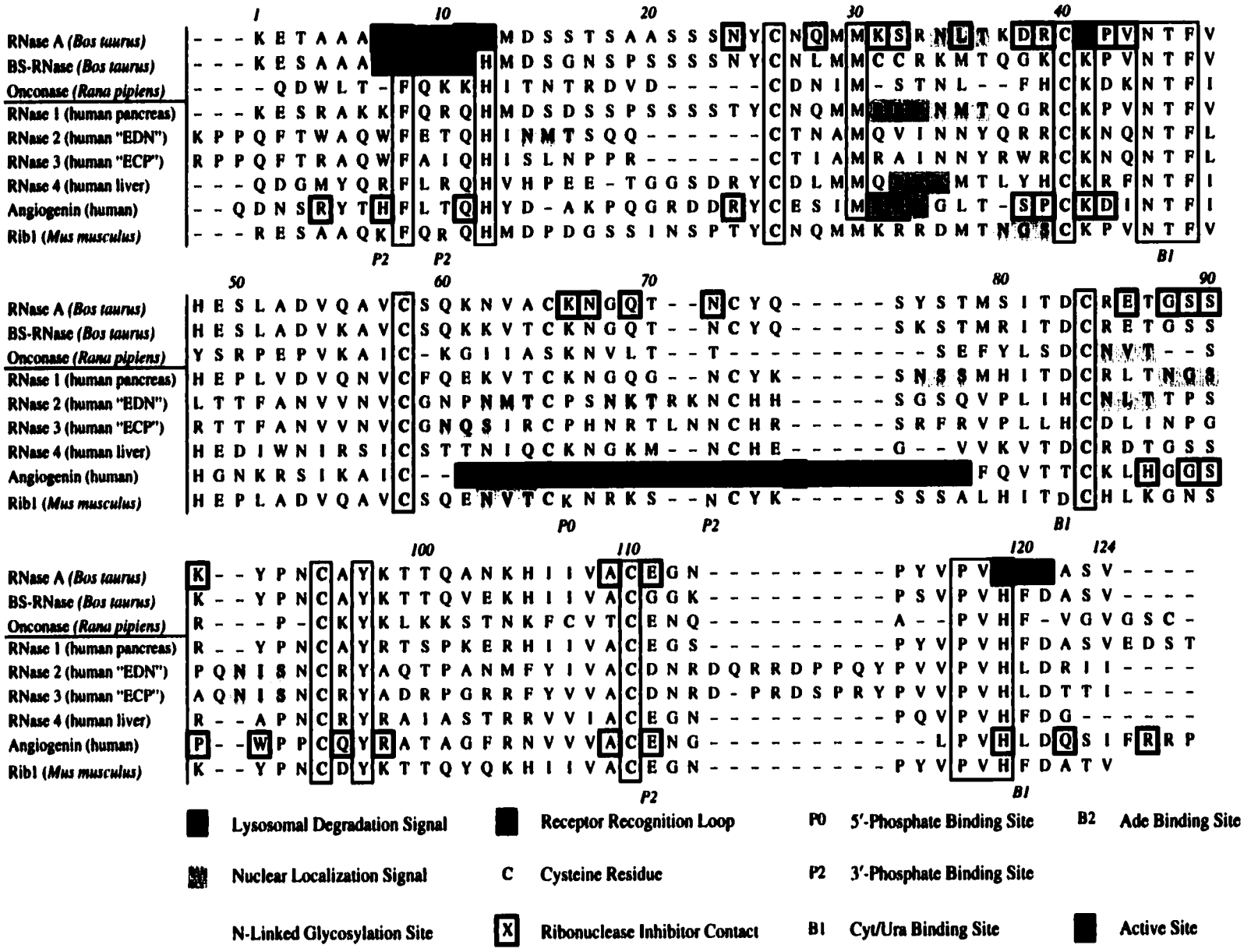
RNase A (Bos taurus)
BS-RNase (Bos taurus)
Onconase (Rana pipiens)
RNase 1 (human pancreas)
RNase 2 (human "EDN")
RNase 3 (human "ECP")
RNase 4 (human liver)
Angiogenin (human)
Rib1 (Mus musculus)
Lysosomal Degradation Signal
Nuclear Localization Signal
N-Linked Glycosylation Site
Receptor Recognition Loop
C Cysteine Residue
X Ribonuclease Inhibitor Contact
P0 5'-Phosphate Binding Site
P2 3'-Phosphate Binding Site
B1 Cyt/Ura Binding Site
B2 Ade Binding Site
Active Site

Figure 1.4 Structure of the ribonuclease inhibitor•ribonuclease A complex. Ribbon diagrams were created by using the atomic coordinates derived by x-ray diffraction analysis (Kobe & Deisenhofer, 1995b) and the program MOLSCRIPT (Kraulis, 1991).

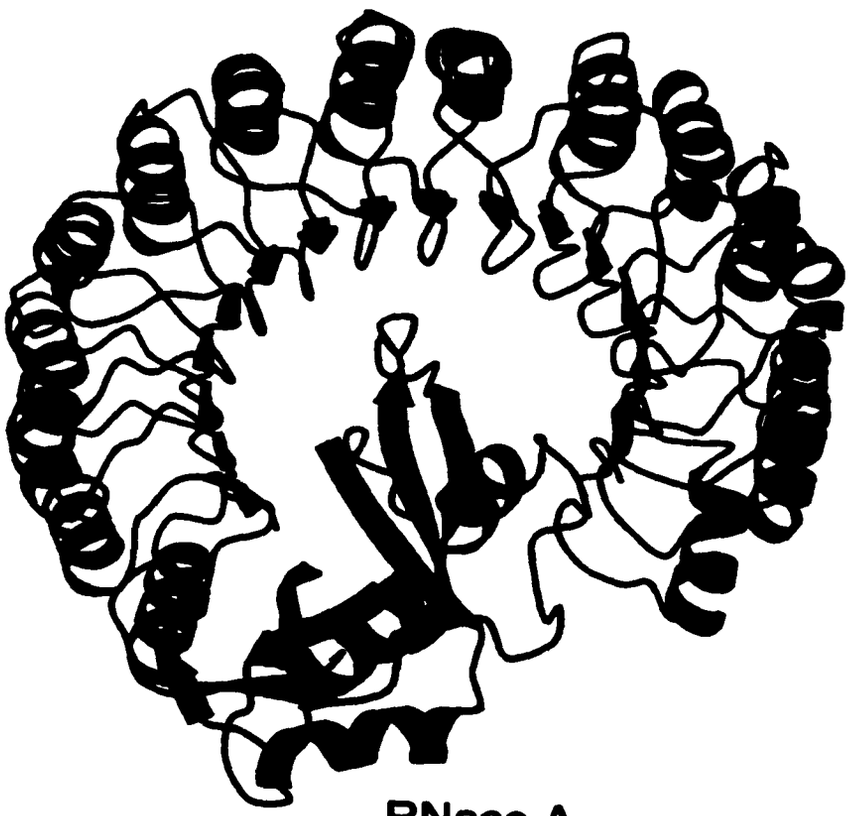
RI
RNase A

Figure 1.5 Putative mechanism for ribonuclease-mediated cytotoxicity. Ribonuclease-mediated toxicity can be described by: (1) cell-surface localization, (2) internalization, (3) translocation to the cytosol, (4) RI evasion and RNA cleavage, and (5) cell death.

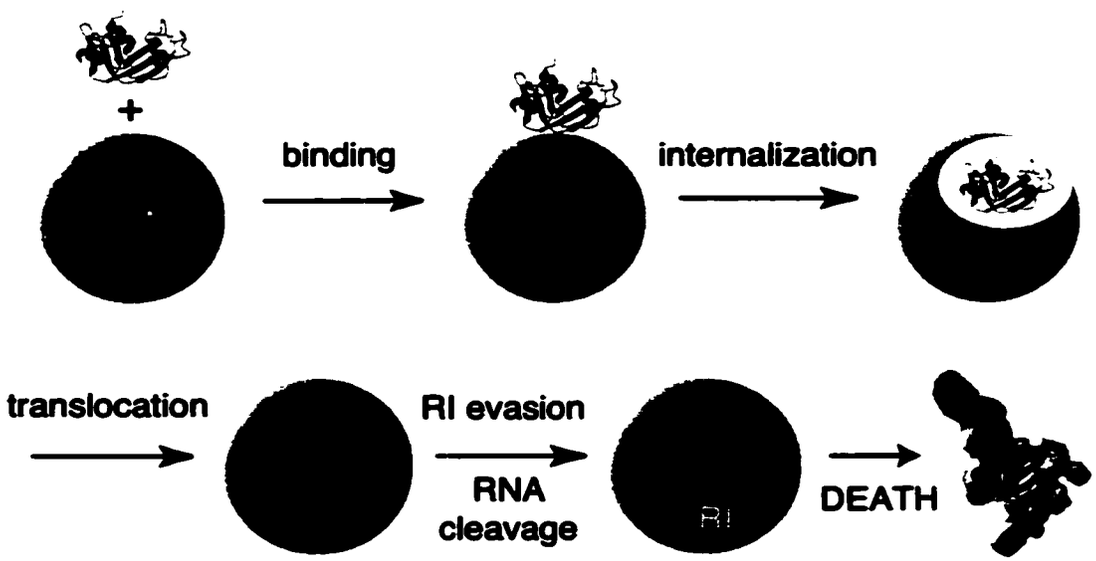
+
binding
internalization
translocation
RI evasion
RNA
cleavage
RI
DEATH

Chapter 2

Intracellular Routing of Toxic Ribonucleases

In preparation as: Marcia C. Haigis, Sandra L. Schmid, and Ronald T. Raines (2002)

Intracellular routing of toxic ribonucleases

ABSTRACT

Cytosolic internalization is a requirement for the toxicity of secretory ribonucleases. Here, we investigate the mechanism of internalization of Onconase® (ONC), a toxic protein, and bovine pancreatic ribonuclease A (RNase A), a homologue that is normally not toxic to cells. Microscopy studies using K-562 cells indicate that ribonucleases readily bind to the cell surface and are internalized via acidic vesicles. The toxicity of ONC, RNase A, and G88R RNase A, a toxic variant, was measured on a HeLa cell line overproducing a dominant-negative dynamin variant. These cells remain vulnerable to the toxicity of ONC and G88R RNase A, indicating that ribonucleases are internalized via a dynamin-independent pathway. As a further probe of the internalization pathway, NH_4Cl, monensin, and brefeldin A were used to perturb acidic vesicles and the Golgi apparatus. We find that cytosolic translocation of ribonucleases does not require an acidic environment or transport to the ER. These data show that ribonucleases are internalized by a pathway distinct from other protein toxins.

INTRODUCTION

Members of the ribonuclease A (RNase A) superfamily possess diverse biological properties. Bovine seminal ribonuclease demonstrates antitumor, antiviral, and immunosuppressive activity (for reviews, see: D'Alessio *et al.*, 1991; D'Alessio *et al.*, 1997; Matousek, 2001). Angiogenin, another homologue, was isolated originally based on its ability to promote angiogenesis (Fett *et al.*, 1985; Shapiro *et al.*, 1987). Angiogenin is also toxic to mixed cultures of primary lymphocytes (Matousek *et al.*, 1995). Onconase® (ONC) is a homologue of RNase A found in *Rana pipiens* and demonstrates both antitumor and antiviral activity (Darzynkiewicz *et al.*, 1988; Youle *et al.*, 1994; Saxena *et al.*, 1996). RNase A itself, however, does not have marked antitumor, antiviral, or angiogenic activity.

The mechanism of ribonuclease-mediated cell death consists of two major steps: (1) internalization and (2) catalytic cleavage of cellular RNA. Several studies have focused on understanding the contribution of intracellular ribonucleolytic activity to toxicity (for reviews, see: D'Alessio, 1993; Schein, 1997; Raines, 1999; Rybak & Newton, 1999; Leland & Raines, 2001; Matousek, 2001). The internalization pathway of ribonucleases is not well characterized. Ribonucleases must reach the cytosol to degrade cellular RNA. Ribonucleases that are microinjected into the cytosol are several fold more toxic than when added to cells externally (Saxena *et al.*, 1991). Even RNase A becomes toxic when microinjected directly into the cytosol, suggesting that its internalization limits toxicity. The potency of ONC can also be enhanced by adding drugs that alter cellular routing (Wu *et al.*, 1995). Likewise, conjugating ribonucleases to delivery molecules enhances their toxicity (Rybak *et al.*, 1991;

Newton *et al.*, 1992; Suzuki *et al.*, 1999). Hence, the efficiency of its intracellular routing mediates the toxicity of a ribonuclease.

Proteins can be transported from the cell surface to endosomal compartments through clathrin-dependent or various clathrin-independent mechanisms (for a review, see: Marsh, 2001). Dynamin is a GTPase that plays an essential role in clathrin-mediated endocytosis (for reviews, see: Warnock & Schmid, 1996; Urrutia *et al.*, 1997; McNiven, 1998; Schmid *et al.*, 1998; McNiven *et al.*, 2000). A variant of dynamin in which Lys44 is replaced with an alanine residue (K44A Dyn) is defective in GTP binding and hydrolysis (van der Bliek *et al.*, 1993). Previous studies have shown that the overproduction of K44A Dyn in HeLa cells blocks clathrin-mediated endocytosis and inhibits the internalization of both transferrin and epidermal growth factor (van der Bliek *et al.*, 1993; Damke *et al.*, 1994). These HeLa cells demonstrate normal levels of fluid-phase endocytosis.

The toxicity of a molecule can be a powerful tool for assaying the efficiency and delineating the pathway of its intracellular routing. As RNase A is not toxic to cultured cells, this approach has not been used in previous studies to probe the internalization of RNase A. Variants of RNase A can be toxic to cells. For example, substituting the glycine residue at position 88 with arginine (G88R) decreases the affinity of RNase A for ribonuclease inhibitor (RI) and endows RNase A with cytotoxic activity (Leland *et al.*, 1998). This activity is specific for rapidly dividing tumor cell lines, but is not due to differences in intracellular RI concentrations (Haigis *et al.*, 2002c; Chapter 4). Little is known about the mechanism of cell entry of RNase A or whether it differs from that of ONC. Indeed, other workers have reported that RNase A is not bound by cells (Leamon & Low, 1993).

Here, we investigate the internalization of RNase A and ONC with tools from cell biology, pharmacology, and somatic cell genetics. Microscopy studies using K-562 cells provide evidence that RNase A and G88R RNase A, like ONC, are able to bind to the cell surface. Using fluorescently-labeled variants of RNase A and ONC, we visualize their internalization into acidic vesicles, and demonstrate that RNase A and ONC are internalized by the same cellular compartments, in a dose-dependent manner. We have taken advantage of the toxicity of G88R RNase A to probe the mechanism of its cytosolic entry. Ribonucleases can be internalized and are toxic to cells defective in dynamin-mediated endocytosis. Through the use of drugs that target varied components of intracellular trafficking, we demonstrate that cytosolic translocation does not depend on an acidic environment, nor on retrograde transport to the ER. Our results provide a mechanism of the intracellular routing of secretory ribonucleases, as well as the first evidence for differences in trafficking between ONC and RNase A.

MATERIALS AND METHODS

Design of ribonuclease variants. Native RNase A and ONC do not contain a reduced cysteine residue. To visualize the early internalization event(s) of RNase A and ONC in living cells, we introduced a cysteine residue into each protein, which allows for site-specific labeling with a fluorophore. The exact placement of the cysteine residue was determined by several criteria with the goal of not altering the mechanism of ribonuclease internalization. The exact residues involved in ribonuclease internalization are unknown. Therefore, we did

not mutate regions of the protein that could be central for directing internalization. First, active-site residues were not altered, as this cationic region could be important for internalization. In addition, highly conserved residues were not chosen. The selected residue should be solvent accessible, to facilitate labeling to a fluorescent probe. Finally, the mutation should not disrupt the thermal stability of these ribonucleases. Unfolded protein may not be internalized efficiently. Also, unfolded ribonucleases within the cell are substrates for degradation (Klink & Raines, 2000).

The first surface loop of RNase A and ONC satisfied these requirements. In both proteins, this region is located away from active site residues and is variable between members of the RNase A superfamily. Ala19 (RNase A) and Asp16 (ONC) are located in this surface loop, and are solvent exposed (Figure 2.1) (Wlodawer *et al.*, 1988; Mosimann *et al.*, 1994). Mutating Ala19 and Asp16 to a cysteine residue enables site-specific labeling with a thiol-reactive flourescent probe. Addition of a fluorophore should not interfere with ribonucleolytic activity, structural stability, or internalization.

Production of ribonucleases and variants. The pBXR and pONC plasmids direct expression of wild-type RNase A and wild-type ONC in Escherichia coli (delCardayré *et al.*, 1995; Leland *et al.*, 1998). A plasmid that directs the expression of D16C ONC was created by using oligonucleotide-mediated site-directed mutagenesis (Kunkel *et al.*, 1987).

Wild-type RNase A, G88R RNase A, and wild-type ONC were purified using methods described previously (delCardayré *et al.*, 1995; Leland *et al.*, 1998). A19C RNase A and D16C ONC were purified as described for the wild-type proteins, but with the following modifications (Kothandaraman *et al.*, 1998). Refolding solutions were saturated with Ar(g) to

remove molecular oxygen. Immediately after anion-exchange chromatography, the sulfhydryl group of Cys19 (A19C RNase A) or Cys16 (D16C ONC) was protected from oxidation by reaction with 5,5′-dithio-bis(2-nitrobenzoic acid) (DTNB) at pH 9 (Messmore *et al.*, 1995). DTNB-protected protein was isolated from unprotected protein with anion-exchange chromatography. Protein concentrations were determined by UV spectroscopy using $\varepsilon = 0.72$ ml mg^{-1} cm^{-1} at 277.5 nm for RNase A (Sela *et al.*, 1957) and its variants and $\varepsilon = 0.87$ ml mg^{-1} cm^{-1} at 280 nm for ONC. All ribonucleases were dialyzed exhaustively versus phosphate-buffered saline (PBS), which contained (in 1.00 liter) KCl (0.20 g), KH_2PO_4 (0.20 g), NaCl (8.0 g), and Na_2HPO_4 (2.16 g).

Fluorescent labeling of ribonucleases. DTNB-protected A19C RNase A and D16C ONC were deprotected immediatedly prior to fluorescent labeling. Protected protein was incubated with a 3-fold molar excess of dithiothreitol or tris(2-carboxyethyl) phosphine (TCEP) and a 40-fold molar excess of label for 25 min at 22 °C. The fluorescent probes 5-iodoacetamidofluorescein (5-IAF), N-(4,4-difluoro-1,3,5,7-tetramethyl-4-bora-3a,4a-diaza-s-indacene-2-yl)iodoacetamide (BODIPY® 507/545 IA), and 2′,7′-difluorofluorescein-iodoacetamide (Oregon Green™ 488 IA) were from Molecular Probes (Eugene, OR). Excess, unreacted probe was removed by gel filtration chromatography with a NICK column (Pharmacia Biotech; Piscataway, NJ). Protein concentration was determined with eq 1:

$$A_{prot} = A_{meas} - A_{max\,dye}(cf) \tag{1}$$

where A_{prot} is the actual A_{280} of the protein, A_{meas} is the measured absorbance at 280 nm, A_{maxdye} is the absorbance of the coupled dye, and *cf* is the A_{280}/A_{max} ratio of the free dye. The *cf* for fluorescein is 0.2. The degree of protein labeled (*DOL*) was determined with eq 2:

$$DOL = \frac{A_{maxdye}}{\varepsilon} \times \frac{MW_{prot}}{[\text{prot}]} \tag{2}$$

where ε is the molar extinction coefficient of the dye at wavelength of maximum absorption.

Labeled protein was purified away from unlabeled protein by using reverse-phase HPLC as described by Abel *et al.* (Abel *et al.*, 2001). The HPLC peak containing labeled protein was dialyzed exhaustively versus PBS for biological assays.

Assay of thermal stability. Conformational stability assays were performed as described (Eberhardt *et al.*, 1996), with the following modifications. The conformational stability was of RNase A, ONC, and each labeled-variant (in PBS) was determined by monitoring the change in absorbance at 287 nm as the temperature was increased from 25 to 75 °C in 1 °C increments. The absorbance at 287 nm was recorded after a 7-min equilibration at each temperature. The value of T_m represents the midpoint of the thermal denaturation. The data was collected and analyzed with the program Thermal (Varian Analytical Instruments; Walnut Creek, CA).

Assay of catalytic activity. Ribonucleolytic activity was measured by using a fluorogenic substrate (Kelemen *et al.*, 1999). Assays were performed at 23 °C in 2.00 ml of 0.10 M MES–NaOH buffer (pH 6.0) containing NaCl (0.10 M). Solutions contained 6-

FAM~dArU(dA)$_2$~6-TAMRA (50 nM) and enzyme (1.0–5.0 pM). Fluorescence changes were measured using a QuantaMaster 1 photon-counting fluorescence spectrometer from Photon Technology International (South Brunswick, NJ) using glass cuvettes (1.0-cm pathlength) from Starna Cells (Atascadero, CA). Fluorescence was monitored using 493 and 515 nm for the excitation and emission wavelengths, respectively. Kinetic parameters were determined by a linear least-squares regression analysis of the initial velocity using:

$$V / K = \frac{(\Delta F / \Delta t)}{F_{max} - F_0} \tag{3}$$

where V/K is the first-order rate constant, $\Delta F/\Delta t$ is the slope from the linear regression, F_{max} is the final fluorescence intensity after the reaction has reached completion, and F_0 is the fluorescence intensity before the addition of enzyme. The value of k_{cat}/K_M was calculated by dividing V/K by the enzyme concentration.

Cell culture. K-562, JAR, and HeLa cells were obtained from the American Type Culture Collection (Manassas, VA). K-562 and JAR cells were grown in RPMI medium 1640. HeLa cells were grown in DMEM medium. All culture medium contained fetal bovine serum (FBS; 10% (v/v)), penicillin (100 units/ml), and streptomycin (100 μg/ml). Cell culture medium and supplements were from Life Technologies (Gaithersburg, MD). Cells were cultured at 37 °C in a humidified incubator containing 5% CO_2(g). All studies were performed using asynchronous log-phase cultures.

Immunohistochemistry. Wild-type RNase A, G88R RNase A, or ONC was added to a culture of K-562 cells at 4 °C. After 20 min, cells were washed twice with PBS and fixed for 30 min at 4 °C in PBS containing paraformaldehyde (2% w/v) and Triton X-100 (0.1% w/v). After being fixed, the cells were rinsed three times in PBS and incubated for 1 h at 37 °C with primary antibody. Rabbit IgG raised against RNase A was from Biodesign International (Kennebunk, ME), and was used at a concentration of 1 μg/ml in PBS containing Tween-20 (0.1% v/v) (PBST). Chicken antiserum raised against ONC was the generous gift from Alfacell Corporation (Bloomfield, NJ), and was used at a 1:100 dilution in PBST. After incubation with primary antibodies, cells were washed three times in PBST and incubated with the appropriate secondary antibodies (1:500 in PBST) conjugated to fluorescein or rhodamine (Molecular Probes; Eugene, OR). After a 1-h incubation with secondary antibodies, cells were washed three times with PBST, and stained with propidium iodide (1 μg/ml in PBS) for 5 min. Then, cells were washed twice with PBST and mounted onto glass microscope slides using Vectashield (Vector Laboratories; Burlingame, CA). Fluorescence staining of cells was visualized on a Zeiss Axiovert 100 TV microscope (Zeiss; Germany). Images were analyzed with the programs BioRad MRC 1024 Laser Scanning Confocal Imaging System (Hercules, CA) and Adobe Photoshop (San Jose, CA).

Ribonuclease internalization. The internalization of RNase A was visualized directly in living cells. K-562 cells in PBS (1–2 × 10^6 cells/ml) were incubated with either BODIPY-labeled A19C RNase A (BODIPY~RNase A) or fluorescein-labeled A19C RNase A (fluorescein~RNase A) (1 μM) at 4 °C for 20 min. Cells were washed three times with ice-cold PBS to removed unbound protein. Then, cells were incubated for 5 min at 37 °C in a

humidified incubator containing 5% CO_2(g). After incubation, living cells were washed three times in PBS and placed on a microscope slide; fluorescence was monitored immediately.

To probe the co-internalization of ONC and RNase A, JAR or HeLa cells were grown on coverslips in the wells of a 6-well plate for 24 h before the assay. Oregon Green-labeled D16C ONC (OG~ONC) and BODIPY~RNase A (both at a concentration of 1 μM and labeled to ~10%) were incubated with cells at 4 °C for 20 min. Cells were washed three times with ice-cold PBS to remove unbound protein, and then incubated for 5 min at 37 °C or for 15 min at 22 °C. Cells were washed three times with ice-cold PBS, and fixed as described for immunohistochemistry. After fixing, cells were washed three times with PBS, mounted on microscope slides, and visualized immediately.

To study the dose-dependence of RNase A and ONC, both proteins were labeled with Oregon Green, and used at a labeling efficiency of 30%. HeLa cells were incubated with increasing concentrations of either OG~RNase A or OG~ONC (0.01, 0.1, 1, and 10 μM). Samples were pulsed, fixed, and visualized as described previously.

To investigate the internalization of RNase A with endocytic markers, cells were pulsed with BODIPY~RNase A (1 μM), OG~RNase A (1 μM), FM™ 1-43 (1 μg/ml; Molecular Probes; Eugene, OR), BODIPY-FL- or tetramethylrhodamine-transferrin (50 μg/ml; Molecular Probes; Eugene, OR). Endocytosis assays were performed as described (Lamaze *et al.*, 2001).

Assays of cytotoxicity. The effect of ONC, RNase A, and G88R RNase A on cell proliferation was determined by measuring [*methyl*-^{3}H]thymidine uptake into DNA. Briefly, cells (95 μl of a solution of 5×10^4 cells/ml) were incubated with PBS containing a known

concentration of a ribonuclease (5 μl) in a 96-well plate for 20 h at 37 °C in a humidified incubator containing 5% CO_2(g). The proliferation of cells was monitored with a 4 h [*methyl*-^{3}H]thymidine pulse (0.4 μCi/well). Cells were harvested onto glass fiber filters using a PHD Cell Harvester (Cambridge Technology; Watertown, MA). Filters were washed with water, dried with MeOH, and counted in a liquid scintillation counter.

For pharmacological studies, brefeldin A (BFA; 5.0 μg.ml), NH_4Cl (20 mM), or monensin (10 μM) was preincubated with cells for 2 h before the addition of a ribonuclease. Data were analyzed as the percent of [*methyl*-^{3}H]thymidine incorporated compared to drug-treated cells incubated with PBS.

To investigate the role of dynamin in ribonuclease internalization, the toxicity of ONC and G88R RNase A was measured in a cell line overproducing K44A Dyn (Damke *et al.*, 1994). Briefly, transformed tTA HeLa cells were cultured in DMEM containing FBS (10% v/v), penicillin (100 units/ml), streptomycin (100 μg/ml), G418 (400 μg/ml), and tetracycline (2 μg/ml) as described previously (Damke *et al.*, 1994). Cells were cultured at 37 °C in a humidified incubator containing 5% CO_2(g). All studies were performed using asynchronous log-phase cultures. To induce the overexpression of HA-tagged dynamin (or K44A Dyn), subconfluent cultures (<50%) were washed several times in PBS, detached with trypsin, and plated onto 10-cm culture dishes in the absence of tetracycline. After 48 h, the overexpression of dynamin was monitored by immunoblot analysis using antibodies to the HA epitope. Then, toxicity assays were performed as described above using both uninduced and induced cells.

RESULTS

Conformational stability and ribonucleolytic activity. Data from experiments with incubations at 37 °C can be interpreted properly only with information that the protein is folded at that temperature. Fluorescein-labeled A19C RNase A (fluorescein~RNase A) and DTNB-labeled D16C ONC (DTNB~ONC) had T_m values of 61 and 88 °C, respectively (Table 2.1). These values are similar to the reported T_m values for wild-type RNase A and ONC of 63 and 90 °C, respectively (Leland *et al.*, 2000).

The cytotoxicity of ribonucleases relies on their ribonucleolytic activity. Alkylation of ONC results in the loss of catalytic as well as cytotoxic activity (Wu *et al.*, 1993). RNase A variants with altered active-site residues have lowered enzymatic activity and cytotoxic activity (Raines, 1998; Raines, 1999; Bretscher *et al.*, 2000). We measured the ribonucleolytic activity of labeled-ONC and RNase A variants using a fluorogenic substrate, 6-FAM~dArU(dA)$_2$~6-TAMRA (Kelemen *et al.*, 1999). Values of k_{cat}/K_M for ONC, RNase A and their variants were determined for cleavage of this substrate. The values of k_{cat}/K_M for RNase A and ONC were found to be 4.3×10^7 $M^{-1}s^{-1}$ and 3.5×10^2 $M^{-1}s^{-1}$, which are in good agreement with k_{cat}/K_M values reported previously (Kelemen *et al.*, 1999; Leland *et al.*, 2000). The values of k_{cat}/K_M for fluorescein~RNase A and DTNB~ONC were found to be 0.54×10^7 $M^{-1}s^{-1}$ and 1.7×10^2 $M^{-1}s^{-1}$ respectively (Table 2.1). Thus, thermal stability and ribonucleolytic actitivity are retained in the modified variants tested herein.

Binding and internalization of ribonucleases. The first step in the mechanism of ribonuclease-mediated cytotoxicity is an interaction with the cell surface. Previous studies

have reported a high-affinity interaction (K_d = 62 nM) between ONC and the surface of 9L cells (Wu *et al.*, 1993). An interaction between RNase A and the cell surface has not been reported. We investigated the binding of ONC, RNase A, and G88R RNase A to the plasma membrane of human leukemia cells (K-562). We incubated K-562 cells with protein at 4 °C for 15 min, 1 h, or 2 h. As shown in Figure 2.2, ONC, RNase A, and G88R RNase A are bound to the cell surface after a 15-min incubation at 4 °C. The intensity of signal does not increase significantly after incubating for 2 h at 4 °C (data not shown). Our data also show that both ONC and RNase A accumulate at the cell surface at 4 °C and do not cross the plasma membrane, even after 2 h. These results suggests that the internalization of ribonucleases does not occur at 4 °C, and thus likely relies on endocytic processes.

A19C RNase A was labeled with fluorescein (fluorescein~RNase A), which has pH-sensitive fluorescence, or BODIPY (BODIPY~RNase A), which is a pH-insensitive probe. The fluorescence intensity of fluorescein~RNase A or BODIPY~RNase A was measured initially in a 10 mM Tris–HCl buffer (pH 8.0). As expected, the fluorescence intensity of fluorescein~RNase A decreased by >10-fold in a pH 4.5 environment (Figure 2.3A). The fluorescence intensity of the BODIPY~RNase A was not diminished by changes in pH. These data demonstrate that the pH-dependent properties of fluorescein and BODIPY are retained when conjugated to a specific site on ribonucleases.

Next, we examined the initial events of internalization. We pulsed K-562 cells at 37 °C with either fluorescein~RNase A or BODIPY~RNase A and then analyzed their fluorescence. Cells incubated with fluorescein~RNase A demonstrated a lack of detectable fluorescence inside cells (Figure 2.3B). In contrast, cells pulsed with BODIPY~RNase A

revealed vivid fluorescence (Figure 2.3B). As the pH of endosomal compartments are acidic (<6), these data provide evidence that ribonucleases are internalized through acidic endosomes.

Endosomal vesicles can merge with lysosomal compartments during internalization. To verify that RNase A was intact within acidic vesicles, K-562 cells were pulsed with unlabeled RNase A and analyzed by immunohistochemistry. RNase A was detected in inner vesicles similar in morphology to those seen in living cell studies (Figure 2.3C). Thus, the fluorescence visualized in BODIPY~RNase A-pulsed cells represents the internalization of intact protein. In addition, the immunostaining data show that the addition of the fluorescent label does not hinder or alter the mode of ribonuclease internalization.

We then searched for co-internalization of ONC and RNase A in a variety of human cancer cell lines. D16C ONC was labeled at residue 16 with the pH-insensitive fluorescent probe Oregon Green™ (OG~ONC), to allow for colocalization studies with BODIPY~RNase A. We find that K-562 cells internalize OG~ONC using the same compartments that contain BODIPY~RNase A (Figure 2.4). BODIPY~RNase A and OG~ONC are also internalized in the same compartments in cervical epithelioid carcinoma (HeLa) and choriocarcinoma (JAR) cells. Identical results were seen in living cells that were viewed without fixation after incubation with ribonucleases (data not shown).

To compare the dose dependence of ONC and RNase A internalization, we pulsed HeLa cells with increasing concentrations of either OG~ONC or OG~RNase A. We find that the amount of OG~ONC and OG~RNase A internalized by cells increases with increasing protein concentration (Figure 2.5). We also find that HeLa cells are equally sensitive to

external concentrations of OG~ONC and OG~RNase A. Both OG~ONC and OG~RNase A show a similar increase in uptake in the 1 μM versus 10 μM samples. In addition, the 10 μM samples consistently show an increase in the number of ribonuclease-filled punctate vesicles, and not an increase in the size or intensity of each vesicle. For internalization experiments, control samples containing cells incubated with fluorescein, BODIPY, or OG alone showed no fluorescence in either living cells or fixed cells (data not shown).

Fluid-phase endocytosis was analyzed in K-562 cells using the fluorescent small molecule FM 1-43™. K-562 cells undergo constant endocytosis (Figure 2.6). In addition, BODIPY~RNase A colocalizes with FM 1-43 (Figure 2.6). An enhancement in endocytosis was not detectable upon the addition of RNase A (data not shown).

Receptor-mediated endocytosis was analyzed in K-562 cells using a fluorescein-labeled transferrin. We find that transferrin, a marker for receptor-mediated endosomes and recycling endosomes, is readily internalized by K-562 cells (Figure 2.6). Significantly, BODIPY~RNase A did not colocalize with transferrin-containing endosomes. In addition, we observed that the internalization pattern of BODIPY~RNase A was distinct from the process of receptor-mediated endocytosis.

Dynamin-independent toxicity and internalization of ribonucleases. The toxicity of ONC, and G88R RNase A was investigated using tTA HeLa cell lines that overexpress genes encoding for wild-type dynamin or K44A Dyn (Damke *et al.*, 1994). Removal of tetracycline resulted in the overproduction of K44A Dyn, as shown by an immunoblot (Figure 2.7A), as well as morphological changes in these cells similar to those described previously (Damke *et*

al., 1994). Specifically, cells overproducing K44A Dyn are flatter, and have rounder edges and distinct actin formation (Figure 2.7A).

We find that HeLa cells are not equally susceptible to ONC and G88R RNase A-mediated toxicity (Figures 2.7B and 2.7C). ONC kills HeLa cells with an IC_{50} that is greater than 50-fold lower than that of G88R RNase A, with IC_{50} values of 1 and >50 μM, for ONC and G88R RNase A, respectively (Table 2.2). The toxicity of ONC and G88R RNase A was unaffected by the overproduction of wild-type dynamin (Figure 2.7B; Table 2.2).

We next measured the toxicity of ONC and G88R RNase A for cells that were overproducing the K44A Dyn protein (Figure 2.7C). The toxicity of ONC and G88R RNase A for cells not overproducing K44A Dyn was not significantly different from the toxicity of ONC and G88R RNase A for cells containing wild-type dynamin (Table 2.2). Surprisingly, we find that the overproduction of K44A Dyn makes cells *more* susceptible to ribonuclease-mediated toxicity. The IC_{50} value for ONC decreased by 2-fold, from 1.6 to 0.7 μM in uninduced versus induced cells, respectively (Table 2.2). A more dramatic enhancement in cytotoxicity was seen for G88R RNase A, as its IC_{50} value was decreased by more than 3-fold, from >50 to 17 μM in uninduced versus induced cells.

The increase in cytotoxicity upon K44A Dyn overproduction suggests that ONC and G88R RNase A are internalized via a dynamin-independent mechanism. To test this hypothesis, cells overproducing K44A Dyn were pulsed with OG~RNase A and tetramethylrhodamine-labeled transferrin. OG~RNase A is internalized by cells overproducing K44A Dyn (Figure 2.8). In contrast, transferrin is not internalized by these cells (Figure 2.8a). Analysis demonstrated that 80% of the cells overproducing K44A Dyn

were defective in internalization of transferrin, while they remained competent for OG~RNase A uptake (Figure 2.8b). Control cells not overproducing the dynamin variant internalized both OG~RNase A and labeled transferrin (Figure 2.8). These data clearly show that ribonucleases can be internalized in the absence of clathrin- and dynamin-mediated endocytosis.

Routing of toxic ribonucleases to the cytosol. The pharmacological agents NH_4Cl, monensin, and brefeldin A (BFA) have distinct and established effects on cellular compartments (Pelham, 1991; Sciaky *et al.*, 1997; Dinter & Berger, 1998). These drugs were used to examine the intracellular pathway(s) that ribonucleases use to reach the cytosol. In all experiments, K-562 cells were incubated with a drug for 2 h prior to the addition of ribonucleases (Figure 2.9).

NH_4Cl is a weak base that increases the endosomal pH. We find that NH_4Cl (20 mM) had no effect on the cytotoxicity of either ONC or G88R RNase A, indicating that routing to the cytosol is not perturbed in the presence of deacidified vesicles (Figure 2.9; Table 2.3). An NH_4Cl concentration of 30 mM also had no effect on ribonuclease toxicity (data not shown).

Monensin is a carboxylic ionophore that also leads to the deacidification of endosomes and may disrupt Golgi trafficking. Monensin (10 μM) potentiated the cytotoxicity of ONC by 10-fold, but had little effect on the cytotoxicity of G88R RNase A (Figure 2.9). Our data reveal for the first time that G88R RNase A is internalized via a monensin-insensitive pathway, and verify that the internalization of ONC or G88R RNase A is not dependent on a low pH environment.

To investigate whether downstream events in the retrograde pathway are important for cytotoxicity, we analyzed the toxicity of ONC and G88R RNase A in the presence and absence of BFA. BFA disassembles the Golgi stack and disrupts retrograde transport from the Golgi to the ER (Pelham, 1991), and has been a powerful tool for studying the internalization pathway of other protein toxins (Hudson & Grillo, 1991). We found that BFA potentiates the toxicity of both ONC and G88R RNase A by 10-fold (Figure 2.9; Table 2.3). Hence, our data show that retrograde transport from the Golgi to the ER is not an essential component of ribonuclease translocation to the cytosol.

DISCUSSION

Ribonucleases must reach the cytosol to act on their target substrate. Cytosolic internalization of ribonucleases can be broken down into the following components: (1) attraction to the cell surface, (2) internalization, and (3) crossing a cell membrane to reach the cytosol. Here, we have used ONC, RNase A, and their variants to analyze the pathways of ribonuclease internalization with a multifaceted approach. The data are summarized in Figure 2.10, which depicts a detailed model of ribonuclease internalization. First, we have demonstrated that both amphibian and mammalian ribonucleases can bind to the surface of a human cell. After binding, ribonucleases undergo clathrin- and dynamin-independent endocytosis. The acidic environment of these vesicles is not necessary for translocation to the cytosol, and internalized ribonucleases translocate to the cytosol from a pre-ER compartment.

Is there a cell-surface receptor for secretory ribonucleases? ONC and RNase A are homologous to lectins that bind to glycosylated proteins on the cell surface (Sakakibara *et al.*, 1979; Nitta *et al.*, 1987). A protein receptor for these lectins has not been identified. In addition, homologue scanning mutagenesis results suggest that there is not a single protein receptor for bovine seminal ribonuclease (Kim *et al.*, 1995b). One hypothesis is that favorable Coulombic interactions between cationic ribonucleases and the anionic plasma membrane could enhance cell-surface binding. Indeed, Yamada and co-workers found that the random cationization of RNase A increased its cellular uptake and cytotoxicity (Futami *et al.*, 2001).

After binding, internalization occurs through acidic vesicles, although an acidic environment is not necessary for translocation to the cytosol (Figures 2.3 and 2.9). We monitored the internalization of fluorescein~RNase A and BODIPY~RNase A, as well as OG~ONC, in living cells to provide the first direct evidence for the internalization of RNase A in acidic endosomes (Figure 2.3B). We probed the specific nature of these acidic vesicles, and found that found that unlike transferrin, ribonucleases do not require dynamin for internalization (Figure 2.8).

Surprisingly, ribonucleases are more toxic to cells in the absence of clathrin-mediated endocytosis (Figure 2.7; Table 2.2). What is the explanation for this finding? First, the clathrin-mediated endocytic pathway could be an inefficient route for the cytosolic entry of ribonucleases. Dynamin function has also been proposed to be important in caveolae fission from the plasma membrane (Henley *et al.*, 1998). By bypassing a dead-end pathway, ribonucleases could enter the cytosol more efficiently, leading to enhanced toxicity. Second,

a block in dynamin function could alter the translocation of ribonucleases, as well as their initial uptake. In addition to its role in endocytosis, dynamin is required for the formation of vesicles important for trafficking between numerous organelles. For example, dynamin is involved in endosome-to-Golgi transport, and in the formation of clathrin-coated and non-clathrin–coated vesicles from the trans-Golgi network (Jones *et al.*, 1998; Llorente *et al.*, 1998; Cao *et al.*, 2000). Thus, cells overproducing K44A Dyn are deficient in normal Golgi trafficking. Finally, some clathrin-independent pathways, such as pinocytosis, are up-regulated in cells that lack functional dynamin (Damke *et al.*, 1995). Hence, inactivating dynamin-dependent pathways can increase the influx of ribonucleases by cells.

Monensin potentiates the cytotoxicity of ONC by 10-fold, but does not alter significantly the cytotoxicity of G88R RNase A (Figure 2.9). Monensin is a carboxylic ionophore that deacidifies vesicles by exchanging protons for other cations. In addition, monensin can disrupt cellular functions, such as trafficking through the Golgi. Thus, our results provide evidence for a difference between the trafficking of ONC and G88R RNase A through the Golgi.

Perturbing intracellular trafficking by using drugs or by the overproduction of K44A Dyn can have indirect consequences on cellular pathways and must be interpreted with caution. For example, cells overproducing a temperature-sensitive variant of dynamin (G273D) have a block in transferrin receptor recycling to the cell surface at the nonpermissive temperature (van Dam & Stoorvogel, 2002). Such a block could lead to the decrease of a protein or lipid receptor at the cell surface, which would result in a decrease of toxicity. The toxicity of G88R RNase A and ONC is enhanced when treated with BFA

(Figure 2.9) or when dynamin activity is blocked (Figure 2.7). Thus, their toxicity is not diminished by this indirect affect.

Ribonucleases are internalized in a dose-dependent manner (Figure 2.5), which is consistant with their dose-dependent cytotoxicity (Figures 2.7 and 2.9). We propose that as the extracellular concentration of a ribonuclease increases, so does its cytosolic concentration. The arrows in Figure 2.6 indicate the protein concentrations that correspond to IC_{50} values of 1 and >50 μM for ONC and G88R RNase A, respectively (Table 2.2). We were surprised to find that ONC and RNase A have a similar dose-dependent influx for HeLa cells, despite having IC_{50} values that differ by more than 50-fold (Figure 2.6; Table 2.2). What accounts for this discrepancy?

The results of the dose–response experiment imply that ONC and RNase A are equally capable of overcoming the energetic barriers associated with cell-surface binding and internalization. As mentioned, the mechanism for ribonuclease-mediated toxicity also includes translocation across the cell membrane to the cytosol. Once in the cytosol, uninhibited ribonucleolytic activity is required for toxicity. Our data suggests that either (or both) of these hurdles is responsible for the difference in the toxicity of ONC and G88R RNase A for HeLa cells. ONC (104 residues) is smaller than RNase A (124 residues), and could be more efficient at crossing a lipid bilayer. Much work has already demonstrated the importance of RI evasion for cytotoxicity of mammalian ribonucleases (Kim *et al.*, 1995c; Leland *et al.*, 1998; Suzuki *et al.*, 1999; Bretscher *et al.*, 2000; Antignani *et al.*, 2001).

Ribonucleases are internalized by a unique internalization pathway. Ribonucleases are internalized in a manner that is distinct from that of toxins characterized previously (Figure 2.10). Protein toxins characterized to date, that act within the cytosol, cross a phospholipid membrane from either endosomal or post-endosomal compartments (Figure 2.10) (Lord & Roberts, 1998). A toxin that translocates from an endosomal compartment is diphtheria toxin (Collier, 2001); and ricin is among the most characterized toxins that translocates from a post-endosomal compartment (Olsnes & Kozlov, 2001). Diphtheria and ricin-like toxins have evolved special mechanisms for entering and killing mammalian cells. Such toxins are almost universally comprised of distinct domains to provide catalytic activity and facilitate cytosolic entry. During toxin action, these domains physically dissociate. In a striking, structural difference, ribonucleases have a single, globular domain that is responsible for cell-surface binding, internalization, and catalytic activity.

The internalization pathways of ribonucleases and diphtheria toxin differ by their modes of uptake and translocation. The internalization of diphtheria toxin is contingent on clathrin-dependent endocytosis (Simpson *et al.*, 1998). Blocking this pathway by overproduction of a dominant negative variant of dynamin protects cells from diphtheria toxin action (Simpson *et al.*, 1998). In contrast, ribonucleases are *more* toxic in the absence of clathrin-dependent endocytosis (Figure 2.7). The translocation of diphtheria toxin is highly dependent on the low pH of the endosome; this acidic environment induces a conformational change in the B domain that forms a pore through the membrane and allows the A domain to cross (Draper & Simon, 1980; Sandvig & Olsnes, 1980; Sandvig & Olsnes, 1981; Sandvig & Olsnes, 1982). Agents such as NH_4Cl and monensin, which neutralize acidic environments within the

cell, block cytosolic entry and thereby protect cells from diphtheria toxin. These drugs do not protect cells from the toxicity of ribonucleases (Figure 2.9).

The internalization pathway of ribonucleases has similarities and differences with that of ricin (for reviews, see: Sandvig & van Deurs, 2000; Olsnes & Kozlov, 2001). Like many RNase A homologues, ricin is a lectin that binds to carbohydrates on the cell surface. ONC, RNase A, and ricin can be internalized and cytotoxic in the absence of clathrin-mediated endocytosis (Llorente *et al.*, 1998) (Figures 2.7 and 2.8). In addition, a low pH is not required for the cytotoxicity of ONC (Figure 2.9), G88R RNase A, or ricin. Unlike ribonucleases, ricin translocates to the cytosol from the ER after retrograde transport from the Golgi network. Cells with a BFA-disrupted Golgi stack are protected from ricin (Yoshida *et al.*, 1991), but not from ribonucleases (Figure 2.9). These data are consistent with the finding that BFA does not block the toxicity of ONC for 9L cells (Wu *et al.*, 1995). Transport of the ricin A chain from the Golgi to the ER was a prerequisite for translocation (Rapak *et al.*, 1997). Morover, introduction of a KDEL tail to the ricin A chain dramatically enhances its cytotoxicity (Wales *et al.*, 1993; Tagge *et al.*, 1996), but the presence of a KDEL tail on G88R RNase A does not increase its cytotoxicity (P.A. Leland and R.T. Raines, unpublished results). Hence, an increased ribonuclease concentration in the ER does not enhance its cytotoxicity. Combined, these results indicate that ONC and G88R RNase A do not enter the cytosol through the endoplasmic reticulum.

The study of toxin internalization has facilitated important discoveries in the field of intracellular transport (Lord & Roberts, 1998). Studies of Shiga toxin showed for the first time that the secretory pathway is completely reversible (Sandvig *et al.*, 1992). In addition,

Shiga toxin and ricin are models for dissecting retrograde transport and as well as the molecular details of endocytosis (Mallard *et al.*, 1998; Sandvig & van Deurs, 2000). Studies using cholera toxin binding and entry have clarified pathways of lipid trafficking (Orlandi & Fishman, 1998; Radhakrishnan *et al.*, 2000).

Our work has revealed aspects of the route by which a common protein—secretory ribonucleases—enters the cytosol (Figure 2.10). Ribonucleases can be a tool for studying how cationic secretory proteins re-enter cells, as well as for understanding clathrin- and dynamin-independent endocytosis. Although ribonucleases are secreted, every cell contains RI, suggesting a need to protect cells from ribonucleases that re-enter the cytosol. The prevalence of RI in many cell types suggests that ribonuclease internalization is a widespread occurrence.

Acknowledgements. We thank A.K. Menon, S.Y. Bednarek, T.F. Martin, J.A.T. Young, S. Narayan, A.D. Attie, and M.L. Nibert for contributive discussions. We thank K.M. Haigis, R.L. Abel, for helpful suggestions and critical reading of the manuscript. We thank J.F. Wilkins and K.A. Dickson for help in the purification of D16C ONC. We thank J. Kimble for use of the Zeiss Axiovert 100 TV microscope.

Table 2.1 Biophysical and biochemical properties of ribonucleases

Ribonuclease	T_m [a] (°C)	k_{cat}/K_M [b] (M^{-1} s^{-1})
RNase A	63	$4.3 \pm 0.3 \times 10^7$
fluorescein~RNase A	61	$0.54 \pm 0.02 \times 10^7$
ONC	90	$3.5 \pm 0.1 \times 10^2$
DTNB~ONC	88	$1.7 \pm 0.2 \times 10^2$

[a] Values of T_m (± 1 °C) were determined in PBS by UV spectroscopy.
[b] Values of k_{cat}/K_M (± S.E.) are for the catalysis of 6-FAM~dArU$(dA)_2$~6-TAMRA cleavage at (23 ± 2) °C in 0.10 M MES–NaOH buffer (pH 6.0) containing NaCl (0.10 M).

Table 2.2 IC_{50} values of toxic ribonucleases in HeLa cell lines

	IC_{50} (μM)	
Cells Tested	ONC	G88R RNase A
wild-type	1.5 ± 0.1	>50[a]
wild-type dynamin (uninduced)	1.4 ± 0.1	>50
wild-type dynamin (induced)	1.8 ± 0.2	>50
K44A Dyn (uninduced)	1.6 ± 0.1	>50
K44A Dyn (induced)	0.72 ± 0.05	17 ± 3

[a]A protein concentration of 50 μM resulted in <50% cell death.

Table 2.3 Effect of drugs on IC_{50} values of toxic ribonucleases in K-562 cells[a]

	IC_{50} (μM)	
Drug	ONC	G88R RNase A
None	0.89 ± 0.07	7.7 ± 0.9
NH_4Cl	1.2 ± 0.1	8.0 ± 0.8
Monensin	0.15 ± 0.02	8.0 ± 1.4
Brefeldin A	0.23 ± 0.03	0.66 ± 0.07

[a] Cells were preincubated with drug (NH_4Cl, 20 mM; monensin, 10 μM; brefeldin A, 5 μg/ml) for 2 h prior to the addition of ribonucleases.

Figure 2.1 Structural similarity between ribonuclease A and Onconase®. Ribbon diagrams of (A) RNase A and (B) ONC were created using the atomic coordinates derived by x-ray diffraction analysis (Wlodawer, 1985; Mosimann *et al.*, 1994) and the program MOLSCRIPT (Kraulis, 1991). Residues 19 (RNase A) and 16 (ONC), which were changed to a cysteine residue for labeling experiments, are indicated.

A

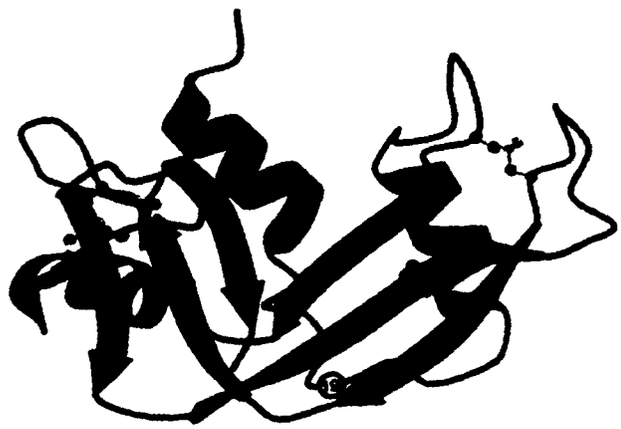

B

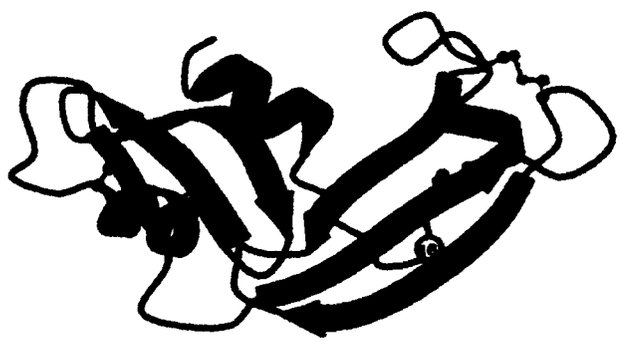

Figure 2.2 Binding to the surface of K-562 cells by Onconase®, ribonuclease A, and G88R ribonuclease A. Cells were incubated with a ribonuclease (1 μM) for 20 min at 4 °C. Cells were then washed, fixed, and processed for indirect immunofluorescence with antibodies generated against either RNase A or ONC. The appropriate FITC or TRITC-conjugated secondary antibody was used to visualize RNase A (green), G88R RNase A (green), and ONC (red) binding. Negative control samples were incubated in PBS in the absence of protein and processed as described above.

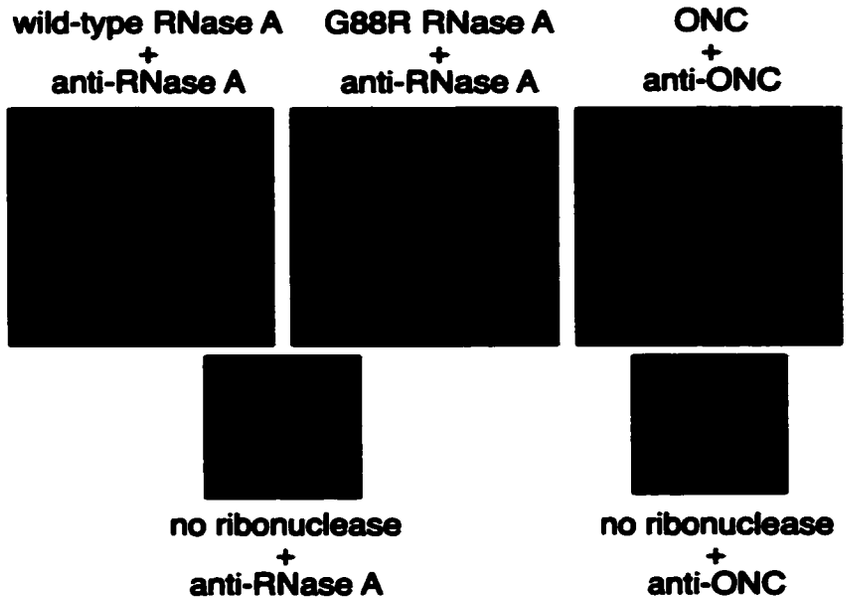
wild-type RNase A
+
anti-RNase A
G88R RNase A
+
anti-RNase A
ONC
+
anti-ONC
no ribonuclease
+
anti-RNase A
no ribonuclease
+
anti-ONC

Figure 2.3 Ribonuclease internalization in acidic vesicles. (A) The pH sensitivity of fluorescein~RNase A and BODIPY~RNase A was investigated by measuring the fluorescence intensity (counts/sec) of labeled protein at pH 8 versus pH 4.5 using a time-based assay. The fluorescence of labeled protein was measured first in 1 mM Tris-acetic acid buffer (pH 8.0). The pH of the solution was then lowered by the addition of 2 M sodium acetate buffer (pH 4.5). (B) K-562 cells were incubated with either fluorescein~RNase A (1 μM, green) or BODIPY~RNase A (1 μM, red) for 30 min at 4 °C. Cells were then washed, and the temperature was shifted to 37 °C for 5 min. Fluorescence was visualized immediately in living cells.
(C) Immunohistochemistry was performed to demonstrate the internalization of unlabeled RNase A. Cells were pulsed with RNase A as described above. After a temperature shift to 37 °C for 5 min, cells were fixed and internalized RNase A was detected by the appropriate primary and secondary antibody (green).

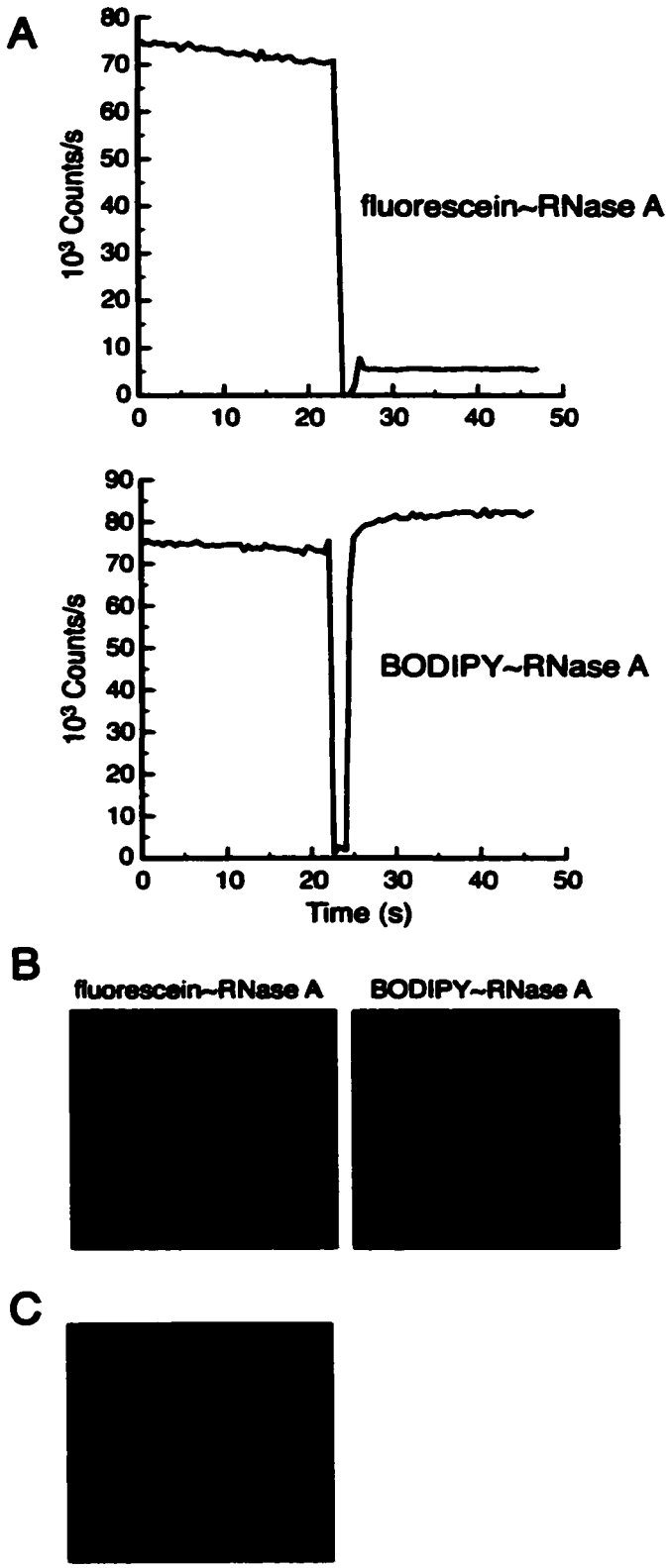
A
80
70
60
50
40
30
20
10
0
10^3 Counts/s
fluorescein~RNase A
0
10
20
30
40
50
90
80
70
60
50
40
30
20
10
0
10^3 Counts/s
BODIPY~RNase A
0
10
20
30
40
50
Time (s)
B
fluorescein~RNase A
BODIPY~RNase A
C

Figure 2.4 Co-internalization of OG~ONC and BODIPY~RNase A in K-562, JAR, and HeLa cells. Cells were pulsed with OG~ONC (green) and BODIPY~RNase A (red; 1 μM, 10% labeled). JAR and HeLa cells were grown on coverslips in the wells of a 6-well plate for 24 h before the assay. Cells were incubated with labeled protein for 20 min at 4 °C and the temperature was shifted to 37 °C. After a 10 min incubation at 37 °C, cells were washed three times with ice-cold PBS, fixed, and the fluorescence was visualized directly.

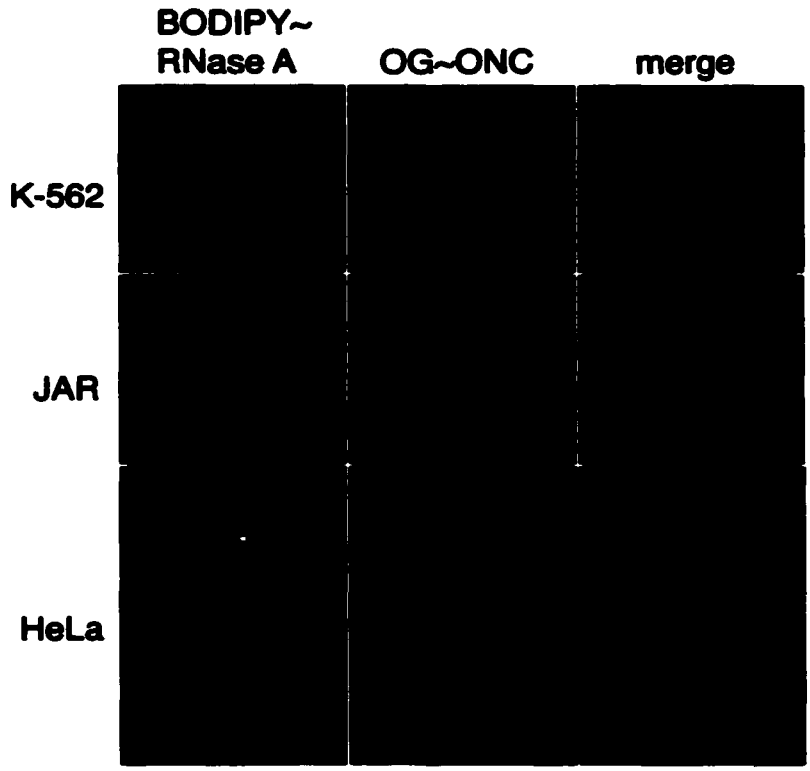
BODIPY~
RNase A
OG~ONC
merge
K-562
JAR
HeLa

Figure 2.5 Dose-dependent internalization of OG~ONC and OG~RNase A. HeLa cells were grown on coverslips in the wells of a 6-well plate. Cells were incubated with 30% labeled OG~ONC and OG~RNase A (0.01, 0.1, 1, or 10 μM protein), washed, and fixed as described for Figure 2.4.

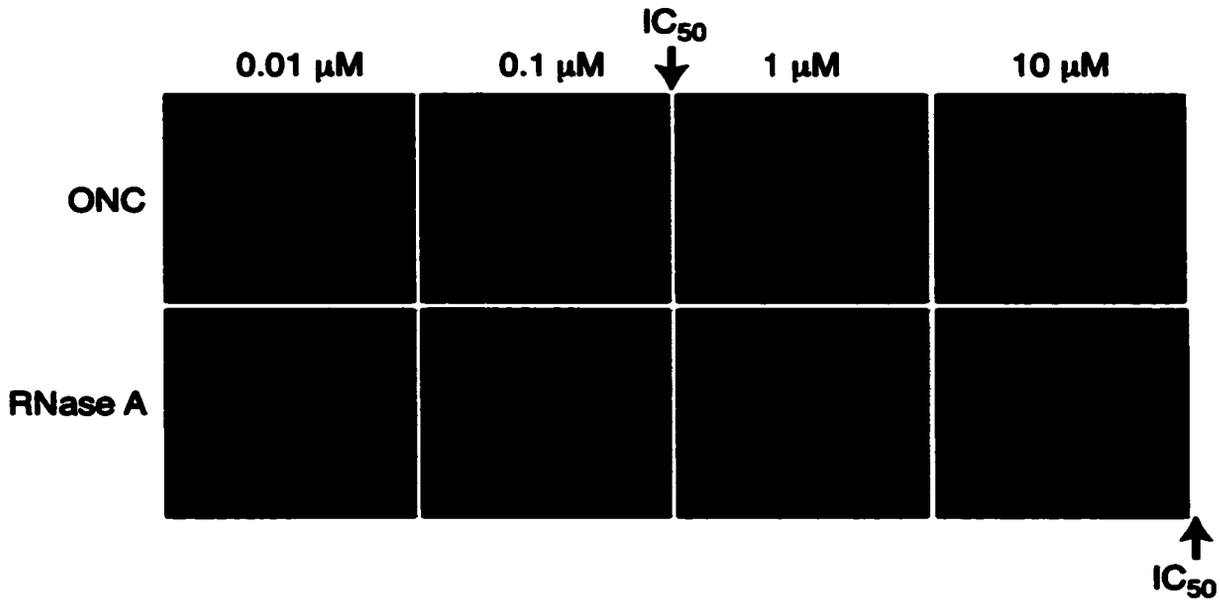
IC50
0.01 μM
0.1 μM
1 μM
10 μM
ONC
RNase A
IC50

Figure 2.6 Endocytosis in K-562 cells. K-562 cells were co-incubated with BODIPY~RNase A (1 μM) and either FM 1-43 (1 μg/ml) or BODIPY-FL-labeled transferrin (50 μg/ml) for 20 min at 4 °C. Cells were pulsed at 22 °C for 15 min, washed, fixed, and the fluorescence of BODIPY~RNase A (red), FM 1-43 (green), and BODIPY-FL-labeled transferrin (green) was visualized directly.

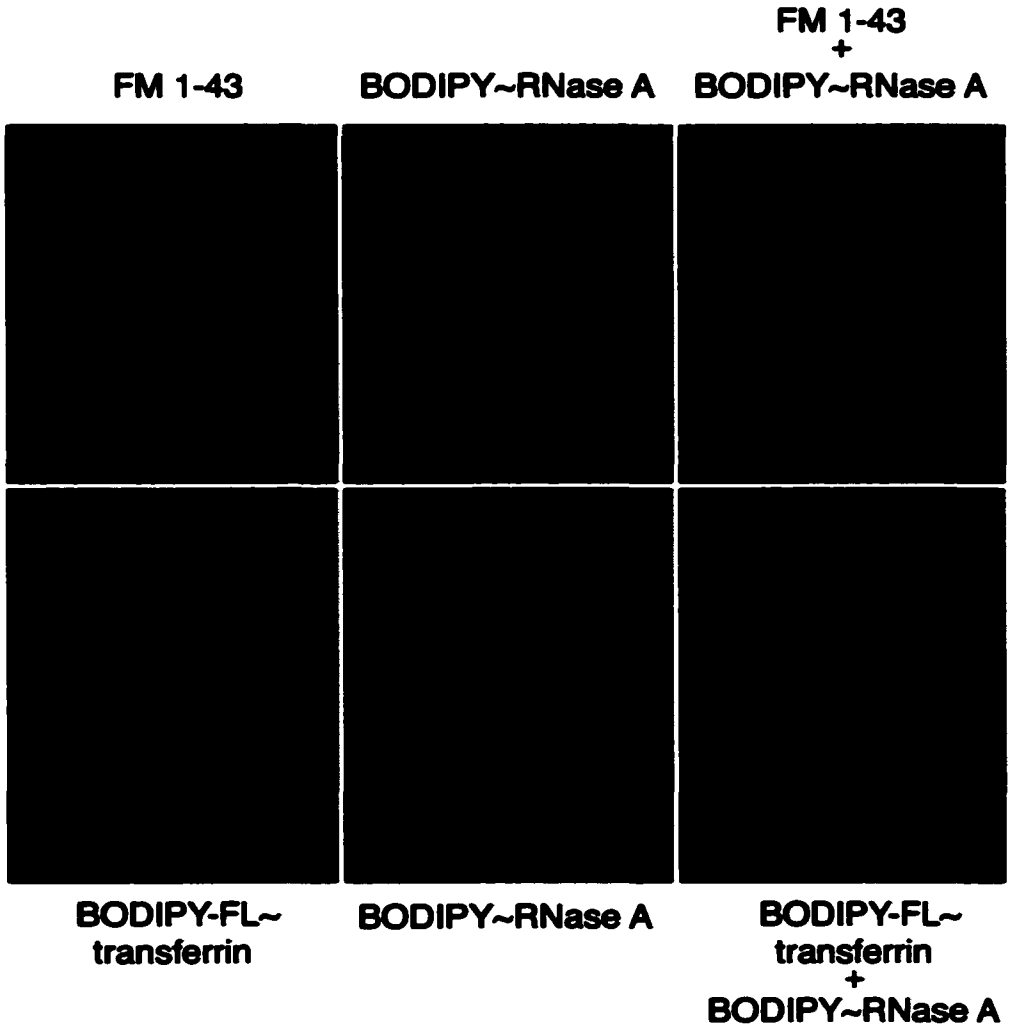
FM 1-43
BODIPY~RNase A
FM 1-43
+
BODIPY~RNase A
BODIPY-FL~
transferrin
BODIPY~RNase A
BODIPY-FL~
transferrin
+
BODIPY~RNase A

Figure 2.7 Role of dynamin in ribonuclease-mediated toxicity. (A) K44A Dyn cells were grown in the presence or absence of tetracycline for 2 days, and analyzed for morphological changes, as well as for protein production. K44A Dyn cells grown in the presence (induced) or absence (uninduced) of tetracycline were fixed and stained with TRITC-conjugated phalloidin to detect actin filaments (red). The production of wild-type dynamin and its K44A variant was monitored by immunoblotting using anti-HA antibodies. A representative immunoblot of uninduced and induced K44A Dyn cell extracts is shown. (C) The toxicity of G88R RNase A and ONC was measured in cells overproducing wild-type dynamin or K44A Dyn. To induce overproduction, cells were grown in the absence of tetracycline for 2 days. Then, increasing concentrations of G88R RNase A and ONC were added. After a 48-h incubation at 37 °C, DNA synthesis was measured as described in Materials and Methods. As a control, the effects of G88R RNase A and ONC were measured on cells not overproducing either form of dynamin. Each point represents the percent of [*methyl*-^{3}H]thymidine incorporated compared to a PBS control. Each point on the plot is the mean (± S.E.) of at least 3 separate experiments with triplicate samples.

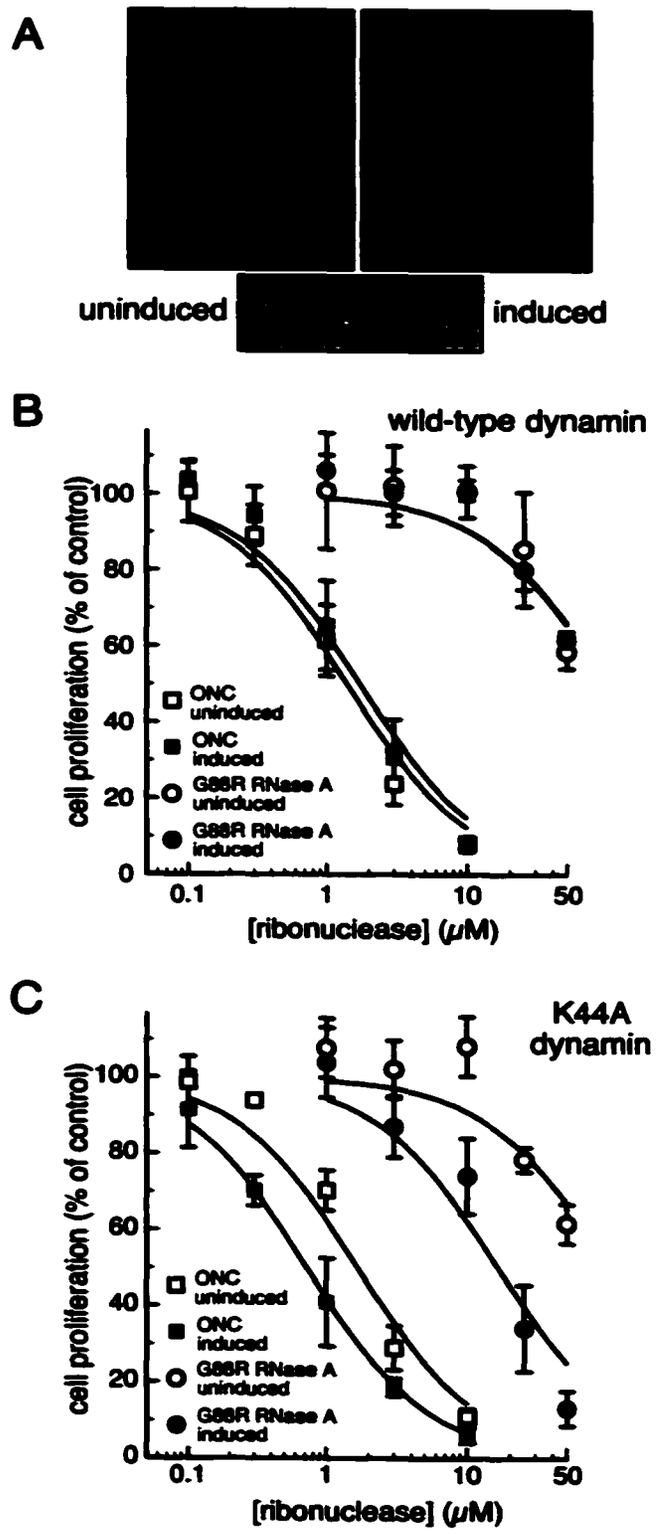
A
uninduced
induced
B
wild-type dynamin
cell proliferation (% of control)
100
80
60
40
20
0
ONC uninduced
ONC induced
G88R RNase A uninduced
G88R RNase A induced
0.1
1
10
50
[ribonuclease] (μM)
C
K44A dynamin
cell proliferation (% of control)
100
80
60
40
20
0
ONC uninduced
ONC induced
G88R RNase A uninduced
G88R RNase A induced
0.1
1
10
50
[ribonuclease] (μM)

Figure 2.8. Dynamin-independent internalization of ribonuclease A. (a) Induced and uninduced K44A Dyn cells were incubated with OG~RNase A (1 μM) and tetramethylrhodamine-labeled transferrin (50 μg/ml) for 20 min at 4 °C. Cells were pulsed at 22 °C for 15 min, washed, fixed, and the fluorescence of OG~RNase A (green) and tetramethylrhodamine-labeled transferrin (red) was visualized directly. (b) The data are expressed as the percentage of total uninduced (no fill) or induced (grey fill) cells that contained internalized OG~RNase A or tetramethylrhodamine-labeled transferrin. The data are the mean (± S.E.) of 2 separate experiments with n = 65 and 105 cells for uninduced and induced samples, respectively.

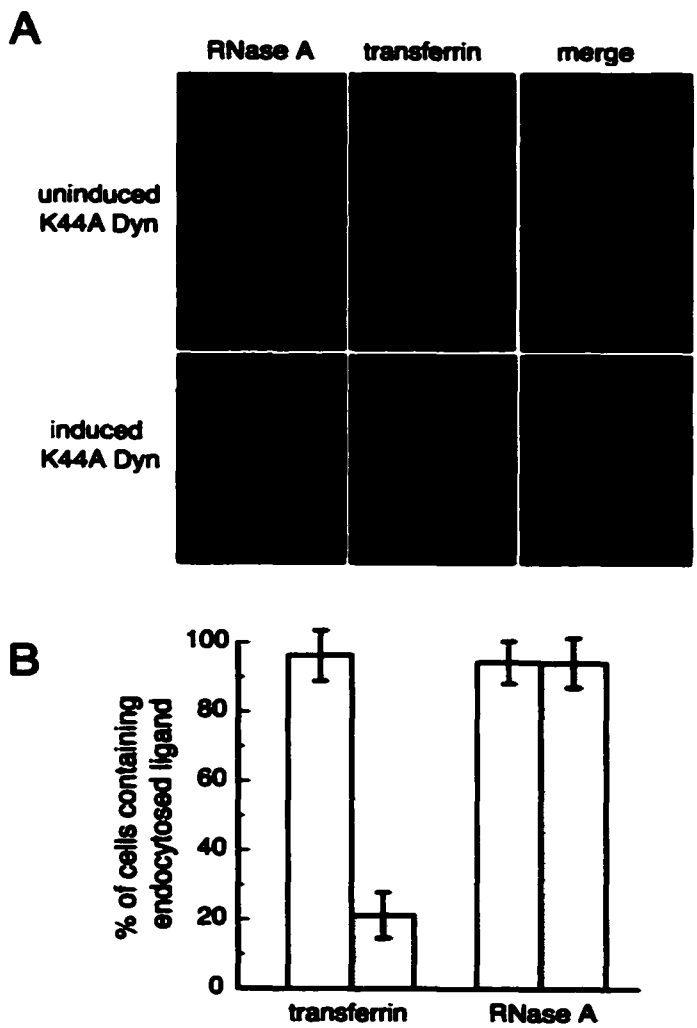
A
RNase A
transferrin
merge
uninduced
K44A Dyn
induced
K44A Dyn
B
% of cells containing
endocytosed ligand
100
80
60
40
20
0
transferrin
RNase A

Figure 2.9 Effect of drugs on the cytotoxicity of G88R ribonuclease A and Onconase®. The effect of G88R RNase A and ONC inhibition of cellular DNA synthesis was measured in the presence of NH_4Cl (20 mM), monensin (10 μM), and BFA (10 μg/ml). K-562 cells were pre-incubated with each drug for 2 h at 37 °C. Increasing concentrations of G88R RNase A (circles) and ONC (squares) were incubated with cells. Open symbols represent control samples without drug treatment, and filled symbols represent samples pre-incubated with drug. Each point represents the percent of [*methyl*-^{3}H]thymidine incorporated compared to a PBS control (with or without drug), and is the mean (± S.E.) of at least 3 separate experiments with triplicate samples.

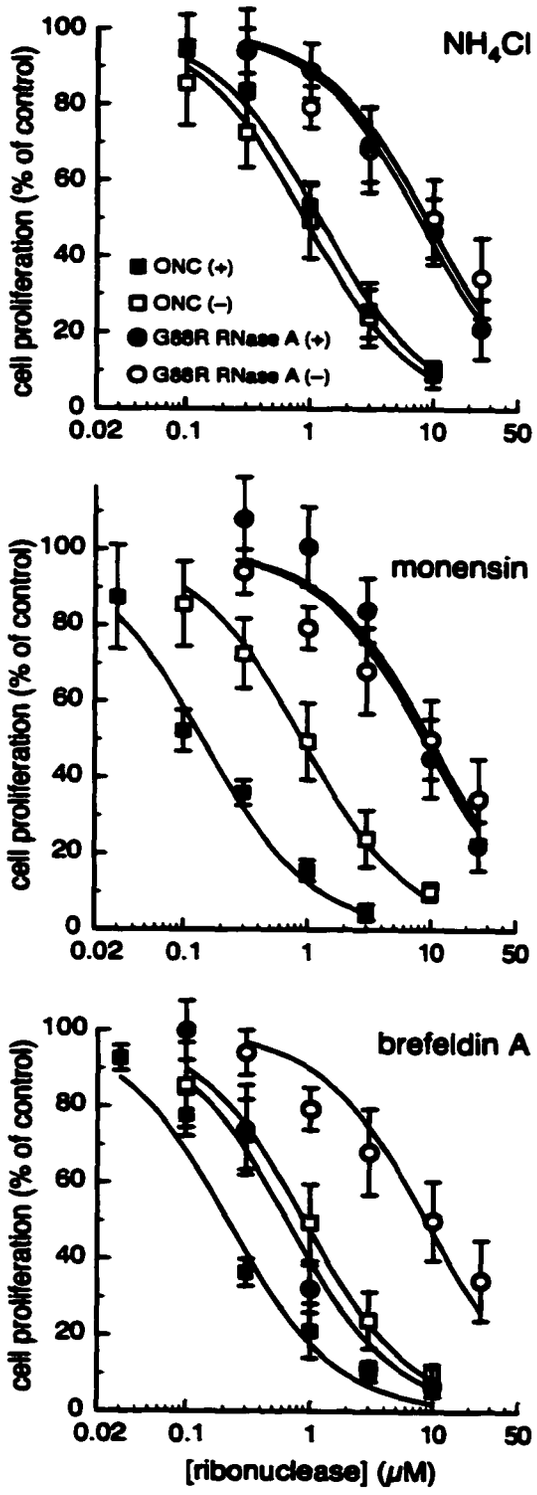
NH4Cl
monensin
brefeldin A
cell proliferation (% of control)
100
80
60
40
20
0
0.02
0.1
1
10
50
ONC (+)
ONC (−)
G88R RNase A (+)
G88R RNase A (−)
[ribonuclease] (μM)

Figure 2.10 Model for the internalization of cytotoxic ribonucleases. RNase A and ONC bind to the cell surface and are internalized by dynamin-independent endocytosis. Unlike diphtheria toxin, the low pH of acidic endosomes is not a prerequisite for the translocation of RNase A and ONC to the cytosol. The internalization pathways of RNase A and ONC are not identical. Unlike ricin, both ribonucleases reach the cytoplasm by translocation from a pre-endoplasmic reticulum (ER) environment.

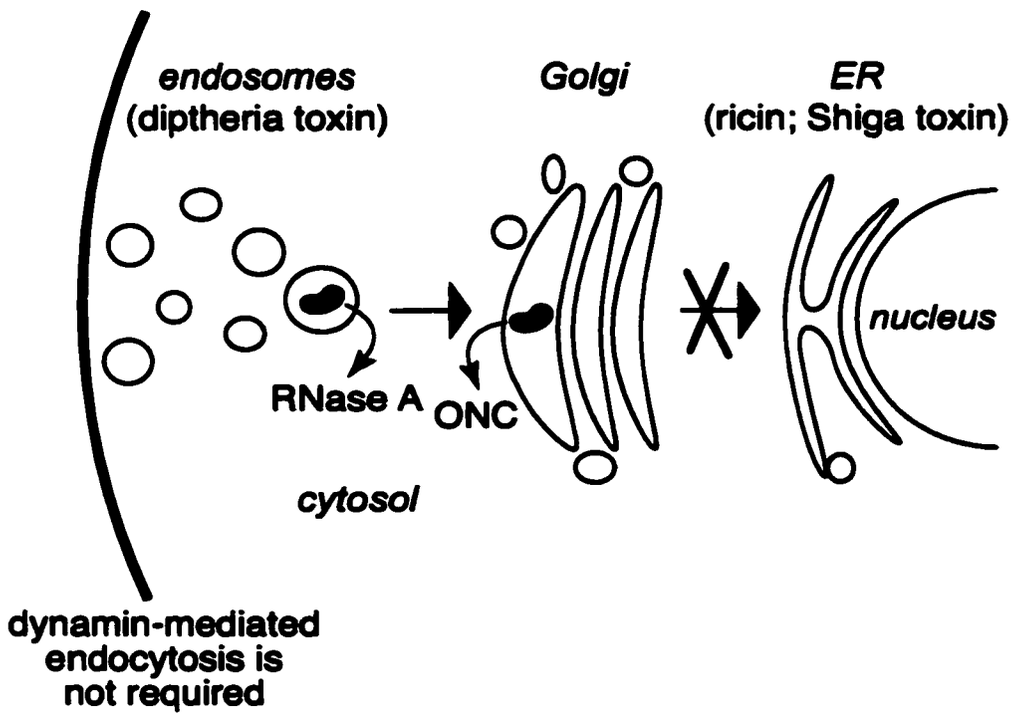
endosomes
(diptheria toxin)
Golgi
ER
(ricin; Shiga toxin)
nucleus
RNase A
ONC
cytosol
dynamin-mediated
endocytosis is
not required

Chapter 3

KFERQ Sequence in Ribonuclease A-Mediated Cytotoxicity

In press as: Marcia C. Haigis, Erin L. Kurten, and Ronald T. Raines (2002) KFERQ sequence in ribonuclease-mediated cytotoxicity. *Journal of Biological Chemistry.*

ABSTRACT

Onconase® (ONC) is an amphibian ribonuclease that is in clinical trials as a cancer chemotherapeutic. ONC is a homologue of ribonuclease A (RNase A). RNase A can be made toxic to cancer cells by replacing Gly88 with an arginine residue, and thereby enabling the enzyme to evade the endogenous cytosolic ribonuclease inhibitor protein (RI). Unlike ONC, RNases A contains a KFERQ sequence (residues 7–11), which signals for lysosomal degradation. Here, replacing Arg10 of the KFERQ sequence is shown to have no effect on either the cytotoxicity of G88R RNase A or its affinity for RI. In contrast, K7A/G88R RNase A is nearly 10-fold more cytotoxic than G88R RNase A, and has more than 10-fold less affinity for RI. Upregulation of the KFERQ-mediated lysosomal degradation pathway has no effect on the cytotoxicity of these ribonucleases. Thus, KFERQ-mediated degradation does not limit the cytotoxicity of RNase A variants. Moreover, substitution of only two amino acids (K7A and G88R) is sufficient to endow RNase A with cytotoxic activity that is nearly equal to that of ONC.

INTRODUCTION

Onconase® (ONC) is a homologue of ribonuclease A (RNase A) from the Northern leopard frog, *Rana pipiens* (Darzynkiewicz *et al.*, 1988; Ardelt *et al.*, 1991). ONC demonstrates both antitumor and antiviral activity, and is in Phase III clinical trials for the treatment of malignant mesothelioma (for reviews, see: Schein, 1997; Youle & D'Alessio, 1997; Irie *et al.*, 1998; Rybak & Newton, 1999; Leland & Raines, 2001; Matousek, 2001). The most damaging side effect from ONC treatment is renal toxicity, which is dosage dependent and reversible (Mikulski *et al.*, 1993; Mikulski *et al.*, 1995). Studies in mice have demonstrated that ONC is retained in the kidneys, in contrast to mammalian ribonucleases (Vasandani *et al.*, 1996). Hence, mammalian ribonucleases could provide a ribonuclease-based anticancer therapy without renal toxicity.

ONC and RNase A share 30% amino acid sequence identity and have similar tertiary structure (Ardelt *et al.*, 1991; Mosimann *et al.*, 1994), yet differ in catalytic activity and affinity for the cytosolic ribonuclease inhibitor protein (RI). RNase A demonstrates 10^4-fold more ribonucleolytic activity than does ONC (Ardelt *et al.*, 1991; Boix *et al.*, 1996). In cells, the high ribonucleolytic activity of RNase A is blocked by its high affinity for RI (Lee *et al.*, 1989; Vicentini *et al.*, 1990; Leland *et al.*, 1998) (Figure 3.1). ONC has low affinity for RI (Wu *et al.*, 1993; Boix *et al.*, 1996).

Several studies have focused on understanding the contribution of ribonucleolytic activity and affinity for RI to cytotoxicity. RNase A itself does not have marked antitumor activity, but variants of RNase A are toxic to cells. For example, substituting the glycine residue at

position 88 with arginine decreases the affinity for RI and endows RNase A with cytotoxic activity (Leland *et al.*, 1998). Replacing Lys41 with an arginine residue results in a decrease in catalytic activity that is compensated by a decrease in affinity for RI (Bretscher *et al.*, 2000a). K41R/G88R RNase A has enhanced toxicity to K-562 cells as compared to G88R RNase A.

Some endosomal pathways end in the lysosomal degradation of proteins. The KFERQ pentapeptide sequence targets cytosolic proteins for lysosomal degradation via an alternative pathway (for reviews, see: Dice, 1987; Dice, 1990; Cuervo & Dice, 1998). Dice and co-workers found that microinjected RNase A associates with lysosomes upon cellular fractionation (McElligott *et al.*, 1985b). Subsequent studies found that the KFERQ pentapeptide, which comprises residues 7–11 of RNase A, regulates lysosomal targeting upon serum removal (Dice *et al.*, 1986; Dice, 1988). The KFERQ sequence of RNase A is recognized by a cytosolic heat shock cognate (hsc) protein of 73 kDa (hsc73) (Agarraberes *et al.*, 1997). ONC does not contain a KFERQ sequence (Figure 3.2). The significance of KFERQ-targeted lysosomal decay in ribonuclease-mediated cytotoxicity is unknown. This sequence, along with RI could serve to protect cells against an invading ribonuclease.

Here, we determine the effect of the KFERQ sequence on G88R RNase A-mediated cytotoxicity. Replacing Lys7 of the KFERQ sequence with an alanine residue has little effect on the conformational stability or catalytic activity of G88R RNase A. K7A/G88R RNase A does, however, have a marked decrease in affinity for RI compared to G88R RNase A and is the most cytotoxic variant of RNase A reported to date. Using other RNase A variants with substitutions in the KFERQ sequence that do not disrupt RI binding, we find that targeted

lysosomal degradation via the KFERQ sequence does not modulate ribonuclease toxicity. Moreover, the toxicity of ribonucleases is not diminished in serum-deprived cells, which have enhanced KFERQ-mediated lysosomal degradation (McElligott *et al.*, 1985b).

MATERIALS AND METHODS

Materials. K-562 and HeLa cells were from the American Type Culture Collection (Manassas, VA). Cell culture medium and supplements were from Life Technologies (Gaithersburg, MD). ONC (Leland *et al.*, 1998) and porcine RI (Klink *et al.*, 2001) were prepared as described. Enzymes used for DNA manipulation were from Promega (Madison, WI) or New England Biolabs (Beverly, MA). [*methyl*-^{3}H]Thymidine was from PerkinElmer Life Sciences (Boston, MA). 6-Carboxyfluorescein~dArU(dA)$_2$~6-carboxytetramethylrhodamine (6-FAM~dArU(dA)$_2$~6-TAMRA) was from Integrated DNA Technologies (Coralville, IA). Yeast rRNA (16 S and 23 S) was from Roche Molecular Biochemicals (Mannheim, Germany). All other chemicals were of commercial reagent grade or better and were used without further purification.

Analytical instruments. Ultraviolet and visible absorption was measured with a Cary model 50 spectrophotometer from Varian (Sugar Land, TX). Fluorescence was measured with a QuantaMaster1 photon-counting spectrofluorometer from Photon Technology International (South Brunswick, NJ), using fluorescence-grade quartz or glass cuvettes (1.0-cm pathlength, 3.0-ml volume) from Starna Cells (Atascadero, CA). Radioactivity was

measured with a Beckman model LS 3801 liquid scintillation counter from Beckman Instruments (Fullerton, CA).

Production of ribonuclease A variants. Plasmids pBXR (delCardayré *et al.*, 1995) and pONC (Leland *et al.*, 1998) direct expression of wild-type RNase A and ONC in *Escherichia coli*. The K7A and R10A RNase A variants were created by using oligonucleotide-mediated site-directed mutagenesis (Kunkel *et al.*, 1987). The K7A/G88R and R10A/G88R substitutions within RNase A were created by ligating DNA fragments using the *Apa*I and *Mun*I restriction sites. The K7A/K41R/G88R RNase A variant was created by ligating the DNA fragments using the *Apa*I and *Cla*I restriction sites.

Protein purification. Wild-type RNase A and its variants were purified by using methods described previously (delCardayre *et al.*, 1995; Messmore *et al.*, 1995; Kothandaraman *et al.*, 1998a; Leland *et al.*, 1998), but with the following modifications. Refolding solutions for RNase A variants with the G88R substitution contained 0.50 M arginine, instead of 0.10 M NaCl. Protein concentrations were determined by UV spectroscopy using $\varepsilon = 0.72$ ml mg^{-1} cm^{-1} at 277.5 nm for RNase A (Sela *et al.*, 1957) and its variants and $\varepsilon = 0.87$ ml mg^{-1} cm^{-1} at 280 nm for ONC. All ribonucleases used in biological assays were dialyzed exhaustively versus phosphate-buffered saline (PBS), which contained (in 1.00 liter) KCl (0.20 g), KH_2PO_4 (0.20 g), NaCl (8.0 g), and Na_2HPO_4 (2.16 g).

Assay of conformational stability. The conformational stability of RNase A variants was determined by monitoring the absorbance at 287 nm (A_{287}) with increasing temperature (Eberhardt *et al.*, 1996). The temperature of solution of protein (0.3 mg/ml) in PBS was increased from 25 to 75 °C in 1-°C increments. The A_{287} was recorded after a 7-min

equilibration at each temperature. The value of T_m is the temperature at the midpoint of reversible thermal denaturation. Data were collected and analyzed with the program Thermal (Varian Analytical Instruments; Walnut Creek, CA).

Assay of catalytic activity. Ribonucleolytic activity was measured by using a fluorogenic substrate (Kelemen *et al.*, 1999). Assays were performed at 23 °C in 2.00 ml of 0.10 M MES–NaOH buffer (pH 6.0) containing NaCl (0.10 M). Solutions contained 6-FAM~dArU(dA)$_2$~6-TAMRA (50 nM) and enzyme (1.0–5.0 pM). Fluorescence was monitored by using 493 and 515 nm for the excitation and emission wavelengths, respectively. Kinetic parameters were determined by a linear least-squares regression analysis of the initial velocity using eq 1 (Kelemen *et al.*, 1999):

$$V / K = \frac{(\Delta F / \Delta t)}{F_{max} - F_0} \tag{1}$$

where V/K is the first-order rate constant, $\Delta F/\Delta t$ is the slope from the linear regression, F_{max} is the final fluorescence intensity after the reaction has reached completion, and F_0 is the initial fluorescence intensity before enzyme is added. The value of k_{cat}/K_M was calculated by dividing V/K by the enzyme concentration.

Fluorescence assay of ribonuclease inhibitor binding. The value of K_d for the complex between porcine RI and RNase A variants was determined by a competitive assay. It has been shown that the fluorescence of fluorescein-labeled A19C/G88R RNase A (fluorescein~G88R RNase A) decreases by approximately 15% upon binding to RI (Abel *et*

al., 2001). Thus, fluorescence spectroscopy can be used to evaluate the ability of an unlabeled ribonuclease to compete with fluorescein~G88R RNase A for binding to RI. Specifically, cuvettes of PBS containing fluorescein~G88R RNase A (50 nM), an unlabeled RNase A variant (1 nM–2 μM), and dithiothreitol (DTT; 1 mM) were incubated at room temperature (23 ± 2 °C). After 15 min, the initial fluorescence intensity was measured using 490 and 511 nm for the excitation and emission wavelengths, respectively. Next, RI was added with stirring (to 50 nM), and the average fluorescence intensity was measured after an additional incubation of 4 min. The maximum fluorescence decrease upon RI binding was measured with samples that lacked unlabeled ribonuclease. The concentration of the RI•fluorescein~G88R RNase A complex was determined by comparing the fluorescence of a sample with the fluorescence decrease observed when all of the fluorescein~G88R RNase A was bound by RI. The K_d value was determined as described (Abel *et al.*, 2001).

Gel assay of ribonuclease inhibitor binding. The effect of RI binding on catalytic activity was monitored directly, but qualitatively, by a gel-based assay as described previously (Leland *et al.*, 1998). Briefly, 0.6-ml siliconized microtubes of MES–NaOH buffer (pH 6.0) containing NaCl (0.10 M), DTT (1 mM), yeast rRNA (4 μg), and a ribonuclease (10 ng) were mixed with RI (0, 10, 20, or 40 units, where 1 unit is the amount required to inhibit the activity of 5 ng of RNase A by 50%). After a 15-min incubation at 37 °C, 10 mM Tris–HCl buffer (pH 7.5) containing EDTA (50 mM), glycerol (30% w/v), xylene cyanol FF (0.25% w/v), and bromophenol blue (0.25% w/v) was added. Samples were analyzed by electrophoresis through an agarose gel (1% w/v) containing ethidium bromide (0.4 μg/ml). Control samples were incubated in the absence of a ribonuclease or RI (or both).

Assay of cytotoxicity. The effect of RNase A, its variants, and ONC on cell proliferation was determined by measuring the incorporation of [*methyl*-^{3}H]thymidine into cellular DNA. K-562 cells were grown in RPMI 1640 medium. Unless indicated otherwise, all culture medium contained fetal bovine serum (FBS; 10% v/v), penicillin (100 units/ml), and streptomycin (100 μg/ml). Cells were cultured at 37 °C in a humidified incubator containing CO_2 (g; 5% v/v). All toxicity studies were performed using asynchronous log-phase cultures. For toxicity assays, cells (95 μl of a solution of 5×10^4 cells/μl) were incubated with a 5 μl solution of ribonuclease or PBS in the wells of a 96-well plate. Cells were incubated for 44 h at 37 °C in a humidified incubator containing CO_2 (g; 5% v/v). Next, the proliferation of cells was monitored with a 4-h pulse of [*methyl*-^{3}H]thymidine (0.4 μCi/well). Cells were harvested onto glass fiber filters using a PHD Cell Harvester (Cambridge Technology; Watertown, MA). Filters were washed with water, dried with MeOH, and their ^{3}H content was measured with liquid scintillation counting.

Serum-deprived cells have enhanced KFERQ-mediated lysosomal degradation of RNase A (McElligott *et al.*, 1985b). To discern the effect of RNase A, its variants, and ONC on the proliferation of cells with enhanced KFERQ-mediated degradation, K-562 cells were grown in RPMI medium without FBS for 18 h prior to the addition of a ribonuclease. Ribonuclease-mediated cytotoxicity was measured as described above.

Cytotoxicity data were analyzed with the programs SigmaPlot (SPSS Science; Chicago, IL) and DeltaGraph (DeltaPoint; Monterey, CA). Each data point represents the mean (± S.E.) of at least three experiments, each performed in triplicate. The IC_{50} value for each ribonuclease was calculated by using eq 2:

$$S = \left(\frac{IC_{50}}{IC_{50} + [\text{ribonuclease}]} \right) \times 100 \qquad (2)$$

where S is the percent of total DNA synthesis after the incubation period (48 h).

RESULTS

Design of ribonuclease A variants. RNase A variants were designed with the primary goal of discerning a role for the KFERQ sequence (residues 7–11) in cytotoxicity. Because RNase A itself is not cytotoxic, the cytotoxic G88R RNase A variant was used as a basis for this work. In addition, amino acid substitutions were combined with the secondary goal of producing variants that have high ribonucleolytic activity, low affinity for RI, and thus (presumably) high cytotoxicity.

Lys7 and Arg10. Lys7 and Arg10 comprise the enzymic P2 subsite, which interacts with a phosphoryl group of an RNA (Boix *et al.*, 1994; Nogués *et al.*, 1995; Fisher *et al.*, 1998). Cuchillo and co-workers found that replacing either Lys7 or Arg10 alone with a glutamine residue has only a minor effect on catalysis of RNA cleavage, but replacing both Lys7 and Arg10 decreases catalytic activity by 60-fold (Boix *et al.*, 1994). Likewise, replacing both Lys7 and Arg10 with alanine residues results in k_{cat}/K_M value that is 60-fold lower than that of wild-type RNase A (Fisher *et al.*, 1998).

The interaction between Lys7 of RNase A and porcine RI was investigated previously by using semisynthetic variants (Neumann & Hofsteenge, 1994). Hofsteenge and co-workers found that replacing Lys7 with an *S*-methyl cysteine residue resulted in a >50-fold decrease in affinity for RI. This result is consistent with the structure of the RI•RNase A complex in which the side-chain nitrogen of Lys7 donates a hydrogen bond to the C-terminal carboxyl group of RI (Figure 3.1) (Kobe & Deisenhofer, 1995b). Arg10 makes no contact with RI in this complex.

Accordingly, we replaced Lys7 and Arg10 of RNase A independently with an alanine residue. The resulting K7A and R10A variants are designed to disrupt the KFERQ sequence, without decreasing ribonucleolytic activity. By systematically incorporating these changes in a cytotoxic variant, G88R RNase A, we were able to investigate the contribution of Lys7 and Arg10 to cytotoxicity.

Phe8, Glu9, and Gln11. Phe8, Glu9, and Gln11, are important to the structure and function of RNase A. Replacing Gln11 with an alanine, glutamine, or histidine residue enables the enzyme to bind a substrate in a nonproductive manner (delCardayré & Raines, 1995). The contributions of Phe8 and Glu9 have been explored in RNase S (or RNase S′), which is a noncovalent complex of residues 1–20 (or 1–15) and 21–124. In this complex, replacing Phe8 (Scoffone *et al.*, 1967) or Glu9 (Dunn & Chaiken, 1975) with other residues decreases its conformational stability or catalytic activity (or both). Because these three residues of the KFERQ sequence play roles other than in lysosomal degradation, we left them intact.

Lys41. The side chain of Lys41 of RNase A donates a hydrogen bond to the transition state during RNA cleavage (Messmore *et al.*, 1995). Changing Lys41 to an arginine residue results in a 10^2-fold decrease in catalytic activity. Although K41R/G88R RNase A has low catalytic activity, it binds RI with less affinity than does G88R RNase A. Moreover, K41R/G88R RNase A is more cytotoxic than G88R RNase A (Bretscher *et al.*, 2000b). Hence, we used the K7A/K41R/G88R RNase A variant to explore the additivity of single substitutions that disrupt RI binding, as well as the relationship between catalytic activity, RI affinity, and cytotoxicity.

Conformational stability. The conformational stability of the RNase A variants was measured to ensure that the proteins were folded properly during all assays. Values of T_m for RNase A, its variants, and ONC are listed in Table 3.1. The T_m values of both wild-type RNase A and G88R RNase A in PBS were determined to be 63.0 °C; this value is similar to those reported previously (Leland *et al.*, 1998; Quirk *et al.*, 1998). K7A RNase A, K7A/G88R RNase A, R10A RNase A, and R10A/G88R RNase A were found to have T_m values of 63, 62, 60, and 62 °C, respectively. Both K41R RNase A and K7A/K41R/G88R RNase A were found to have a T_m value of 63.0 °C. Hence, all RNase A variants were essentially completely folded during assays at room temperature and at 37 °C. The T_m value of ONC in PBS was reported previously to be 90 °C (Leland *et al.*, 2000b).

Catalytic activity. The cytotoxicity of ribonucleases relies on their ribonucleolytic activity (Wu *et al.*, 1993; Kim *et al.*, 1995c; Bretscher *et al.*, 2000). Ribonucleolytic activity was measured using a fluorogenic substrate, 6-FAM~dArU$(dA)_2$~6-TAMRA, which exhibits a nearly 200-fold increase in fluorescence upon cleavage of the P–$O^{5'}$ bond on the 3′ side of the

single ribonucleotide-embedded residue (Kelemen *et al.*, 1999). Values of k_{cat}/K_M for RNase A, its variants, and ONC are listed in Table 3.1. The values of k_{cat}/K_M for RNase A and ONC were 4.3×10^7 and 3.5×10^2 $M^{-1}s^{-1}$, respectively, which is in good agreement with those reported previously (Kelemen *et al.*, 1999; Leland *et al.*, 2000b). The values of k_{cat}/K_M for K7A RNase A and R10A RNase A were 9.2×10^6 and 8.2×10^6 $M^{-1}s^{-1}$, respectively, which are lower by 4–5-fold than that of the wild-type enzyme. These values are not reduced by the G88R substitution; the k_{cat}/K_M values for K7A/G88R RNase A and R10A/G88R RNase A were 8.8×10^6 and 1.2×10^7 $M^{-1}s^{-1}$, respectively. As expected, the K41R variants have greatly diminished catalytic activity. The k_{cat}/K_M value of 4.1×10^5 $M^{-1}s^{-1}$ for K41R/G88R RNase A is in good agreement with the activity reported previously (Bretscher *et al.*, 2000b). The value of k_{cat}/K_M for K7A/K41R/G88R RNase A is 0.70×10^5 $M^{-1}s^{-1}$.

Ribonuclease inhibitor binding. RI is a modulator of ribonucleolytic activity. The values of K_d for the RI•RNase A, RI•G88R RNase A, and RI•fluorescein~G88R RNase A complexes were found previously to be 67 fM (Vicentini *et al.*, 1990), 0.57 nM (Abel *et al.*, 2001), and 0.55 nM (Abel *et al.*, 2001), respectively. Here, the K_d values for the complex between RI and other RNase A variants were measured by using a competition assay (Table 3.1). The K7A substitution disturbs the interaction of RI and RNase A, giving K_d values of 0.07 pM and 7.2 nM for K7A RNase A and K7A/G88R RNase A, respectively. In contrast, the R10A substitution has no significant effect on affinity for RI, as the value of K_d for the RI•R10A/G88R RNase A complex is indistinguishable from that of the RI•G88R RNase A complex. The K_d value for the RI•K41R/G88R RNase A complex is 2.9 nM, which is

comparable to the value of K_i = 3.0 nM reported previously (Bretscher *et al.*, 2000b). Addition of the K41R substitution to K7A/G88R RNase A decreases the affinity for RI by 5-fold, giving a K_d value of 47 nM for the triple variant. These K_d values were used to calculate the change in the free energy of interaction for RI and the RNase A variants. These values of $\Delta\Delta G$ are listed in Table 3.1.

An agarose gel-based assay was used to verify that affinity for RI correlates with inhibition of catalytic activity. In this assay, ribonucleases were incubated with increasing amounts of RI in the presence of yeast rRNA as substrate. The samples were subjected to electrophoresis through an agarose gel, and degraded RNA was observed by its faster mobility and less efficient staining compared to control samples without ribonuclease. K7A/G88R RNase A degrades yeast rRNA more thoroughly in the presence of RI than does either G88R RNase A or K7A RNase A (Figure 3.3).

Cytotoxicity assays. The toxicity of each ribonuclease was measured with the K-562 human leukemia cell line. The resulting IC_{50} values are listed in Table 3.1. ONC, G88R RNase A, and K41R/G88R RNase A had IC_{50} values similar to those reported previously (Leland *et al.*, 1998; Bretscher *et al.*, 2000b). Like wild-type RNase A, K7A RNase A and R10A RNase A were not cytotoxic, even at protein concentrations of 25 μM. The cytotoxicity of R10A/G88R RNase A did not differ from that of G88R RNase A. In contrast, the IC_{50} value of K7A/G88R RNase A was 7-fold lower than that of G88R RNase A (Figure 3.4A). The IC_{50} value of K7A/G88R RNase A was within 2-fold of that of ONC. Unexpectedly, the triple variant, K7A/K41R/G88R RNase A had an IC_{50} value

that was similar to that of G88R RNase A, and 2- and 12-fold greater than that of K41R/G88R RNase A and K7A/G88R RNase A, respectively.

To test further whether KFERQ-mediated degradation contributes to differences between the cytotoxicity of ONC and RNase A variants, assays were performed with serum-deprived K-562 cells. The IC_{50} values of ONC, K7A/G88R RNase A, and G88R RNase A did not change significantly in serum-deprived cells as compared to control cells cultured with FBS (Figure 3.4B, Table 3.2).

DISCUSSION

Secretory ribonucleases can be potent cytotoxins by virtue of their ability to enter the cytosol and catalyze the cleavage of cellular RNA (Schein, 1997; Youle & D'Alessio, 1997; Irie *et al.*, 1998; Rybak & Newton, 1999; Leland & Raines, 2001; Matousek, 2001). The ribonucleolytic activity within the cytosol is regulated by two factors: (1) the concentration of enzyme within the cytosol, and (2) how much of that enzyme is bound by RI. The cytosolic concentration of a ribonuclease is dependent on the balance between import and degradation. The ability of a ribonuclease to reach the cytosol is known to limit its toxicity. For example, even wild-type RNase A is toxic to cells when injected directly into the cytosol (Saxena *et al.*, 1991). ONC and variants of RNase A are more toxic to cells in the presence of drugs that alter intracellular trafficking (Wu *et al.*, 1995) (M.C. Haigis and R.T. Raines, unpublished results). The contribution of protein degradation in ribonuclease toxicity has been less studied, but its importance can be inferred. For example, ONC is more cytotoxic in

the presence of protease inhibitors (Mikulski *et al.*, 1998). In addition, the degradation of fluorescein-labeled RNase A in murine L cells can be blocked by preincubation with lysosomal protease inhibitors (Kothandaraman *et al.*, 1998b).

The sequence-specific, lysosome-targeted degradation of cytosolic proteins can also lower the cellular concentration of a protein. RNase A, unlike ONC contains a KFERQ sequence (Figure 3.2). This sequence is required for the targeted lysosomal degradation of cytosolic RNase A (McElligott *et al.*, 1985a; Dice *et al.*, 1986). The targeted degradation of RNase A or toxic RNase A variants would lead to a decrease in cytosolic ribonucleolytic activity, and a hence, a decrease in cytotoxicity. Dice and co-workers found that certain fragments of the RNase A KFERQ sequence (residues 1–10 and 2–8) are not degraded in a serum-dependent manner (Dice *et al.*, 1986). In addition, although the order of the KFER residues is unimportant (Dice, 1990), the biochemical nature of the side chains needs to be conserved. Thus, disrupting residues of the KFERQ sequence could enhance the cytotoxicity of an RNase A variant.

Arg10 of RNase A is located in the KFERQ sequence, but does not form any contact with RI. Hence, we used the R10A variant to isolate the consequence of lysosomal degradation from RI evasion. R10A RNase A is not toxic to cells. In addition, R10A/G88R RNase A has an IC_{50} value similar to that of G88R RNase A. We also investigated the toxicity of a G88R RNase A variant with Gln11 replaced by a histidine or alanine residue. The cytotoxicity of Q11H/G88R RNase A and Q11A/G88R RNase A does not differ from that of G88R RNase A (data not shown). Hence, disrupting the KFERQ sequence has no effect on ribonuclease-mediated cytotoxicity.

We measured the cytotoxicity of ribonucleases in cells with up-regulated lysosomal degradation. This experiment was based on the hypothesis that if KFERQ-mediated degradation limits the concentration of cytosolic ribonuclease, then enhancing this pathway would result in decreased toxicity. Cells cultured in the absence of serum show enhanced degradation of cytosolic RNase A (McElligott *et al.*, 1985b). The data demonstrate that toxic variants of RNase A do not have lowered potency in serum-deprived cells (Figure 3.4B, Table 3.2). These results indicate that the KFERQ-mediated degradation of cytosolic ribonucleases does not limit their potency.

RI binds to members of the RNase A superfamily in a 1:1 stoichiometry (Blackburn *et al.*, 1977). The interaction between RNase A and porcine RI buries 2550 $Å^2$ of protein surface and forms one of the tightest noncovalent complexes known, with K_d values near the fM range (Lee *et al.*, 1989; Lee & Vallee, 1989; Kobe & Deisenhofer, 1995b). Upon binding to RI, the activity of RNase A is abolished completely.

We have shown that Lys7 of RNase A is an important residue in the RI–RNase A interaction. In the crystalline structure of the RI•RNase A complex, Lys7 is proximal to Ser456 of porcine RI (Figure 3.1B) (Kobe & Deisenhofer, 1995b), which corresponds to Ser460 of human RI. The distance between the side chain nitrogen of Lys7 and the side-chain oxygen of Ser456 is 3.1 Å. The side-chain nitrogen is 3.5 Å and 4.1 Å away from the two oxygens of the C-terminal carboxyl group of RI. Replacing Lys7 with an alanine residue removes the hydrogen bonds and favorable Coulombic interactions with Ser456 of RI. The value of K_d for the RI•K7A RNase A complex is 69 pM (Table 3.1). The cooresponding

value of K_d for the double variant, K7A/G88R RNase A is 7.2 nM. Moreover, K7A/G88R RNase A is endowed with enhanced cytotoxicity.

Surprisingly, we find that the interactions of Lys7, Lys41, and Gly88 with RI are not additive. Single substitutions at Lys7 or Gly88 result in decreases of binding free energy of 4.1 and 5.3 kcal/mol, respectively (Table 3.1). The double variants, K7A/G88R RNase A and K41R/G88R RNase A have lost 6.9 and 6.3 kcal/mol of binding free energy, respectively. Yet, the triple variant, K7A/K41R/G88R RNase A, has only lost 8.0 kcal/mol of binding free energy. If the interactions had been additive, then the effect of single substitutions would contribute fully to the loss of binding free energy. Such conservation in binding free energy loss would suggest rigidity between the interface of the complex. For example, the effect of single substitutions at Lys1 and Lys7 of RNase A on RI binding is indeed additive, suggesting that changing Lys1 does not effect RI binding interactions at Lys7 (Neumann & Hofsteenge, 1994). In contrast, our data show that the interface between RI and RNase A is not rigid. Rather, compensatory changes upon perturbation of key contacts. A similar conclusion was reached by Shapiro and co-workers, who measured the affinity of RI variants for wild-type RNase A (Shapiro *et al.*, 2000). Thus, the dynamic nature of this interface must be addressed when engineering new ribonuclease variants to evade RI.

In conclusion, we have shown that the KFERQ sequence does not contribute to a decrease in ribonuclease-mediated cytotoxicity. We find that Lys7 of RNase A contributes to a key interaction that tethers the N-terminus of RNase A with the C-terminus of RI. The K7A/G88R RNase A variant has $>10^5$-fold lower affinity for RI than does wild-type RNase A. The ribonucleolytic activity of K7A/G88R RNase A is, however, within 10-fold of

that of the wild-type enzyme. Together, its high ribonucleolytic activity and low affinity for RI make K7A/G88R RNase A the most cytotoxic known variant of RNase A, with an IC_{50} value within two-fold of that of ONC. Finally, we find that the RI–RNase A interface is dynamic—disrupting one contact can alter others.

Acknowledgements. We thank K.J. Woycechowsky, K.A. Dickson, and Dr. B.G. Miller for contributive discussions.

Table 3.1 Attributes of ribonuclease A, its variants, and Onconase®

Ribonuclease	T_m[a]	IC_{50}[b]	k_{cat}/K_M[c]	K_d[d]	$\Delta\Delta G$[e]
	°C	μM	(10^6 $M^{-1}s^{-1}$)	nM	kcal/mol
RNase A	63	>25	43 ± 0.3	67 × 10^{-6}	0.0
G88R RNase A	63	7.3 ± 0.4	15 ± 3	0.54 ± 0.07	5.3
K7A RNase A	63	>25	9.2 ± 1.6	0.07 ± 0.01	4.1
K7A/G88R RNase A	62	1.0 ± 0.1	8.8 ± 2.6	7.2 ± 0.4	6.8
R10A RNase A	60	>25	8.2 ± 0.8	ND[f]	ND[f]
R10A/G88R RNase A	62	6.9 ± 0.8	12 ± 1	0.56 ± 0.07	5.3
K41R/G88R RNase A	63	3.9 ± 0.4	0.41 ± 0.05	2.9 ± 0.4	6.3
K7A/K41R/G88R RNase A	63	12.3 ± 1.9	0.07 ± 0.01	47 ± 4	7.9
ONC	90	0.54 ± 0.04	0.00035 ± 0.00001	≥10^3	≥9.7

[a] Values of T_m (± 1 °C) were determined in PBS by UV spectroscopy. The T_m value of ONC is from Ref. (Leland *et al.*, 2000a) and was determined by CD spectroscopy.

[b] Values of IC_{50} are for incorporation of [*methyl*-^{3}H]thymidine into the DNA of K-562 cells.

[c] Values of k_{cat}/K_M (± S.E.) are for the catalysis of 6-FAM~dArU$(dA)_2$~6-TAMRA cleavage at 25 °C in 0.10 M MES–NaOH buffer (pH 6.0) containing NaCl (0.10 M).

[d] Values of K_d were determined at (23 ± 2) °C in PBS. The K_d value for RNase A is from Ref. (Vicentini *et al.*, 1990). The K_d value for ONC is an estimate from Ref. (Boix *et al.*, 1996).

[e] Values of $\Delta\Delta G$ were calculated with the equation: $\Delta\Delta G = -RT\ln(K_d^{\text{RNase A}}/K_d)$.

[f] ND, not determined.

Table 3.2 Toxicity of ribonuclease A, its variants, and Onconase® for serum-deprived cells

Ribonuclease	IC_{50}[a]
	μM
RNase A	>25
G88R RNase A	5.0 ± 0.4
K7A/G88R RNase A	0.62 ± 0.04
ONC	0.48 ± 0.03

[a] Values of IC_{50} are for incorporation of [*methyl*-^{3}H]thymidine into the DNA of K-562 cells grown in the absence of fetal bovine serum for 18 h prior to the addition of a ribonuclease.

Figure 3.1 Molecular interactions between porcine ribonuclease inhibitor and ribonuclease A. This figure was created by using atomic coordinates derived by x-ray diffraction analysis (Kobe & Deisenhofer, 1995b) and the program MOLSCRIPT (Kraulis, 1991). (A) Crystalline structure of the RI•RNase A complex. (B) Close-up of the interaction between Lys7 (RNase A) and Ser456 (RI).

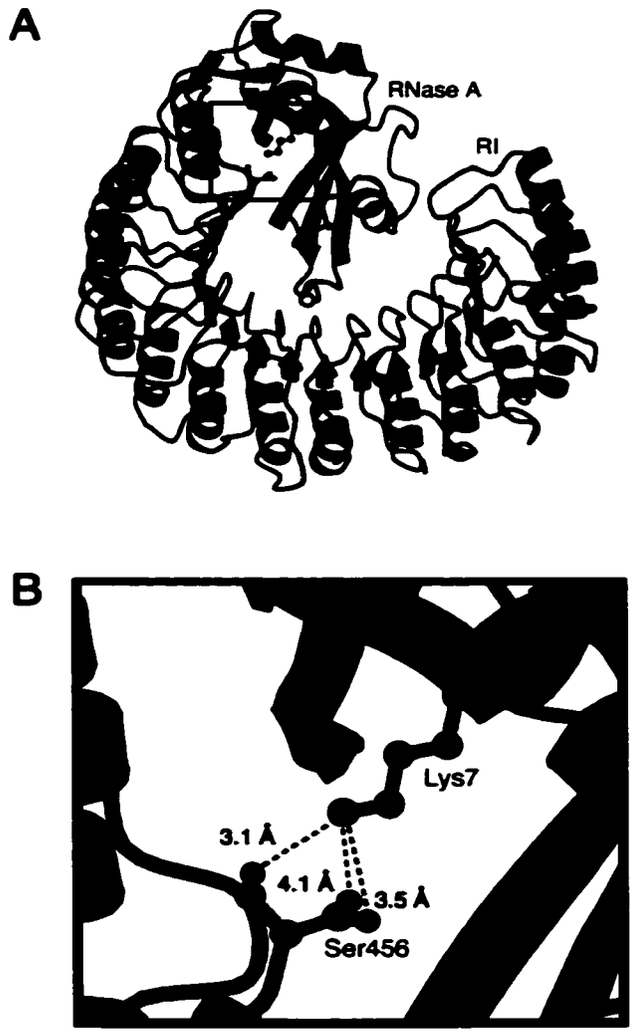
A
RNase A
RI
B
Lys7
3.1 Å
4.1 Å
3.5 Å
Ser456

Figure 3.2 Amino acid sequence of residues 1–20 of ribonuclease A and the corresponding residues of Onconase®.

```
                    7   10
RNase A   K E T A A A K F E R Q H M D S S T S A A
Onconase® - Q D W L T - F Q K K H I T N T R D V D
```

Figure 3.3 Agarose gel-based assay for inhibition of ribonucleolytic activity by porcine ribonuclease inhibitor. Inhibition was assessed by visualizing the cleavage of rRNA by 10 ng of a ribonuclease in the absence or presence of RI (10, 20, or 40 units).

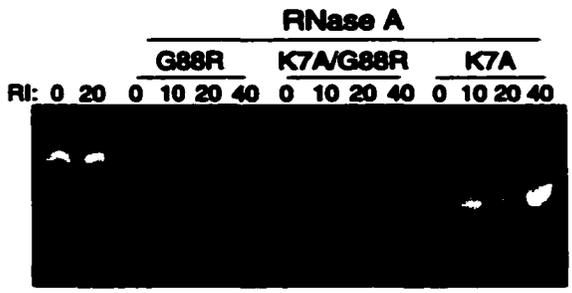
RNase A
G88R
K7A/G88R
K7A
RI: 0 20 0 10 20 40 0 10 20 40 0 10 20 40

Figure 3.4 Effect of ribonucleases on the proliferation of K-562 cells. Cell proliferation was measured by the incorporation of [*methyl*-^{3}H]thymidine into cellular DNA after a 48-h incubation at 37 °C with a ribonuclease. Each value is the mean (± S.E.) of at least 3 independent experiments with triplicate samples and is expressed as a percentage of the PBS control. (A) Assays in the presence of fetal bovine serum (10% v/v). (B) Assays on cells deprived of fetal bovine serum for 18 h prior to the addition of a ribonuclease.

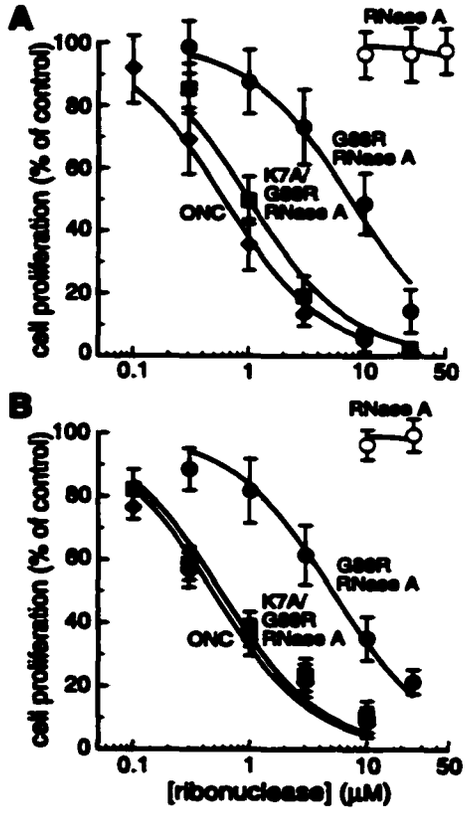
A
B
RNase A
G88R RNase A
K7A/ G88R RNase A
ONC
cell proliferation (% of control)
100
80
60
40
20
0
0.1
1
10
50
[ribonuclease] (μM)

Chapter 4

Ribonuclease Inhibitor is an Intracellular Sentry

Submitted as: Marcia C. Haigis, Erin L. Kurten, and Ronald T. Raines (2002) Ribonuclease inhibitor is an intracellular sentry.

ABSTRACT

Onconase® (ONC) is a homologue of ribonuclease A (RNase A) that is in clinical trials as a cancer chemotherapeutic. The toxicity of such secretory ribonucleases relies on their ability to degrade cellular RNA. Here, we reveal a biological role for the cytosolic ribonuclease inhibitor protein (RI), which binds tightly to wild-type RNase A, but not to ONC. Although wild-type RNase A was not toxic to nine human cell lines of a cancerous or normal origin, the toxicity of both ONC and G88R RNase A (which evades RI) correlates with the growth rate of cells. The endogenous level of RI varies by less than two-fold between these cell lines. Overproduction of RI diminishes the potency of toxic RNase A variants, but has no effect on the cytotoxicity of ONC. Thus, RI can act as an intracellular sentry that constrains the toxicity of RNase A. These insights on the molecular basis of ribonuclease-mediated cell death could aid in achieving an optimal ribonuclease-based cancer therapy.

INTRODUCTION

For most of the last century, bovine pancreatic ribonuclease (RNase A) was an important model for the study of protein chemistry, protein folding and stability, and enzymatic catalysis (Raines, 1998). Recent work on the RNase A superfamily has focused instead on exploring the biological functions and medical applications of ribonucleases (for reviews, see: D'Alessio, 1993; Schein, 1997; Raines, 1999; Rybak & Newton, 1999; Leland & Raines, 2001; Matousek, 2001). In 1973, bovine seminal ribonuclease (BS-RNase), a homologue of RNase A, was shown to reduce transplanted Crocker tumors in mice (Matousek, 1973). The toxicity of BS-RNase is not limited to tumor cells *in vivo*; it is also toxic to embryonic cells (Matousek, 1975), testicular tissue (Dostál & Matousek, 1972; Matousek, 1994), and oocytes (Slavik *et al.*, 2000). Onconase® (ONC) (Darzynkiewicz *et al.*, 1988), an RNase A homologue found in *Rana pipiens*, has anticancer and antiviral activity (Youle & D'Alessio, 1997). ONC is also toxic to noncancerous cells, and high concentrations lead to renal toxicity in mice. ONC is now in Phase III clinical trials for the treatment of malignant mesothelioma (Juan *et al.*, 1998).

Nearly 50 years ago, RNase A itself was shown to be cytotoxic, but only at extremely high levels (Ledoux, 1955a; Ledoux, 1955b). Recently, variants of RNase A have been shown to be cytotoxic at low concentrations. For example, G88R RNase A, which is a monomeric variant with Gly88 replaced with an arginine residue, is toxic to human leukemia cells (Leland *et al.*, 1998). Replacing Lys7 with an alanine residue in G88R RNase A

(K7A/G88R RNase A) creates an even more potent toxin (Haigis *et al.*, 2002b). The tumor cell specificity for toxic variants of RNase A has not been demonstrated previously.

The molecular basis for cell susceptibility to toxic ribonucleases is poorly understood. The proposed mechanism of ribonuclease-mediated cytotoxicity involves cell-surface binding and internalization, translocation to the cytosol, evasion of the cytosolic ribonuclease inhibitor protein (RI), and degradation of cellular RNA. Differences in the efficiency of any of these steps could enhance or decrease the amount of active ribonuclease within the cytosol and, hence, alter cell susceptibility.

One modulator of intracellular ribonucleolytic activity is RI (for a review, see: Hofsteenge, 1997). Every mammalian cell studied produces RI. RI is a cytosolic, horseshoe-shaped protein (Kobe & Deisenhofer, 1993) that binds to RNase A and other members of the RNase A superfamily. The binding of ribonucleases to RI results in the complete loss of ribonucleolytic activity. The crystalline structure of porcine RI complexed with RNase A reveals that extensive contacts are made with the active site of RNase A (Kobe & Deisenhofer, 1995b). RI interacts with RNase A with extremely high affinity [K_d of 10^{-13} M (Lee *et al.*, 1989; Vicentini *et al.*, 1990)]. The affinity of RI for ONC has been estimated at $\geq 10^{-6}$ M (Boix *et al.*, 1996). The G88R RNase A and K7A/G88R RNase A variants have an intermediate affinity for RI, with K_i values of 0.4 and 7×10^{-9} M, respectively (Leland *et al.*, 1998; Haigis *et al.*, 2002b). Ribonucleolytic activity in the cytosol is required for cytotoxicity (Bretscher *et al.*, 2000), and the affinity for RI appears to correlate with the toxicity of RNase A and variants (Leland *et al.*, 1998; Bretscher *et al.*, 2000; Haigis *et al.*, 2002b). Nonetheless, the importance of intracellular RI concentration to cell vulnerability is not

known, as both low and high levels of RI in tumor cells have been previously reported (Lee & Vallee, 1993).

Here, we investigate the role of RI in cell susceptibility. We have measured the toxicity of ONC, G88R RNase A, and RNase A for a broad spectrum of human cell lines. Human cell lines derived from normal tissue along with those derived from a cancerous origin are used to compare the potential therapeutic efficacy of both ONC and G88R RNase A. In addition, we probe characteristics of these cells that could contribute to their susceptibility toward toxic ribonucleases. We find that although RI is present in all tested cell lines, RI levels do not vary significantly. The overproduction of RI makes cells resistant to toxic RNase A variants, but not ONC, revealing an important constraint on the toxicity of RNase A and direct evidence that RI acts as an intracellular sentry.

MATERIALS AND METHODS

Construction of pECFP–RI. A plasmid containing human RI cDNA was the generous gift of Promega (Madison, WI). The RI cDNA was amplified by PCR with the oligonucleotides RI-2b (5′ CGACTGCAGAATTCTCAGGAGATGACCCTCAGG 3′) and RI-1f (5′ ACGAGCTGTACAAGGGCGGAGGCATGAGCCTGGACATCCAGAGCC 3′). The PCR fragment was ligated into pCR®-TOPO® (Invitrogen; Carlsbad, CA). The RI cDNA fragment was digested at the underlined sites with *Eco*RI and *Bsr*GI, and the resulting fragment was inserted into the pECFP-C1 expression vector (Clontech; Palo Alto, CA) that

had been digested with the same enzymes. The resulting plasmid, pECFP–RI, directs the overexpression of RI in human cells.

Production of ribonucleases. Wild-type RNase A, G88R RNase A, K7A/G88R RNase A, and ONC were produced by using methods described previously (delCardayré *et al.*, 1995; Leland *et al.*, 1998; Haigis *et al.*, 2002b). Protein concentrations were determined by UV spectroscopy using $\varepsilon = 0.72$ ml mg^{-1} cm^{-1} at 277.5 nm for RNase A (Sela *et al.*, 1957) and its variants and $\varepsilon = 0.87$ ml mg^{-1} cm^{-1} at 280 nm for ONC (Pace *et al.*, 1995). For cytotoxicity assays, ribonucleases were dialyzed versus phosphate-buffered saline (PBS), which contained (in 1.00 liter) KCl (0.20 g), KH_2PO_4 (0.20 g), NaCl (8.0 g), and Na_2HPO_4 (2.16 g).

Cell lines. K-562, JAR, HeLa, WI-38, IMR-90, SK-HEP-1, and 293 cells were obtained from the American Type Culture Collection (Manassas, VA). HL-60 and Jurkat cells were kindly provided by L.L. Kiessling (Madison, WI). K-562, JAR, and Jurkat cells were grown in RPMI medium 1640. HeLa, HL-60, and 293 cells were grown in DMEM. WI-38, IMR-90, and SK-HEP-1 cells were grown in MEM with Earle's salts, L-glutamine (2 mM), non-essential amino acids (0.1 mM), and sodium pyruvate (1 mM). All culture medium contained fetal bovine serum (FBS; 10% v/v), penicillin (100 units/ml), and streptomycin (100 μg/ml). Cell culture medium and supplements were from Life Technologies (Gaithersburg, MD). Cells were cultured at 37 °C in a humidified incubator containing 5% CO_2 (g). All studies were performed using asynchronous log-phase cultures.

Transfection of human cells. 24-h before transfections, HeLa cells (3×10^6) were plated in 10-cm dishes, and K-562 cells were split (0.5×10^4 cells/ml) with fresh medium. 5–6-h before transfections, the culture medium was refreshed. HeLa cells (10×10^6) were treated

with trypsin, and collected by centrifugation at 150 × *g*. Cell pellets were resuspended in PBS (0.8 ml) and incubated with pECFP or pECFP–RI (20 μg) in a 4.0-mm electroporation cuvette for 10 min at 25 °C. K-562 cells were collected and incubated with DNA as described for HeLa cells. Cells were transfected by electroporation with a Gene Pulser (Bio-Rad; Hercules, CA) at 320 and 230 V for HeLa and K-562 cells, respectively.

ECFP and ECFP–RI production was visualized directly in living cells 24 h after transfection. HeLa cells were grown on coverslips in the wells of a 6-well plate. ECFP fluorescence was visualized by using a Zeiss Axiovert microscope with 433 and 475 nm for the excitation and emission wavelengths, respectively.

Flow cytometry and sorting. Flow cytometry and fluorescence-activated cell sorting (FACS) were performed with a FACSVantage SE (Becton Dickinson; San Jose, CA). Cells were sorted 24 h after transfection, on the basis of their ECFP fluorescence, with 413 and 470 nm as the excitation and emission wavelengths, respectively. Wild-type HeLa and K-562 cells were used to establish the background fluorescence. Only single cells were collected.

Cytotoxicity assays for transformed cell lines. The effect of ONC, RNase A, and G88R RNase A on cell proliferation was determined by measuring the incorporation of [*methyl*-^{3}H]thymidine into newly synthesized DNA. Briefly, cells (95 μl of a solution of 5×10^4 cells/ml) were added to the wells of 96-well plates. Next, a solution (5 μl) of ONC, RNase A, G88R RNase A, or PBS was added in triplicate. Cells were incubated for 44 h at 37 °C, pulsed by the addition of [*methyl*-^{3}H]thymidine (0.20 μCi per well), and then incubated for an additional 4 h at 37 °C. Cells were harvested onto glass fiber filters using a PHD Cell Harvester (Cambridge Technology; Watertown, MA). Filters were washed with

several volumes of water to promote cell lysis and remove unincorporated [*methyl*-^{3}H]thymidine. Filters were dried by washing with methanol, and the radioactivity was measured with a liquid scintillation counter. Data were expressed as the percent of [*methyl*-^{3}H]thymidine incorporated as compared to the PBS control samples.

The effect of ONC, wild-type RNase A, G88R RNase A, and K7A/G88R RNase A was determined on flow-sorted HeLa or K-562 cells that produce ECFP or ECFP–RI. Assays were performed as described previously for wild-type cells.

Data were analyzed with the programs SigmaPlot (SPSS Science; Chicago, IL) and DeltaGraph (DeltaPoint; Monterey, CA). Each data point represents the mean (± S.E.) of at least three experiments, each performed in triplicate. The IC_{50} value for each variant was calculated by using eq 1:

$$S = \left(\frac{IC_{50}}{IC_{50} + [\text{ribonuclease}]} \right) \times 100 \qquad (1)$$

where S is the percent of total DNA synthesis after the incubation period (48 h).

Microscopy. The cytotoxicity of ONC, RNase A, and G88R RNase A was visualized directly by fluorescence microscopy. JAR or HeLa cells (5×10^4 cells/ml) were grown on coverslips in the wells of a 6-well plate. Cells were incubated with ONC, RNase A, or G88R RNase A (10 μM) at 37 °C in a humidified incubator containing 5% CO_2(g) for 48 h. After incubation, the cells were washed with PBS, fixed with paraformaldehyde (4% w/v) for 15 min, and then permeabilized for 5 min with Triton X-100 (0.1% v/v). Samples were then washed with PBS, and stained for 5 min with TOTO-3 iodide (0.1 μM) (Molecular Probes; Eugene, OR). Stained cells were viewed with a Zeiss Axiovert 100 TV microscope.

Growth curves. Cells (2.5×10^5) were added in duplicate or triplicate to the wells of a 24-well plate. The plates of cells were incubated at 37 °C in a humidified incubator containing 5% CO_2(g). Cells were counted every 24 h, until cultures reached confluency, in the presence of trypan blue (0.2% w/v) using a hemacytometer. The exponential portion of the growth curves was fitted with eq 2 (Segel, 1980):

$$N_t = N_o e^{kt} \tag{2}$$

where N_t is the number of cells at time t, N_o is the initial number of cells, and k is the growth rate constant. Population doubling time (τ) was calculated with eq 3:

$$\tau = \frac{\ln 2}{k} \tag{3}$$

Cytoplasmic protein purification. Protein was extracted from each cell line as described by Hofsteenge and co-workers (Blázquez *et al.*, 1996). All steps were completed at 4 °C using ice-cold solutions. Briefly, cells were grown on 10-cm plates to 70% confluency and washed three times with PBS. Cells were lysed in lysis buffer [400 µl of 10 mM Tris–HCl buffer, pH 7.5, containing EDTA (1 mM), dithiothreitol (0.5 mM), saccharose (0.25 M), Triton X-100 (0.1% w/v), leupeptin (0.1 µg/ml), pepstatin A (0.1 µg/ml), benzamidine HCl (1 µg/ml), and phenylmethylsulfonyl fluoride (0.1 mM)] and harvested with a rubber cell scraper. Cells were vortexed and incubated on ice for 10 min. Samples were centrifuged at

3,000 × *g* for 10 min, and supernatants were centrifuged at 270,000 × *g* for 30 min. The resulting supernatants were analyzed immediately or stored in aliquots at –80 °C until further use. The total protein concentration in cytoplasmic extracts was determined by using the Bradford method (Bradford, 1976) as adapted by Pierce (Rockford, IL).

Immunoblotting. Cytoplasmic protein extracts (5–15 μg) or whole cell lysates (50,000–100,000 cells/lane) were analyzed by gel electrophoresis in 10% (w/v) polyacrylamide gels according to the method of Laemmli (Laemmli, 1970). Human RI (50–200 ng) from Promega (Madison, WI) was used as a standard. Proteins were transferred to nitrocellulose and then blocked overnight in TBS-T [20 mM Tris–HCl buffer, pH 7.6, containing NaCl (0.137 M) and Tween 20 (0.1% w/v)] containing nonfat dry milk (2% w/v). An antibody raised in rabbit against recombinant porcine RI was the generous gift of J. Hofsteenge (Basil, Germany). Blots were incubated in blocking buffer containing a $1:10^3$ dilution of anti-RI antibody for 1 h at room temperature or overnight at 4 °C. Next, blots were washed three times for 10 min in TBS-T. Blots were then incubated with a goat anti-rabbit secondary antibody conjugated to alkaline phosphatase (Sigma; St. Louis, MO) at a $1:10^4$ dilution. After the blots were washed, RI was detected using the Atto Phos Plus substrate from JBL Scientific (San Luis Obispo, CA). Bands were visualized using a Vistra Flourimager SI and analyzed with ImageQuant software (both from Molecular Dynamics; Sunnyvale, CA).

Ribonuclease inhibition assays. Lysates from wild-type, ECFP, and ECFP–RI HeLa cells were prepared as described previously. The RI activity from each lysate was determined by measuring the inhibition of the ribonucleolytic activity of RNase A. Assays were performed

at 23 °C in 2.00 ml of 0.10 M MES–NaOH buffer (pH 6.0) containing NaCl (0.10 M), in the presence of RNase A (10 pM) and the 6-FAM~dArU$(dA)_2$~6-TAMRA fluorescent ribonuclease substrate (50 nM) (Kelemen *et al.*, 1999). Inhibitory activity was recorded as percent inhibition per μg of cytosplasmic protein.

RESULTS

Ribonuclease-mediated toxicity to immortalized cell lines. The ability of ONC and G88R RNase A to inhibit cellular DNA synthesis was assessed with a series of human cell lines, derived from both cancerous and noncancerous origins. A description of each cell line is listed in Table 4.1. Data for representative cell lines are shown in Figure 4.1. The toxicity of ONC and G88R RNase A towards each cell line tested, described as IC_{50} values, is listed in Table 4.1.

ONC was highly toxic to all transformed cells tested, with IC_{50} values in the sub-μM range (Figure 4.1A; Table 4.1). ONC was most toxic to the JAR choriocarcinoma cell line, with an IC_{50} value of 0.07 μM. The leukemia-derived K-562, HL-60, and Jurkat cell lines were susceptible, with IC_{50} values of 0.5, 0.4, and 0.2 μM, respectively. The adenocarcinoma-derived HeLa and SK-HEP-1 cell lines were also susceptible to ONC-mediated toxicity, with IC_{50} values of 0.8 and 0.4 μM, respectively. The transformed cell line of a noncancerous origin, 293, was more resistant to ONC, with an IC_{50} value of 3 μM. Thus, ONC was more toxic to tumor cell lines than to this nontumor cell line. Nonetheless, 10 μM ONC resulted in >90% cell death for every cell line tested.

G88R RNase A was toxic only to a few of the tumor cell lines (Figure 4.1B; Table 4.1). As for ONC, the JAR cell line was the most susceptible to G88R RNase A-mediated toxicity, with an IC_{50} value of 4 μM. K-562 and Jurkat cells, both leukemia-derived, were also susceptible, with IC_{50} values of 6 and 10 μM, respectively. The HL-60 leukemia-derived cell line was, however, not susceptible to G88R RNase A. HeLa and SK-Hep-1 cells were also resistant to G88R RNase A. Cells from these three lines began to die only when exposed to ≥25 μM protein, and IC_{50} values could not be determined from the experimental data. When exposed to 25 μM G88R RNase A, <10% of 293 cells died. Wild-type RNase A was not toxic to any cell line at the levels tested.

Toxicity to normal cell lines. To investigate further the toxicity to primary, normal cells, we measured the IC_{50} values of ONC and G88R RNase A for the IMR-90 and WI-38 cells. ONC was toxic to both cell lines, with IC_{50} values of 1 and 5 μM, respectively. G88R RNase A concentrations of 25 μM did not result in significant cell death. These results indicate that normal cells are resistant to G88R RNase A-mediated toxicity.

Cell microscopy. To verify that inhibition of cell proliferation was due to cell death, the effect of ONC compared to G88R RNase A was observed directly in HeLa or JAR cells using fluorescence microscopy (Figure 4.2). RNase A had no detectable effect on cell viability, morphology, or staining of the nucleus. HeLa cells treated with 10 μM G88R RNase A showed nuclear staining similar to that of cells treated with RNase A. HeLa cells treated with ONC demonstrated two characteristics of apoptosis: nuclear condensation and fragmentation. JAR cells treated with either G88R RNase A or ONC showed the presence of apoptotic bodies. These results are consistent with measured IC_{50} values, as JAR

cells are more susceptible than are HeLa cells to G88R RNase A, with IC_{50} values of 4 μM and >25 μM, respectively (Table 4.1).

Cell growth curves. To determine whether the growth rate of a cell correlates with its vulnerability to ribonucleases, population doubling times were measured and compared to IC_{50} values. As listed in Table 4.1, cells derived from a cancerous origin had a more rapid growth rate than did those derived from normal tissue. In addition, cells derived from a similar origin did not necessarily have similar growth rates. The trend observed was an increase in cell susceptibility with faster doubling times.

Intracellular RI levels. The cytotoxicity of a ribonuclease depends upon its ability to evade cytosolic RI, and degrade cellular RNA. We investigated whether cellular RI levels correlated with the apparent resistance of cell lines. Control experiments using RI standards showed that the amount of RI (ng) could be detected accurately by integrating each band (data not shown). Figure 4.3 demonstrates that RI was readily detectable in all cells tested. The intensity of each band was compared to the RI standard to determine RI levels in each cell line (Figure 4.3C). No cell lines differed by more than twofold in RI level. In addition, RI levels did not vary between cell extracts from different protein purifications (data not shown). Thus, differences in RI concentrations did not correlate with susceptibility to toxic ribonucleases. RI represents approximately 0.08% (= 120 ng/15 μg) of total cytoplasmic protein (Figure 4.3). A similar value had been reported previously for HeLa cells (Blázquez *et al.*, 1996) and brain tissue (Nadano *et al.*, 1994), but higher than had been observed for RI purified from tissues extracts (Blackburn & Moore, 1982; Lee & Vallee, 1993).

Design of RI expression construct. To explore further the role of RI, we designed a system to overproduce RI in mammalian cells. Our system had to meet several criteria. Most importantly, the RI had to retain the characteristics of endogenous RI, that is, it had to be located in the cytosol and be able to bind and inhibit the ribonucleolytic activity of RNase A. Also, the overproduced RI had to be easy to detect.

The ECFP–RI fusion protein satisfies these requirements. ECFP is an enhanced fluorescent analog of GFP (Heim *et al.*, 1994; Cubitt *et al.*, 1995; Heim & Tsien, 1996; Tsien, 1998); thus, monitoring its production is facile. The C-terminus of RI provides many contact points with RNase A in the RI•RNase A complex (Figure 4.4A) (Kobe & Deisenhofer, 1995b; Kobe & Deisenhofer, 1996). In contrast, the N-terminus of RI is not involved in binding RNase A. In addition, the N-terminus of human RI contains four residues that extend away from the plane of the RI-fold (Papageorgiou *et al.*, 1997), acting as a natural linker (Figure 4.4B). As GFP is a compact, cylindrical protein (Figure 4.4C) (Yang *et al.*, 1996), we hypothesized that a fusion of ECFP with the N-terminus of human RI could still bind and inhibit the activity of RNase A. To increase the distance between ECFP and RI, three glycine residues were added as a spacer.

Production of ECFP–RI fusion protein. Under control of the CMV IE promoter, the ECFP–RI fusion protein was produced in the cytosol of HeLa and K-562 cells. ECFP alone was produced in these cells as a control. Transfection efficiencies were determined by FACS and ranged from 15–50 and 5–10% for HeLa and K-562 cells, respectively. Fluorescence microscopy was used to monitor the ECFP fluorescence of K-562 and HeLa transfected cells. A representative transfection in HeLa cells is shown in Figure 4.5A. Untransfected HeLa

cells did not have detectable ECFP fluorescence. Cells transfected with pECFP had a strong fluorescence that is diffuse throughout the nucleus and cytoplasm. Cells producing ECFP–RI had a stronger fluorescence in the cytoplasm than in the nucleus.

FACS was used to obtain a homogenous population of cells that overproduce ECFP–RI. The sorting window was adjusted to collect only the 50% most fluorescent cells. A representative histogram for ECFP–RI production in HeLa cells is shown in Figure 4.5B. Prior to fluorescence-based sorting, only 15% of the total cell population produced ECFP–RI, but after sorting, 95% of the cells were fluorescent. All experiments were performed on sorted cells.

Production of the ECFP–RI fusion protein was monitored by immunoblot analysis using a rabbit polyclonal antibody, which is specific for RI (Figure 4.5C). As described previously, endogenous RI can be detected in all cell lines tested. Likewise, a 50-kDa band corresponding to the human RI control was detected in cells that were transfected with pECFP and pECFP–RI. HeLa and K-562 cells that were transfected with pECFP–RI produced an additional, high molecular weight band that was consistent with the addition of the 238 residues of ECFP to RI. The production of ECFP–RI in K-562 and HeLa cells results in a 2- and 10-fold increase, respectively, in total RI concentration as compared to endogenous RI levels in the same cells.

To verify that the ECFP–RI fusion protein contained a functional RI domain, the ability of ECFP–RI HeLa cell lysates to inhibit ribonucleolytic activity was measured. ECFP–RI lysates inhibited RNase A activity 5-fold more than did lysates containing the same concentration of protein from wild-type or ECFP-producing HeLa cells (Figure 4.6).

Cytotoxicity to transiently-transfected cells. The toxicity of ribonucleases was measured for K-562 and HeLa cells that produced ECFP or the ECFP–RI fusion protein. As wild-type HeLa cells are normally resistant to the toxicity of G88R RNase A, we also tested a more toxic variant of G88R RNase A, K7A/G88R RNase A (Haigis *et al.*, 2002b). In K-562 cells, production of ECFP had no effect on the toxicity of either ONC, G88R RNase A, or K7A/G88R RNase A as compared to wild-type cells (Figure 4.7A; Table 4.2). K-562 cells that produced the ECFP–RI fusion protein were 3–4-fold more resistant to the toxicity of G88R RNase A and K7A/G88R RNase A. In contrast, the toxicity of ONC was unaffected by the higher levels of RI in these cells.

In HeLa cells, the toxicity of ribonucleases was not affected by ECFP production (Figure 4.7B; Table 4.2). Although G88R RNase A was not toxic to wild-type or ECFP producing HeLa cells, K7A/G88R RNase A was toxic to these cells, with IC_{50} values of 11 and 14 μM, respectively. HeLa cells that produced the ECFP–RI fusion protein were highly resistant to the toxicity of K7A/G88R RNase A. These cells were not susceptible, even at a K7A/G88R RNase A concentration of 25 μM. The toxicity of ONC was not affected by the production of ECFP–RI in HeLa cells.

DISCUSSION

The mechanism of ribonuclease-mediated cell death consists of two main steps: uptake into cells and catalytic cleavage of cellular RNA. Internalization of a ribonuclease is critical to its cytotoxic activity. After internalization, ribonucleases must be able to cleave cellular

RNA. The cytoplasm of every cell contains RI. The physiological role of RI is not known, but *in vivo* and *in vitro* experiments have provided insight into its biological function. Increasing levels of RI seem to result in decreased angiogenesis and tumor growth (Botella-Estrada *et al.*, 2001). When bound in a complex with RI, ribonucleases are no longer able to degrade RNA (Lee & Vallee, 1993). Thus, evasion of RI binding is necessary to maintain ribonucleolytic activity and correlates with the toxicity of RNase A variants (Leland *et al.*, 1998; Bretscher *et al.*, 2000). Here, we investigated the role of RI as a modulator of intracellular ribonuclease activity.

The toxicity of ribonucleases towards a variety of transformed cell lines reveals several distinctions between G88R RNase A and ONC. First, G88R RNase A is a less potent toxin than is ONC (Figure 4.1; Table 4.1). At a concentration of 10 μM, ONC killed 90% of every cell population tested herein. The same concentration of G88R RNase A resulted in significant toxicity to only three cell lines: K-562, JAR, and Jurkat. Second, the relative vulnerability of cell lines differs for the two ribonucleases. Cells that are highly susceptible to ONC are not necessarily vulnerable to G88R RNase A-mediated cell death. For example, HL-60 cells are sensitive to ONC, with an IC_{50} value of 0.3 μM. Yet, G88R RNase A does not kill HL-60 cells effectively at protein concentrations up to 25 μM.

The different rank order of cell vulnerability for G88R RNase A and ONC suggests that the mechanism of action for these two ribonucleases is not identical. Plasma clearance assays in mice showed that the organ distribution pattern of ONC differs from that of mammalian ribonucleases (Vasandani *et al.*, 1996). Hence, ONC and G88R RNase A could preferentially target different cells. They could also be internalized into different cells with differing

efficiency. In addition, they could degrade a different cellular substrate. *In vitro*, the preferred homopolymeric substrate of ONC [poly(U)] does indeed differ from that of RNase A [poly(C)] (Youle & D'Alessio, 1997). The *in vivo* substrate specificity also differs between RNase A and ONC (Lin *et al.*, 1994). RNase A inhibits protein synthesis in *Xenopus* oocytes by degrading rRNA, but ONC degrades tRNA. Moreover, ONC and G88R RNase A have different affinities for RI (Boix *et al.*, 1996; Leland *et al.*, 1998). These and other differences are manifested as differences in cytotoxic activity and specificity.

In general, the cytotoxicity of ONC and G88R RNase A correlates with cellular growth rate (Table 4.1). The cancer-derived cell lines in this study have a faster population doubling time than do cells isolated from normal tissue. These lines are vulnerable to both ONC and G88R RNase A. In contrast, cell lines derived from noncancerous tissues are the most resistant to ONC, and completely resistant to G88R RNase A. One explanation for tumor cell susceptibility is that the molar ratio of ethanolamine phospholipids to choline phospholipids in the plasma membrane increases upon neoplastic transformation (Kojima, 1993). This increase results in a more anionic membrane that is more attractive to ribonucleases, which are cationic proteins (p*I* > 8.9 for ONC (Ardelt *et al.*, 1991)).

Are some cells more susceptible to ribonuclease-mediated toxicity because of a low RI level? We hypothesized that intracellular RI levels modulate ribonuclease-mediated toxicity. To test this hypothesis, the RI levels between the different cell lines were compared. Intracellular RI levels are difficult to measure accurately. To prevent RI oxidation and its subsequent degradation, we prepared cytoplasmic extracts in a reducing environment and in the presence of multiple protease inhibitors. Moreover, we compared intracellular RI levels

by using immunoblots, so our data are not dependent on RI activity. RI levels differed by less than two-fold among the wild-type cell lines tested herein (Figure 4.3).

We find that the intracellular RI level does not explain the difference in susceptibility between the different cell lines tested herein. Instead, modulators other than RI must account for these differences in susceptibility. Two such modulators are cell surface affinity (discussed previously) and internalization. When ribonuclease internalization is enhanced, so is its cytotoxicity. For example, ribonucleases that are microinjected into the cytosol are several fold more toxic than are ribonucleases added to cells externally (Saxena *et al.*, 1991). The toxicity of ribonucleases can also be enhanced by adding drugs that alter cellular routing (Wu *et al.*, 1993; Wu *et al.*, 1995), or by conjugation to delivery molecules (Newton *et al.*, 1992; Suzuki *et al.*, 1999).

Although the intracellular RI levels did not vary with differences in cell susceptibility in the cells tested herein (Figure 4.3), we hypothesized that RI is still a modulator of toxicity in these cells. This hypothesis was based on the previous finding that RNase A variants that evade RI are potent cytotoxins (Leland *et al.*, 1998; Bretscher *et al.*, 2000; Haigis *et al.*, 2002b). In the absence of RI variation, it is impossible to determine the contribution of intracellular RI on toxicity. In order to generate variation in RI levels, we overproduced RI as a fusion protein in mammalian cells (Figure 4.5). Oxidized and (presumably) misfolded RI is degraded rapidly in cells (Blázquez *et al.*, 1996). The ECFP–RI fusion protein is stable in mammalian cells (Figure 4.5C) and can be detected up to 72 h after DNA transfection (data not shown). The ECFP–RI fusion protein is functional, as it can inhibit the ribonucleolytic

activity of RNase A (Figure 4.6). The RI fusion protein can be used to explore its biological role.

RI does not modulate ONC-mediated cytotoxicity (Figure 4.7). Thus, RI is not involved in regulating the intracellular activity of ONC. This finding has significant implications for understanding the mechanism of a toxic ribonuclease. Most importantly, the mechanism of ONC-mediated toxicity differs from that of toxic mammalian ribonucleases. Every cytosolic molecule of ONC is free to degrade cellular RNA. The only barriers to ONC cytotoxicity are entry into the cytosol and its low ribonucleolytic activity. Second, cell susceptibility to ONC toxicity is not modulated by intracellular RI levels *in vivo* or *in vitro*. The IC_{50} values measured herein and the tumor cell susceptibility documented for ONC (*vide supra*) are presumably due to differences in the cell surface binding and cytosolic internalization of ONC. Alternatively, cell susceptibility to ONC toxicity could be due to specific mRNA requirements by the cell.

RI does indeed modulate the intracellular activity of toxic RNase A variants, as evidenced by the protection conferred upon cells that produce ECFP–RI (Figure 4.7). Thus, the requirement for cytotoxicity by RNase A variants is more complex than for ONC; toxic RNase A variants have the additional challenge of evading RI. These data reveal a potential biological role for RI—as an intracellular sentry against endogenous secretory ribonucleases that become internalized to the cytosol. Although the cell lines tested herein do not differ dramatically in RI levels, RI levels can vary *in vivo*, according to temporal and spatial regulation (Hofsteenge, 1997). In addition, pancreatic ribonucleases are secretory proteins that can circulate systemically through the sera (Weickmann *et al.*, 1984; Futami *et al.*,

1997). As a result, many cells are exposed to ribonucleases. Thus, differences in RI levels *in vivo* could lead to enhanced cellular protection or susceptibility to endogenous ribonucleases.

Our findings demonstrate that intracellular fluctuations of RI can modulate a biological event—cell death. RI is sensitive to oxidation, and as such, can be regulated by the reduction potential of the cytosol (Blázquez *et al.*, 1996). Intracellular redox potential changes can regulate cellular events, such as circadian rhythm (Rutter *et al.*, 2001). Whether RI levels fluctuate in biological pathways remains to be determined.

In summary, we have revealed new aspects in the toxicity of ONC and toxic RNase A variants for human cells. We have measured the toxicity of ONC and G88R RNase A towards a variety of human cell lines and found that cellular growth rate correlates with ribonuclease susceptibility. Cytoplasmic RI levels do not vary substantially among these cell lines. Nonetheless, overproducing RI does diminish the toxicity of RNase A variants. This finding provides the first direct evidence that RI acts as an intracellular sentry against invading secretory ribonucleases. In contrast, the toxicity of ONC is unaffected by RI levels, indicating that this ribonuclease (unlike toxic RNase A variants) cannot be made more toxic by decreasing its affinity for RI. Our findings provide a basis for designing more potent variants of RNase A, as well as choosing which tumor cell types to target with ribonuclease-based cancer chemotherapeutics.

Acknowledgements. This work was supported by grant CA73808 (NIH). We thank L.L. Kiessling for the HL-60 and Jurkat cell lines, and J. Hofsteenge for the RI antibody and

for helpful discussion. We thank K.M. Haigis and R.L. Abel for insightful discourse and critical reading of the manuscript. We thank K. Schell and J.M. Batchelder at the University of Wisconsin–Madison Comprehensive Cancer Center for assistance with FACS experiments.

Table 4.1 Properties of cell lines and IC_{50} values for cytotoxic ribonucleases

Cell line	Tissue/Origin[a]	Doubling time (h)	IC_{50} (μM) ONC	G88R RNase A
K-562	Chronic myelogenous leukemia	18	0.54 ± 0.04	5.7 ± 0.4
JAR	Placenta, choriocarcinoma	21	0.074 ± 0.005	4.1 ± 0.3
Jurkat	T cell leukemia	22	0.22 ± 0.02	10 ± 1
HeLa	Cervix, adenocarcinoma	25	0.83 ± 0.05	>25 [b]
SK-Hep-1	Liver, adenocarcinoma	27	0.41 ± 0.03	>25 [b]
HL-60	Promyelocytic leukemia	30	0.42 ± 0.03	>25 [b]
IMR-90	Lung, fibroblast	34	0.57 ± 0.07	—[c]
WI-38	Lung, fibroblast	36	4.5 ± 0.3	—[c]
293	Kidney, epithelial	40	3.2 ± 0.7	—[c]

[a]Data from American Type Culture Collection catalog.
[b]A protein concentration of 25 μM resulted in >30% but <50% cell death.
[c]A protein concentration of 25 μM resulted in <10% cell death.

Table 4.2 Toxicity of ribonucleases to transiently-transfected K-562 and HeLa cells

	IC_{50} (μM)		
Cell	ONC	G88R RNase A	K7A/G88R RNase A
K-562	0.54 ± 0.04	5.7 ± 0.4	1.0 ± 0.1
K-562 ECFP	0.47 ± 0.02	4.2 ± 0.5	1.0 ± 0.1
K-562 ECFP–RI	0.51 ± 0.03	15 ± 2	2.5 ± 0.3
HeLa	0.83 ± 0.05	>25[a]	14 ± 1
HeLa ECFP	0.60 ± 0.04	>25[a]	11 ± 1
HeLa ECFP–RI	0.65 ± 0.06	>25[a]	>25[a]

[a]A protein concentration of 25 μM resulted in <50% cell death.

Figure 4.1 Cell proliferation assay. Cells were incubated with increasing concentrations of Onconase® (A) and G88R ribonuclease A (B). Cells (5×10^4) were plated and incubated with varying concentrations of RNase A. Plots for representative cell lines are shown to illustrate the potency of ONC and G88R RNase A. Each point represents the mean (± S.E.) of at least 3 sets of triplicate experiments.

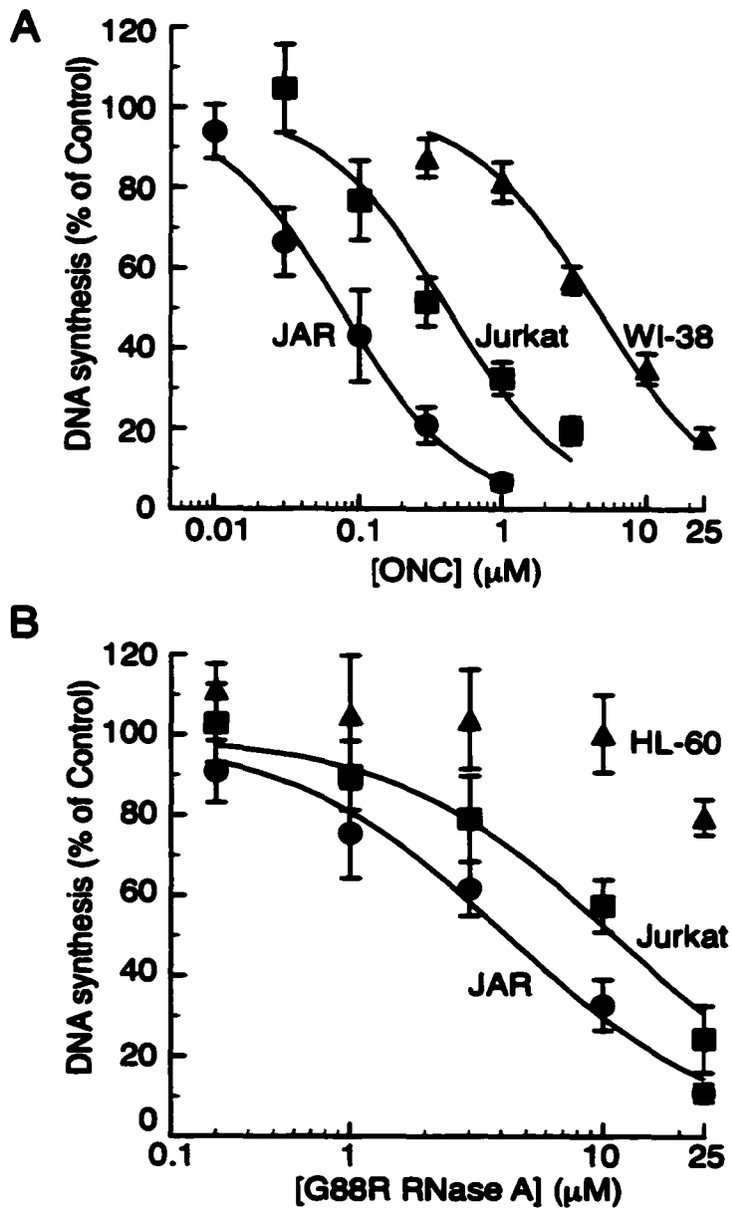
A
DNA synthesis (% of Control)
120
100
80
60
40
20
0
JAR
Jurkat
WI-38
0.01
0.1
1
10
25
[ONC] (μM)
B
DNA synthesis (% of Control)
120
100
80
60
40
20
0
HL-60
Jurkat
JAR
0.1
1
10
25
[G88R RNase A] (μM)

Figure 4.2 Cell microscopy of ribonuclease-mediated toxicity. HeLa and JAR cells were grown, and exposed to 10 μM ribonuclease A, G88R ribonuclease A or Onconase® for 48 h. Cell nuclei were stained using TOTO-3 iodide immunofluorescent reagent.

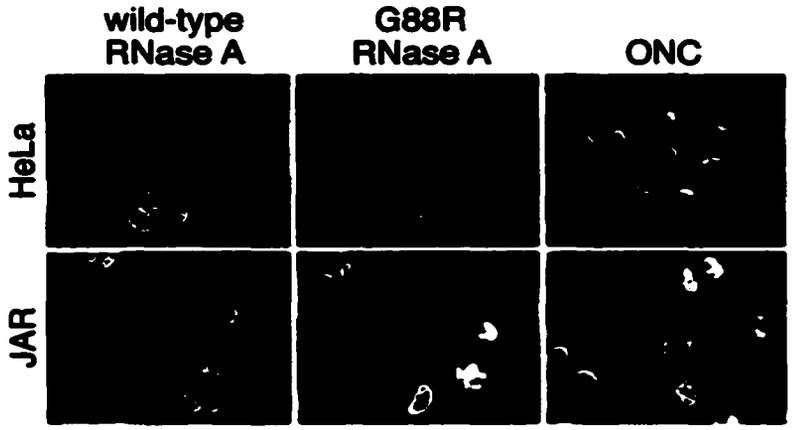
wild-type
RNase A
G88R
RNase A
ONC
HeLa
JAR

Figure 4.3 Immunoblot of cytoplasmic ribonuclease inhibitor. Lanes contain protein (15 μg) from cytoplasmic extracts or a human RI standard (A, 100 ng; B, 50 ng). After electrophoresis, gels were probed with rabbit anti-porcine RI antibody. The quantity of RI in each lane is depicted in a bar graph (C).

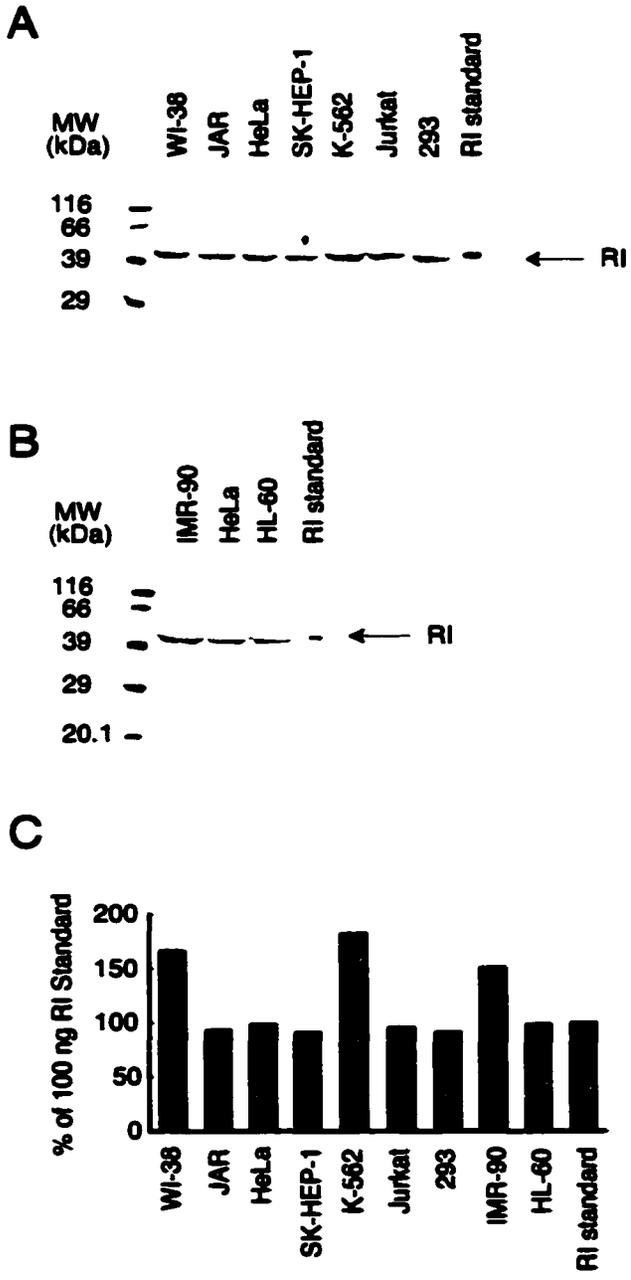
A
MW (kDa)
116
66
39
29
WI-38
JAR
HeLa
SK-HEP-1
K-562
Jurkat
293
RI standard
RI
B
MW (kDa)
116
66
39
29
20.1
IMR-90
HeLa
HL-60
RI standard
RI
C
% of 100 ng RI Standard
200
150
100
50
0
WI-38
JAR
HeLa
SK-HEP-1
K-562
Jurkat
293
IMR-90
HL-60
RI standard

Figure 4.4 Structural components of the ECFP–RI fusion protein. (A) Ribbon diagram of the porcine RI•RNase A complex (Kobe & Deisenhofer, 1995b), (B) human RI (Papageorgiou *et al.*, 1997), and (C) GFP (Yang *et al.*, 1996) were created using the atomic coordinates derived by x-ray diffraction analysis and the program MOLSCRIPT (Kraulis, 1991). Shown in ball and stick is Tyr66 of GFP, which is replaced with a tryptophan residue to give ECFP fluorescent properties.

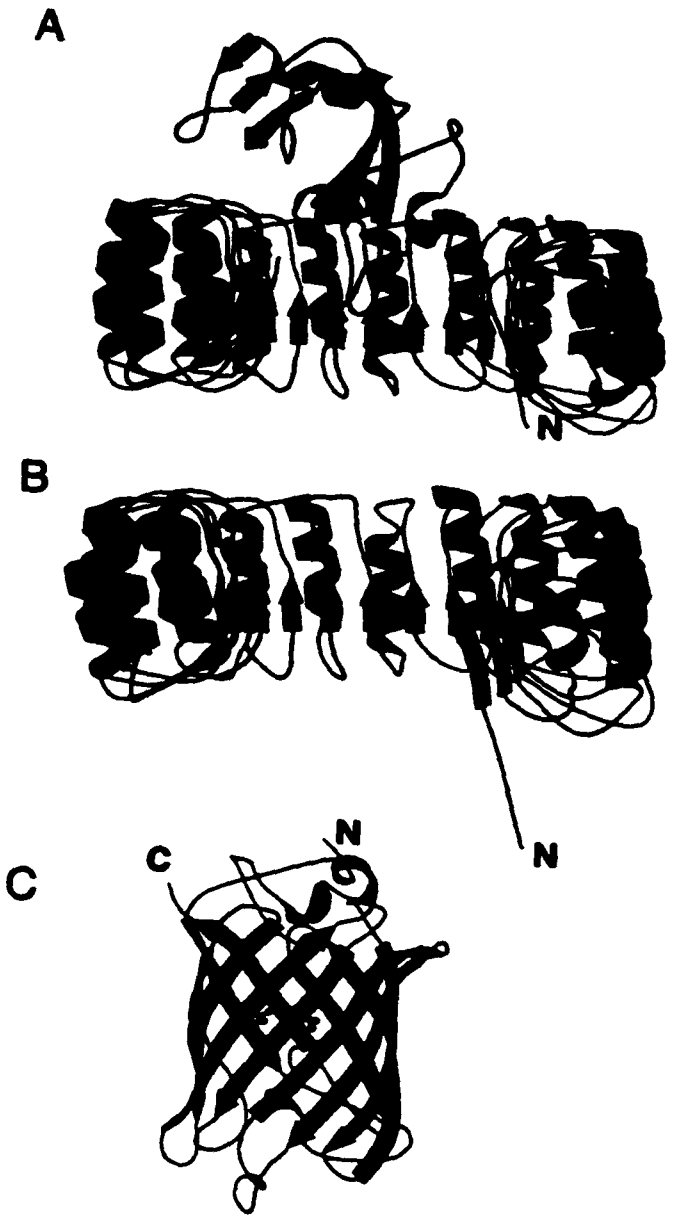
A
N
B
N
C
C
N

Figure 4.5 Transient overproduction of ribonuclease inhibitor. (A) ECFP fluorescence was detected 24 h after transfection with pECFP or pECFP–RI. Bar represents 20 μm. (B) Representative flow-sorting experiment. HeLa cells producing ECFP–RI before sorting for ECFP fluorescence (purple) represented 14.8% of the total cell population. 94.6% of the post-sorted cells overproduced eCFP–RI (cyan). (C) Lanes contain flow-sorted K-562 or HeLa cell lysates (50,000–100,000 cells/lane), which produced ECFP or ECFP–RI. RI was detected with an anti-porcine RI antibody, and bands were compared to a human RI control.

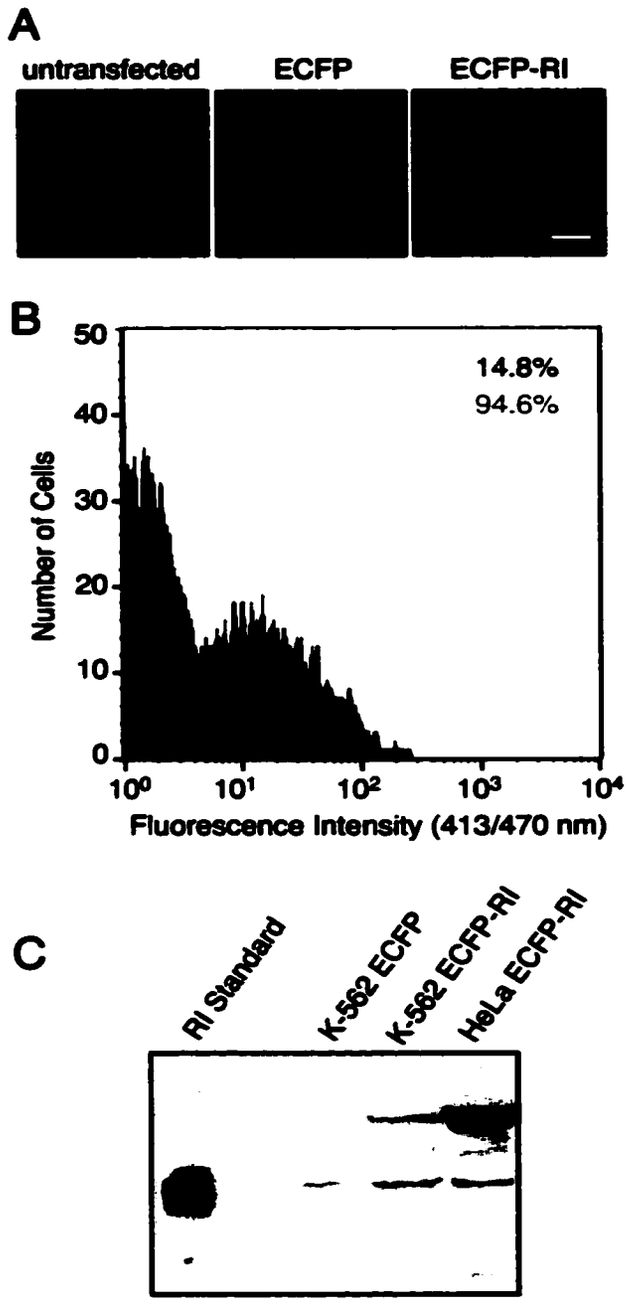
A
untransfected
ECFP
ECFP-RI
B
14.8%
94.6%
Number of Cells
50
40
30
20
10
0
10^0
10^1
10^2
10^3
10^4
Fluorescence Intensity (413/470 nm)
C
RI Standard
K-562 ECFP
K-562 ECFP-RI
HeLa ECFP-RI

Figure 4.6 Inhibition of ribonuclease activity by HeLa cell extracts. Extract (20 ng of protein) from HeLa cells and flow sorted HeLa cells producing ECFP–RI was added to a solution containing RNase A (10 pM) and 6-FAM~dArU$(dA)_2$~6-TAMRA (50 nM). Less than 10% of the 6-FAM~dArU$(dA)_2$~6-TAMRA substrate was cleaved during the assay.

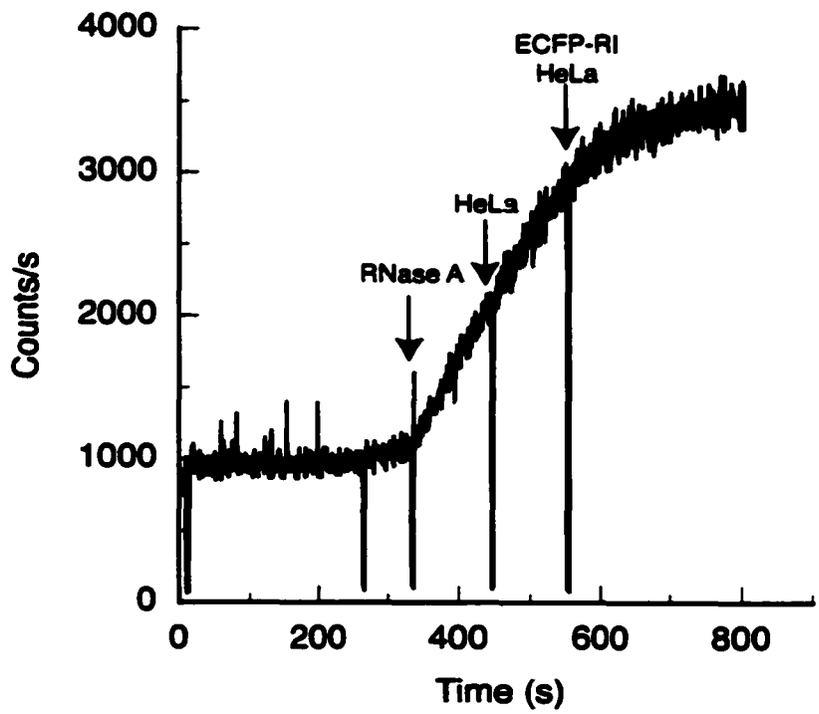
4000
3000
2000
1000
0
Counts/s
0
200
400
600
800
Time (s)
ECFP-RI
HeLa
HeLa
RNase A

Figure 4.7 Cell proliferation assay in cells overproducing ribonuclease inhibitor. Flow-sorted K-562 (A) or HeLa (B) cells overproduced ECFP (filled symbols) or ECFP–RI (open symbols). Cells were incubated with increasing concentrations of ONC (A,B, squares), G88R RNase A (A, circles), or K7A/G88R RNase A (B, circles). Cytotoxicity was analyzed as described for Figure 4.1.

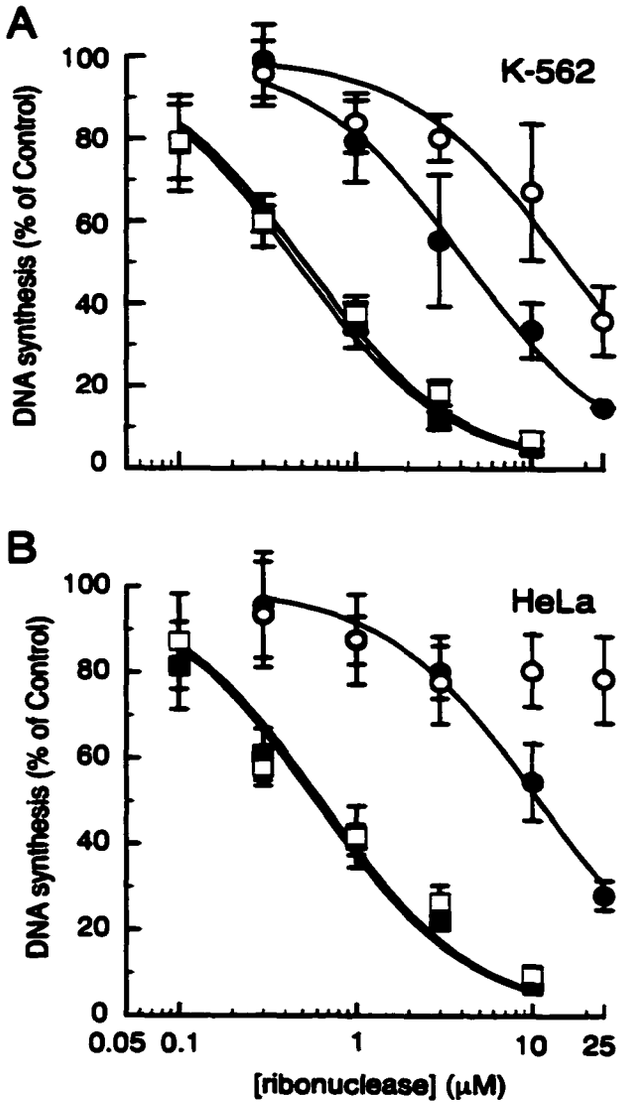
A
K-562
DNA synthesis (% of Control)
100
80
60
40
20
0
B
HeLa
DNA synthesis (% of Control)
100
80
60
40
20
0
0.05
0.1
1
10
25
[ribonuclease] (μM)

Chapter 5

Evolution of Ribonuclease Inhibitor by Exon Duplication

In press as: Marcia C. Haigis, Eric S. Haag, and Ronald T. Raines (2002) Evolution of ribonuclease inhibitor by exon duplication. *Molecular Biology and Evolution.*

ABSTRACT

The leucine-rich repeat (LRR) is a prevalent structural motif that mediates protein–protein interactions. LRRs are found in proteins performing diverse biological functions. Ribonuclease inhibitor (RI) is a non-globular protein that consists entirely of tandem LRR units. We have determined the genomic structure of the human RI gene. We find that the nine coding exons are precisely in phase with the individual LRR units, and sequence analyses indicate that the internal exons within RI duplicated rapidly and then diverged slowly. These data suggest a general mechanism for the evolution of proteins with tandem repeats.

INTRODUCTION

The leucine-rich repeat (LRR) is a prevalent structural motif that mediates specific protein–protein interactions (Kobe & Deisenhofer, 1995a; Kobe & Kajava, 2001). The LRR is defined by a region of 20–29 residues that contains the consensus sequence: XLXXLXLXXN, where L, N, and X are leucine, asparagine, and any residue, respectively. Typically, LRRs are displayed in 1–30 tandem copies within a protein.

The first crystalline structure of an LRR-containing protein revealed a new protein fold (Kobe & Deisenhofer, 1993) (Figures 5.1A and 5.1B). In porcine ribonuclease inhibitor (RI), the LRRs are arranged tandemly in a horseshoe shape with 16 α-helices encasing a parallel β-sheet of 17-strands. Hydrophobic forces between the consensus leucine residues appear to stabilize the β-sheet. RI is able to bind tightly to members of the ribonuclease (RNase) A superfamily, which not only catalyze RNA degradation but also mediate angiogenesis, cytotoxicity, and the host-defense response (for reviews, see: D'Alessio & Riordan, 1997; Hofsteenge, 1997; Raines, 1998; Leland & Raines, 2001).

The RI fold is conserved in other proteins containing LRRs. Human U2A′ is a small nuclear protein that contains 5 LRRs and binds to U2B″ to form an active spliceosomal complex. Another protein, Skp2, contains both 10 LRRs that function as a protein-binding domain and an F-box motif that binds to the catalytic core of ubiquitin–protein ligases. The LRRs in U2A′ and Skp2 adopt an RI-like fold (Price *et al.*, 1998; Schulman *et al.*, 2000). The crystalline structure of U2A′ bound to U2B″ and those of RI bound to RNase A and angiogenin reveal that the parallel β-sheet formed by the LRRs furnishes the surface for

interacting with other proteins (Kobe & Deisenhofer, 1995b; Papageorgiou *et al.*, 1997; Price *et al.*, 1998).

The modularity of the LRR is consistent with the evolution of RI by gene duplication. To test this hypothesis, we investigated the genomic structure of human RI. Our findings provide new insight into the evolution of RI as well as the many proteins containing LRRs or other modules.

MATERIALS AND METHODS

RI Genomic Locus. Using the National Center for Biotechnology Information (NCBI) nr database (http://www.ncbi.nlm.nih.gov), we identified three potential transcripts obtained from human placental (Lee *et al.*, 1988), HeLa (Schneider *et al.*, 1988), and testis cDNA libraries (GI = 186260, 35843, and 7328055, respectively). Using these transcripts, we searched the NCBI database for a corresponding genomic sequence and identified a region of DNA on human chromosome 11 overlapping cosmids cSRL125c1 and cSRL135f4 that contained the RI gene (GI = 2281060). The presence of consensus splice donor and acceptor sites enabled the identification of the intron/exon positions.

The mouse intron/exon positions were determined by analyzing existing sequences and generating new sequence data. First, genomic sequences were identified in the NCBI mouse genome database, containing several exons of mouse RI. To obtain the mouse RI locus, a mouse 129/Sv library (Genome Systems; St. Louis, MI) was screened by PCR using the following primers: 5′ GGTGCAAAGACATCAGCTCAGCAGTCCAAGC 3′ and

5′ CCTGGAGCACCAGACCCACACC 3′. This locus is described further in Chapter 6. Predicted intron/exon junctions were verified by DNA sequencing. The pig exons were inferred from the cDNA for pig RI (Vicentini *et al.*, 1990)(GI = M58700) by using the genomic structures of human and mouse RI.

Analysis of RI Exons. RI exons were aligned using the PILEUP program from Wisconsin Package of Genetics Computer Group (Madison, WI). Phylogenetic trees were built by the PAUP (phylogenetic analysis using parsimony) program (Swofford, 1998). The rate of nonsynonymous vs synonymous substitutions for exons 3–9 were measured as described previously (Nei & Gojobori, 1986).

RESULTS AND DISCUSSION

Human RI consists of alternating 28- or 29-residue LRR units (Kobe & Deisenhofer, 1993; Papageorgiou *et al.*, 1997; Kajava, 1998). RI transcripts from human placental, HeLa, and testis were identified and are 1682, 1921, and 2982 bp, respectively. Although alternative splice forms of the 5′-untranslated region have been identified in placenta, Northern blot analysis revealed that the RI gene is expressed as a single transcript in placental and HeLa cells (Lee *et al.*, 1988; Schneider *et al.*, 1988; Crawford *et al.*, 1989).

The genomic locus of human RI is situated on chromosome 11 and spans more than 12 kb (Figure 5.1C). All three transcripts identified possess a colinear open reading frame encoded by nine 3′-terminal exons, numbered 2–10, as determined by the presence of consensus splice donor and acceptor sites. The transcripts differ in their 5′-untranslated region, and contain

zero, one, or two alternatively spliced exons. As all transcripts encode an identical protein sequence, the functional significance of alternative splice forms is unknown. Remarkably, all but the first and last coding exons are *exactly* 171 bp in length. In addition, all introns are of phase 2, which denotes codon interruption after the second nucleotide. Hence, any of the internal exons could be moved or removed without disrupting the alignment of LRRs encoded by neighboring exons.

A striking relationship exists between the intron–exon structure and the tertiary structure of RI (Figure 5.1). Each of the internal exons encodes 57 residues. Except for the junction after the N-terminus, which occurs within a longer β-strand, every exon translation product correlates with a pair of β-strands and α-helices without any disruption (Figures 5.1A and 5.1B). Thus, the LRR motif within RI is defined completely by its intron–exon structure.

The phasing and position of the RI introns are consistent with exon amplification during evolution (de Souza *et al.*, 1997; Gilbert *et al.*, 1997; Fedorov *et al.*, 1998). To test this hypothesis, we investigated the similarity of the coding exons. Although the terminal exons (2 and 10) have low sequence identity, the internal exons (3–9) can be aligned without gaps and have considerable sequence identity (Figure 5.2A). Pairwise comparisons revealed that exons 3–9 are 50–60% identical. In addition, translation products corresponding to exons 3–9 were aligned and determined to be 30–50% identical (Figure 5.2C).

The high degree of similarity and their identical length strongly suggests that the internal exons of RI are homologues related by exon duplication. We wished to know whether these duplications had occurred all at once or in distinct phases, and whether inter-exonic conversion events had occurred since different RI-containing genomes diverged. To

distinguish between these distinct mechanisms, phylogenetic analyses was performed on the internal coding exons of human, mouse, and pig RI. The mouse RI exons were identified by a two-fold approach: analyzing existing sequences and generating new sequence data. Like the human gene, mouse RI consists of 7 internal exons that are 171 bp in length and are separated by phase 2 introns. The intron/exon positions in pig RI were inferred from the human and mouse data. The internal exons from human, pig, and mouse were aligned as described above (Figure 5.2A). Sequence alignment reveals strong identity between analogous exons. Neighbor-joining phylogenetic trees built by using a Kimura 2-parameter correction have strongly supported clades for analogous exons between species with bootstrap values of 99–100% (Figure 5.2B). A maximum parsimony analysis of the data set also strongly supports the existence of clades for each exon with bootstrap values of 98–100%. Apparently, the tandem repeats within RI are extremely stable and homogenization has not taken place, as that would have resulted in a tree in which the internal exons from each species form a strongly supported clade. A consistent internal branching pattern did not emerge with strong support from either analysis. Furthermore, the branches leading to each exon clade are extremely long, which is consistent with a nearly simultaneous divergence of each clade. Thus, we conclude from this analysis that exons 3–9 were most likely duplicated in a "radiation" that occurred rapidly early in the history of RI. Members of the RNase A superfamily apparently exist in all tetrapods (D'Alessio & Riordan, 1997). Thus, it is likely that RI was assembled after the origin of tetrapods in the late Devonian, approximately 360 million years ago, but before the divergence of eutherian mammals.

The data indicate several unusual features about the evolution of RI. The internal exons of RI are homologous and stable. In addition, the branching pattern suggests that the internal exon duplications occurred rapidly and then diverged over a long period of time. To assess whether positive selection has been a factor in the divergence of the RI exons, we measured the rate of nonsynonymous versus synonymous changes in human exons 3–9 (Nei & Gojobori, 1986). The ratios of nonsynonymous-to-synonymous changes range from 0.31 to 1.00. Although the nonsynomous-to-synonymous ratio is not always a definitive indicator of positive selection (Wyckoff *et al.*, 2000), the low ratios for RI do not provide support for positive selection. Moreover, these ratios can be overestimated if the GC content in the third codon position is high (Moriyama & Gojobori, 1992; Bielawski *et al.*, 2000). In human RI, the GC content is indeed high, being 79–93%. We conclude that the divergence of the RI exons from one another is unlikely to have been promoted by positive selection.

Why did the RI exons duplicate? There are no known RI homologues that vary in the number of LRR units (Hofsteenge *et al.*, 1988; Lee *et al.*, 1988; Schneider *et al.*, 1988; Kawanomoto *et al.*, 1992; Hofsteenge, 1997). In contrast, other LRR-containing proteins have a variable number of repeats. For example, the tomato *Cf-2* and *Cf-5* genes encode homologues that do differ in LRR unit number (Dixon *et al.*, 1998). Modular mutagenesis of RI has demonstrated that not all of its LRRs are required for binding to RNase A (Lee & Vallee, 1990). In other words, RI progenitors with fewer than the extant number of LRRs could be functional. The contemporary RI could, however, have an increased affinity for a broad spectrum of RNases. The crystalline structures of human RI complexed with angiogenin and porcine RI complexed with RNase A support this hypothesis (Kobe &

Deisenhofer, 1995b; Papageorgiou *et al.*, 1997). These structures reveal that only 17 of the 28 RI residues that contact RNase A also contact angiogenin (Papageorgiou *et al.*, 1997). Yet, the affinity of RI for both angiogenin and RNase A is extreme. The K_d values of the RI·angiogenin and RI·RNase A complexes are near 10^{-15} M, among the lowest for known biomolecular interactions (Lee *et al.*, 1989; Vicentini *et al.*, 1990). High LRR unit number could be critical for the evolution of both broad specificity and high affinity by RI.

RI and RNase have co-evolved. The amino acid sequence of RI has been determined only for the protein from human, pig, rat, and mouse (Hofsteenge *et al.*, 1988; Lee *et al.*, 1988; Schneider *et al.*, 1988; Kawanomoto *et al.*, 1992) (GI = AF071546). In contrast, the amino acid sequence of RNase A homologues has been determined for >40 species, and reveals expansion through gene duplication (Beintema *et al.*, 1997; Beintema, 1998). The binding of RI to members of the RNase A superfamily is class specific. For example, porcine RI binds tightly to human RNase A, but no mammalian RI inhibits the activity of RNase A homologues isolated from frogs, and vice versa (Roth, 1962; Nagano *et al.*, 1976; Tomita *et al.*, 1979; Wu *et al.*, 1993). Likewise, mammalian RI does not inhibit the activity of the RNase A homologue from chicken liver (Hayano *et al.*, 1993). Uninhibited ribonucleolytic activity can result in cell death by the degradation of cellular RNA (Leland *et al.*, 1998; Leland & Raines, 2001). Co-evolution of RI and RNases maintains a safeguard against this circumstance.

The precise exon phasing seen in RI exists in some, but not all, LRR-containing proteins. For example, *Mus musculus* MATER (*M*aternal *A*ntigen *T*hat *E*mbryos *R*equire) has similar phasing. Several of its repeats are encoded by 171-bp exons (Tong *et al.*, 2000). In contrast,

the protein FBL2 contains 6 LRRs, which do not coincide with its exon structure (Ilyin *et al.*, 1999). These examples suggest the independent evolution for the LRR motif and that not all LRR-containing proteins have evolved by exon duplication.

RI has no obvious homologues in invertebrates. Yet, RI does share significant amino acid similarity to other proteins with LRRs. Two such proteins are U2A′ (*vide supra*) and rna1p (Hillig *et al.*, 1999). These proteins are not homologues of RI, but are extremely similar in LRR arrangement and tertiary structure.

The β/α barrel is a common structural scaffold in soluble proteins. Like RI, β/α barrel proteins are formed by an alternating pattern of parallel β-strands and α-helices, with the α-helices situated peripheral to inner β-strands. Members of this group are often enzymes that bind and catalyze the interconversion of small-molecule metabolites (Reardon & Farber, 1995). The versatility of the β/α barrel in enabling protein–small-molecule interactions resembles that of LRRs in enabling protein–protein interactions (Kobe & Deisenhofer, 1994). An investigation of the ancestry of β/α barrels suggests that many β/α proteins have evolved from a stable intermediate—a primordial half-barrel (Lang *et al.*, 2000; Miles & Davies, 2000). In contrast, our data are not consistent with the existence of such an intermediate during the evolution of RI (Figure 2B).

In summary, the intron–exon junctions of RI reveal a remarkable mechanism of molecular evolution by gene duplication. These junctions are precisely in phase with the tandem LRR modules. RI evolved through rapid duplication of its LRR modules and their subsequent divergence. These modules are highly stable and have not homogenized since the divergence of human, pig, and mouse. RI thus acquired a malleable, modular scaffold with which to

mediate protein–protein interactions. We conclude that the accumulation of functional units can be a driving force for exon duplication. Our mechanism for the evolution of RI could also apply to the evolution of the many other proteins containing LRRs, as well as guide the study of modular proteins in general.

Acknowledgements. I thank K.M. Haigis and Drs. N.T. Perna and C. Park for discussion and critical reading of the manuscript, and Dr. A.M. Dean for a helpful suggestion.

Figure 5.1 Correlation of the exons of human ribonuclease inhibitor with its LRR units. (A) Ribbon diagram of RI was created using the atomic coordinates derived by x-ray diffraction analysis (Papageorgiou *et al.*, 1997) and the program MOLSCRIPT (Kraulis, 1991). Each exon-encoded sequence is in a different color. The N- and C-termini are labeled. (B) Same as (A), except rotated by ~90° around the horizontal axis. (C) Physical map of the human RI gene. Alternate forms isolated from placenta, HeLa cells, and testes are depicted as RIα, RIβ, and RIγ, respectively. Exons and introns are drawn to scale. Start and stop codons are indicated. Exon colors match those of exon-encoded sequences in (A) and (B).

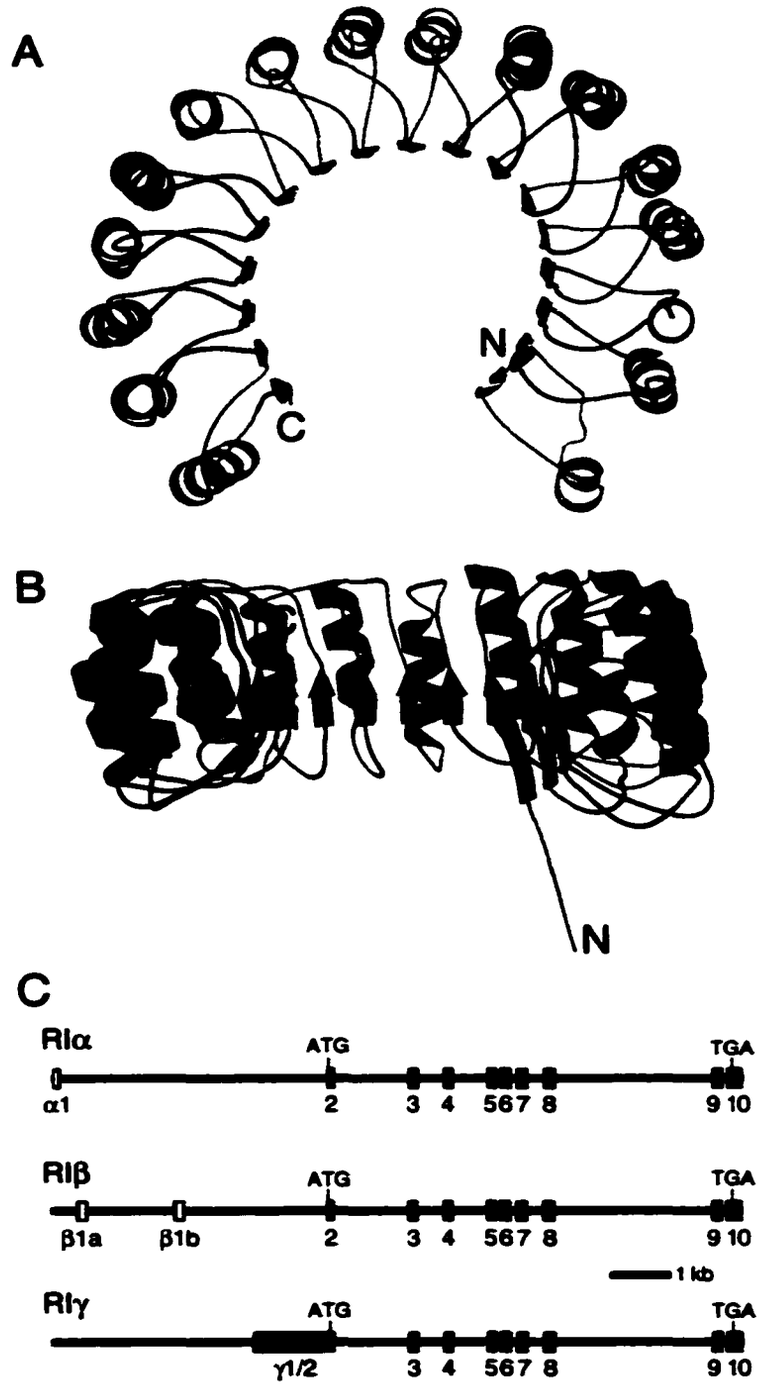
A
N
C
B
N
C
RIα
ATG
TGA
α1
2
3 4
567 8
9 10
RIβ
ATG
TGA
β1a
β1b
2
3 4
567 8
9 10
1 kb
RIγ
ATG
TGA
γ1/2
3 4
567 8
9 10

Figure 5.2 Analysis of the internal exon sequences of ribonuclease inhibitor. (A) An alignment of DNA sequences that corresponds to each internal exon from human (h), pig (p), and mouse (m) was generated with the program PILEUP. Sequences are listed in order of decreasing identity. Nucleotides present in at least 10 of 21 exons are in black boxes. (B) A neighbor-joining tree for all codon positions in *A* was generated from the first and second codon positions with the PAUP program (Swofford, 1998) using a Kimura 2-parameter correction. Bootstrap values are indicated at the nodes. The bar indicates the distance for 0.1 nucleotide substitutions per site for the 171 positions of RI.

A

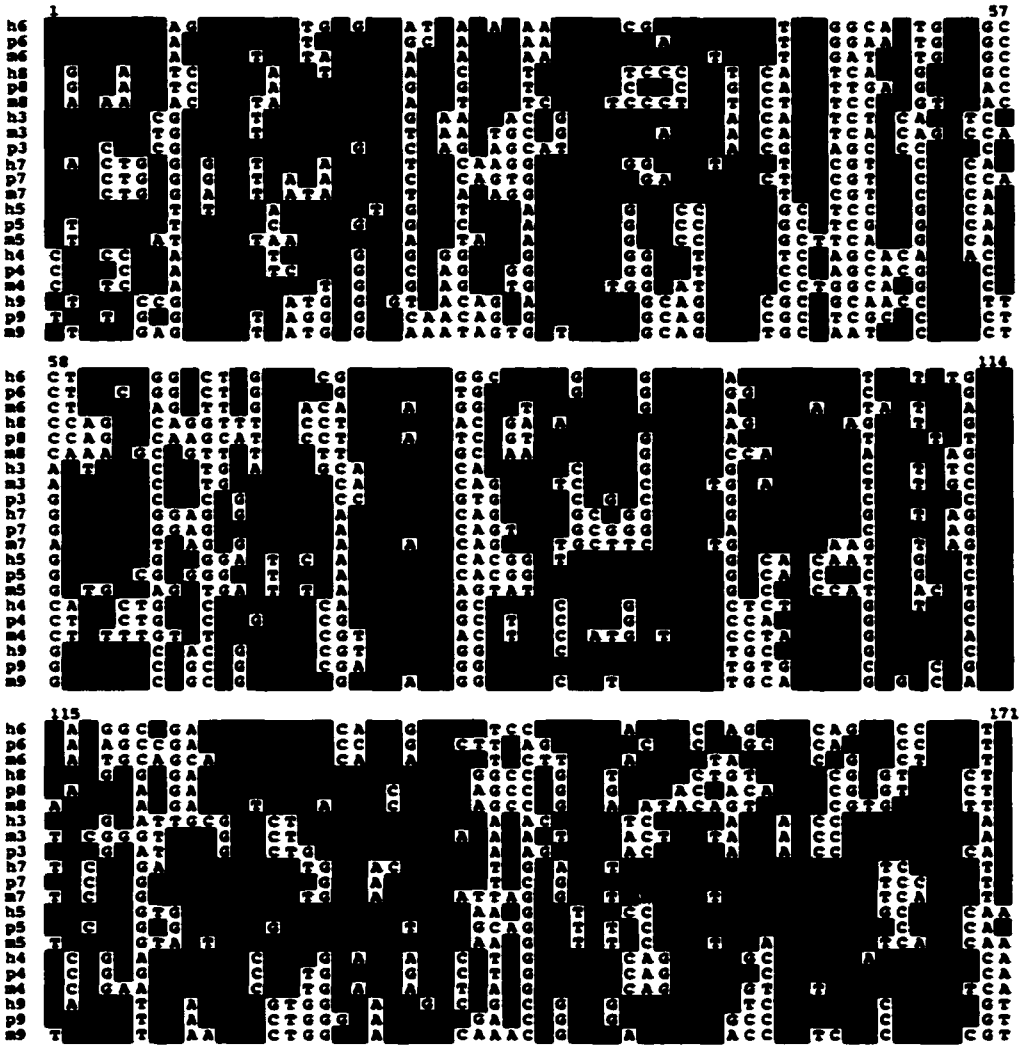

B

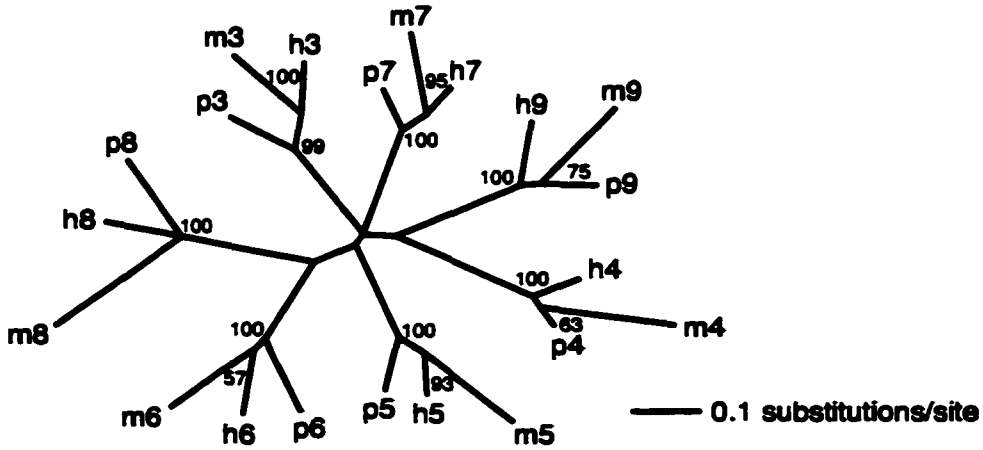
m7
m3
h3
100
p7
95
h7
p3
99
100
h9
m9
p8
100
75
p9
h8
100
100
h4
m8
100
63
m4
p4
100
57
93
m6
h6
p6
p5
h5
m5
0.1 substitutions/site

Chapter 6

Targeted Gene Disruptions of *Rib1* and *Rnh*

ABSTRACT

Bovine pancreatic ribonuclease (RNase A) is a model protein for the study of enzyme catalysis, protein folding stability, and protein engineering. Ribonuclease inhibitor (RI) is a cytosolic protein that inhibits the activity of RNase A and several of its mammalian homologues. Despite the wealth of information on the *in vitro* activities of pancreatic ribonucleases and RI, little is known about their physiological functions. Here, I investigate the physiological roles of mouse pancreatic ribonuclease (Rib1) and RI (Rnh). I have created targeting constructs to replace the first coding exons of *Rib1* and *Rnh* with a *Neomycin phosphotransferase* (*Neo*) resistance gene. These constructs were used to generate targeted gene disruptions of *Rib1* and *Rnh* in murine embryonic stem cells. The correctly targeted stem cells will lead to the creation of nullizygous animals, which will provide important information on the *in vivo* function of pancreatic ribonuclease and RI.

INTRODUCTION

Pancreatic ribonuclease. The ribonucleolytic activity of bovine pancreatic ribonuclease (RNase A) and its homologues has unexpected biological manifestations (for reviews, see: D'Alessio, 1993; Schein, 1997; Youle & D'Alessio, 1997; Irie *et al.*, 1998; Rybak & Newton, 1999; Leland & Raines, 2001; Matousek, 2001). For example, high concentrations of RNase A are toxic to tumor cells growing in culture (Ledoux, 1955a; Ledoux, 1955b), or when injected directly into NIH/3T3 cells (Smith *et al.*, 1999). RNase 1, the human homologue of RNase A, kills Kaposi's sarcoma cells *in vitro* (Griffiths *et al.*, 1997). Bovine seminal ribonuclease, a dimeric homologue, also has antitumor and antispermatogenic properties (Matousek, 2001). Angiogenin, another member of the RNase A superfamily, promotes neovascularization in a variety of *in vitro* assays (Fett *et al.*, 1985), and is cytotoxic to some cell types (Matousek *et al.*, 1995).

Despite the growing information on pancreatic ribonucleases, their biological purpose remains a mystery. In 1969, Barnard proposed that pancreatic ribonucleases function physiologically as a dietary aid (Barnard, 1969). Yet, levels of RNase A do not change with food consumption. In humans, pancreatic ribonuclease (RNase 1) is expressed in nearly all tissues, except peripheral blood leukocytes (Futami *et al.*, 1997; Sasso *et al.*, 1999). In addition, RNase 1 protein has been found in the seminal plasma (De Prisco *et al.*, 1984; Sorrentino *et al.*, 1989), and urine (Iwama *et al.*, 1981). The diverse distribution of RNase 1 is particularly curious because of the paucity of extracellular RNA in these locations.

Pancreatic ribonucleases are secretory proteins, and may exert a biological effect in tissues where they are not expressed. Therefore, to completely investigate the biological role of pancreatic ribonuclease, it must be studied in an organism. The only existing ribonuclease knockout animal has a disruption in its *RNase L* gene (Zhou *et al.*, 1997). RNase L, which is not a member of the RNase A superfamily, functions in the interferon-inducible RNA-decay pathway. *RNase* $L^{-/-}$ mice demonstrate an impairment in interferon α response against encephalomyocarditis virus and have suppressed apoptosis in the thymus.

Ribonuclease inhibitor. Ribonuclease inhibitor (RI) is a 50-kDa cytosolic protein that binds and thereby inactivates the pancreatic-type ribonucleases in a 1:1 stoichiometric complex (Blackburn *et al.*, 1977). Human RI binds RNase A, RNase 1, and angiogenin with fM affinity (for review, see: Hofsteenge, 1997). Interestingly, RI does not bind to all pancreatic-type ribonucleases in exactly the same manner, but uses somewhat different intermolecular contacts (Papageorgiou *et al.*, 1997; Chen & Shapiro, 1999). RI may also interact with eosinophil cationic protein and eosinophil-derived neurotoxin, which are homologues of RNase A found in secretory granules of eosinophils.

RI is found in all cells (Hofsteenge, 1997). The mRNA for RI is also ubiquitously expressed in all tissues (Futami *et al.*, 1997). The subcellular location of RI, beyond the cytosol, has not been established. Because of the close, regulatory relationship with ribonucleases, a more complete understanding of ribonuclease inhibitor function would provide insight into the biological roles of the ribonucleases, themselves.

Here, we use reverse genetics to determine the physiological roles of mouse pancreatic ribonuclease (Rib1) and the mouse ribonuclease inhibitor (Rnh) proteins. We hypothesize that the role of Rib1 may extend beyond being a digestive aid. We hypothesize that Rnh will function *in vivo* to regulate multiple pancreatic-type ribonucleases. To test these hypotheses, we created targeted gene disruptions within *Rib1* and *Rnh* in murine embryonic stem cells. These cells are precursors to experiments in nullizygous animals.

MATERIALS AND METHODS

Cloning of murine Rib1 genomic fragments. We isolated a *Rib1* cDNA from an EST library (Research Genetics; Huntsville, AL), and verified its identity through sequence analysis. This cDNA was used as a probe to identify a clone containing the *Rib1* genomic locus from a mouse 129/SvJ lambda phage library (Stratagene; La Jolla, CA). The cDNA probe was used to clone a 6.6 kb-SacI fragment containing the *Rib1* genomic locus. Characterization of this clone revealed that it contained mostly 3′ genomic sequence.

To obtain a 5′ genomic clone, PCR primers were designed from *Rib1* genomic sequence data (Samuelson *et al.*, 1991) and had the following sequences: MHa (5′ GTGTAAGGAAGCTGAGGTGGGAGAG 3′) and MHb (5′ GGATCCATGTGCTGCCGCTGAAACTTC 3′). These primers were used to screen a mouse 129/SvEv bacteria artificial chromosome (BAC) library (Genome Systems; St. Louis, MI). The resulting PCR product was used to identify and subclone a 6.6 kb-*Eco*RI fragment that contained the 5′ region of the *Rib1* locus.

Rib1 targeting constructs. The *Rib1* targeting constructs (pRib1-TC and pRib1-TC2) were prepared from the 6.6 kb-*Eco*RI and *Sac*I fragments. The targeting constructs were designed to replace the entire *Rib1* coding region, contained in exon 2, with the *Neomycin phosphotransferase* (*Neo*) resistance gene cassette. The original vector plasmid, pPNT-3, also contained the gene encoding herpes simplex virus thymidine kinase (*TK*) for negative selection during gene targeting (University of Wisconsin–Madison Transgenic Animal Facility).

Cloning of an Rnh genomic fragment. PCR primers were designed from *Rnh* cDNA sequence data (Blake *et al.*, 1997) and had the following sequences: MHRI7 (5′ GGTGCAAAGACATCAGCTCAGCAGTCCAAGC 3′) and MHRI5 (5′ CCTGGAGCACCAGACCCACACC 3′). These primers were used to screen a mouse 129/SvEv BAC library (Genome Systems; St. Louis, MI). This PCR fragment was used to subclone a 6.3 kb-*Hin*dIII fragment, which contained exons 2 and 3 of the *Rnh* locus. A 3′ *Sac*I fragment was used to identify and clone a 4.4 kb-*Bgl*II fragment, which contained more genomic sequence 3′ of exon 3.

Fluorescent in situ hybridization on karyotypes. Fluorescent *in situ* hybridization (FISH) was performed on mouse NIH3T3 cells using the *Rnh* BAC probe using a protocol developed by KM Haigis. To obtain metaphase karyotypes, cells were grown in DMEM, containing fetal bovine serum (FBS; 10% v/v), until they were 70% confluent. At this point, the medium was replaced with fresh medium containing colchicine (5 μg/ml). Plates were incubated for 30 min at 37 °C. Cells were harvested by trypsin treatment and centrifugation at 400 × *g* for 10 min. The supernatant was removed, and 2–3 ml of KCl (75 mM) was added. The cells

were resuspended gently and incubated for 30 min at 37 °C. Cells were prefixed by adding 5 drops of fixative (methanol:acetic acid, 3:1 v/v). After 10 min at room temperature, cells were harvested by centrifugation at 500 × *g* for 10 min. The resulting cell pellet was resuspended gently in 3–4 ml of fixative and incubated at room temperature for 30 min. Cells were run over a charged microscope slide (Fisher Scientific; Pittsburgh, PA) and air dried.

After generating karyotypes, microscope slides were soaked in 2X standard saline citrate (SSC) for 30 min at 37 °C. 1X SSC, pH 7.0, contains (in 1.00 liter) NaCl (8.76 g) and sodium citrate (4.41 g). Then, the samples were dried at room temperature through a series of 2 min incubations in 70, 80, 90, and 100% (v/v) ethanol. Samples were denatured for 3 min at 72 °C in 70% formamide (w/v in 2X SSC), and dried down again through an ice cold ethanol series. BAC Probes were labeled with digoxygenin using a DIG Nick translation kit from Roche Molecular Biochemicals (Mannheim, Germany). Probes were prewarmed to 37 °C, added to samples, and then incubated at 37 °C overnight. The slides were then washed by incubating twice with 2X SSC and twice with 0.1X SSC for 10 min each at 60 °C. Slides were incubated for 15 min at 37 °C with FITC anti-digoxygenin, followed by incubations with AlexaFluor 488 anti-FITC, and then AlexaFluor 488 goat anti-rabbit. Fluorescent antibodies were from Molecular Probes (Eugene, OR). Between incubations, the slides were washed at 37 °C with 1X phosphate-buffered detergent, which is PBS containing IGEPAL-630 (0.1% v/v). Then samples were counterstained with DAPI (1 μg/ml). Samples were visualized with a Zeiss Aviovert 100TV microscope.

Rnh targeting construct. The *Rnh* targeting construct (pRnh-TC) was prepared from the 6.3 kb-*Hin*dIII and 4.4 kb *Bgl*II fragments. The targeting construct was designed to replace

exon 2, which contains the start codon, with *Neo*. pRnh-TC also contained *TK* downstream of the 3′ homology region.

Cell culture. Low-passage murine AB2.2 embryonic stem (ES) cells, derived from 129/SvEv (Simpson *et al.*, 1997), were obtained from Stratagene (La Jolla, CA). SNLP (STO mice, Neomycin resistant, LIF secreting, Puromycin resistant) cells were the generous gift of J. Petrini (Madison, WI). SNLP cells were cultured in DMEM with newborn calf serum (NBCS; 10% v/v). SNLP cells were inactivated by a 4-h incubation with mitomycin C (MMC, 0.01 mg/ml; Sigma-Aldrich; St. Louis, MO). After incubation, cells were washed with phosphate-buffered saline (PBS), which contained (in 1.00 liter) KCl (0.20 g), KH_2PO_4 (0.20 g), NaCl (8.0 g), and Na_2HPO_4 (2.16 g). Cells were trypsin-treated, and plated onto gelatinized plates at a density of 2–3 × 10^5 cells/ml. ES cells were cultured in DMEM, which contained FBS (15% v/v), leukemia inhibitory factor (LIF; 1% v/v), β-mercaptoethanol (5 μl/500 ml), and L-glutamine (2 mM). ES cells were grown on a layer of 1–7-day-old inactivated feeders, and ES medium was refreshed every day. FBS was from HyClone (Logan, UT). LIF was a generous gift of J. Petrini. All other cell culture reagents were from Life Technologies (Gaithersburg, MD). Cells were cultured at 37 °C in a humidified incubator containing CO_2 (g; 5% v/v).

Embryonic stem cell transformation. ES cells (1.0 × 10^7 cells in 0.8 ml of PBS) were electroporated with linearized targeting vector (25 μg). For transfections, DNA was purified using a Qiagen Plasmid Midi Kit (Valencia, CA). Cells were electroporated with a Gene Pulser (Bio-Rad; Hercules, CA) using a 500-μF capacitor charged to 230 V. The cells were then plated on MMC-inactivated feeder cells in 10-cm tissue culture plates. 24-h after

electroporation, the medium was replaced with ES medium containing G418 (230 μg/ml) and ganciclovir (2 μg/ml). Clones resistant to both drugs were isolated after 10 days of selection. These clones were individually dispersed into the wells of a 96-well plate and grown without selection for 3 days. The cells were split into duplicate plates. Half of the cells were frozen at –80 °C, while the remaining cells were analyzed for the homologous recombination event. To confirm the targeting event, Southern blot analysis was performed on ES cell genomic DNA with various restriction enzymes and probes.

RESULTS

Disruption of Rib1 by gene targeting. The mouse genome does not contain *Rib1* psuedogenes (Samuelson *et al.*, 1991). Sequence analysis verified that the fragments subclones from the genomic libraries contained the *Rib1* genomic locus (data not shown). The targeting constructs were designed to remove the entire *Rib1* coding sequence, which is in exon 2 (Figure 6.1A), and should prevent Rib1 protein production. The pRib1-TC construct contained a 5′ homology region subcloned from a 1.3 kb-*Nhe*I–*Nco*I fragment. The 3′ homology region was the 2.4 kb-*Hin*dIII fragment. The linearized construct (pRib1-TC) was electroporated into murine AB2.2 cells, and drug resistant colonies were isolated. Southern blot analysis was performed with genomic DNA from expanded colonies using an *Eco*RI restriction digest and a probe upstream of the 5′ homology region. In a total of 918 clones, 0 were targeted correctly (data not shown).

The *Rib1* targeting construct was redesigned to have a 5 kb-longer 5′ homology region (pRib1-TC2) (Figure 6.1A). pRib1-TC2 was linearized by *Not*I and transfected into murine AB2.2 cells, and drug resistant colonies were obtained. Targeted cells were identified by Southern blot analysis of genomic DNA from expanded colonies using a *Sac*I restriction digest and a probe downstream of the 3′ homology region. In a total of 176 clones, 3 were targeted correctly. Figure 6.1B shows a Southern blot with a positive clone that is flanked by two negative clones.

Disruption of Rnh by gene targeting. The murine *Rnh* genomic locus had not been characterized prior to the experiments discussed in Chapter 5. An initial library screen with primers that spanned the coding region of *Rnh* identified an *Rnh* pseudogene, which did not contain introns, but contained a premature stop codon. In addition, the *Rnh* pseudogene did not retain the leucine-rich consensus sequence that is strictly adhered to by mammalian homologues of RI (see Chapter 5). The BAC library was rescreened with the primers MHRI7 and MHRI5, which amplified exon 3 in *Rnh*, but did not amplify the psuedogene (data not shown). FISH analysis using the new BAC clone showed that it hybridized to mouse chromosome 7 (Figure 6.2), as predicted, because *Rnh* is located on human chromosome 11 (Weremowicz *et al.*, 1990; Zneimer *et al.*, 1990). The *Rnh* pseudogene and genomic locus were accounted for by genomic Southern blot analysis using cDNA fragments (data not shown).

The strategy used to disrupt the murine *Rnh* gene was to replace the first coding exon with *Neo* (Figure 6.3A). This deletion removes the translational start codon along with the first 29 residues, and should prevent Rnh protein production. The targeting construct was

linearized by *Not*I and electroporated into murine AB2.2 cells; drug resistant colonies were isolated. Targeted cells were identified by Southern blot analysis of genomic DNA from expanded colonies using a *Hin*dIII restriction digest and a probe upstream of the 5′ homology region. In a total of 288 clones, 9 were targeted correctly. Figure 6.3B shows a Southern blot with a positive clone next to two negative clones.

DISCUSSION

The creation of a *Rib1* or *Rnh* null animal can be divided into a few major steps (for reviews, see: (Capecchi, 1989; Melton, 1994; Bradley *et al.*, 1998). First, a targeting vector is created to generate a null allele. Second, embryonic stem (ES) cells, derived from the inbred mouse strain 129/SvEv, are transformed by electroporation with the targeting construct, and clones are screened for homologous recombination events by Southern blot analysis. Next, the positive clones are microinjected into C57BL/6 embryos and chimeric animals are screened for germline transmission of the targeted allele. Once germline chimeric animals are identified, chimeras are crossed with 129/SvEv animals to obtain heterozygous mice. These animals can be intercrossed to generate null animals on an isogenic background.

The frequency of homologous recombination is dependent on sequence identity and the length of homology. Homologous recombination occurs with a 20-fold higher frequency when isogenic versus non-isogenic homology regions are used in the targeting construct (te Riele *et al.*, 1992; van Deursen & Wieringa, 1992). The pRnh-TC construct was derived from a 129/SvEv genomic library. The pRib1-TC and pRib1-TC2 constructs were derived from

129/SvJ and 129/SvEv genomic libraries, respectively. Likewise, AB2.2 ES cells were derived from 129/SvEv mice (Soriano *et al.*, 1991). The 129/SvEv and 129/SvJ strains do differ (Simpson *et al.*, 1997), and may have contributed to the low targeting frequency of pRib1-TC.

The frequency of recombination events in murine ES cells is a function of the length of the homologous DNA (Hasty *et al.*, 1991; Deng & Capecchi, 1992). Bradley and co-workers found that targeting efficiency increased dramatically as the total length of the homology region was increased from 1–7 kb (Hasty *et al.*, 1991). The targeting constructs, pRib1-TC and pRib1-TC2, had identical 3′ homology domains but differed in the length of their 5′ genomic DNA. pRib-TC had only 1.3 kb of 5′ genomic sequence, and had a 0% recombination frequency. In contrast, pRib1-TC2 had 6.3 kb of 5′ genomic sequence, and had a recombination frequency of 1.7% (3/176). Thus, a difference of 5 kb at the 5′ homology region allowed for successful recombination events.

Presently, the positive clones identified herein are being expanded for further characterization. The clones that are the least differentiated will be injected into early embryos using facilities at the University of Wisconsin–Madison Transgenic Animal Facility. These experiments will lead to the generation of animals that do not produce pancreatic ribonuclease or RI. Studies using these mice will provide the first insight into the biological functions of pancreatic ribonuclease and RI.

Acknowledgements. I thank Dr. J. Petrini for use of tissue culture facilities. I thank Dr. J.Petrini and C.F. Bender for guidance and instruction of ES cell culture. I thank Dr. P.A.

Powers for technical support during construction of the *Rib1* targeting construct. I thank K.M. Haigis for help with FISH.

Figure 6.1 Targeted gene disruption of *Rib1*. (A) Targeting vector pRib1-TC2 was constructed by using the pNT-3 vector (University of Wisconsin–Madison Transgenic Animal Facility). A 6.3-kb 5′ homology unit was inserted upstream of *Neo*, and a 2.4-kb 5′ homology unit was inserted downstream of *Neo*. *Neo* will act as a positive selector for recombined clones. *TK* will act as a negative selector to prevent the growth of clones with random, non-homologous insertions within the genome. (B) The DNA from embryonic stem cell colonies was digested with *Sac*I and screened for homologous recombination with a 3′ probe. Colonies that were not targeted (lanes 1 and 3) had a single band at 6.6 kb. A correctly targeted allele (lane 2) was identified by its additional 3.9-kb band.

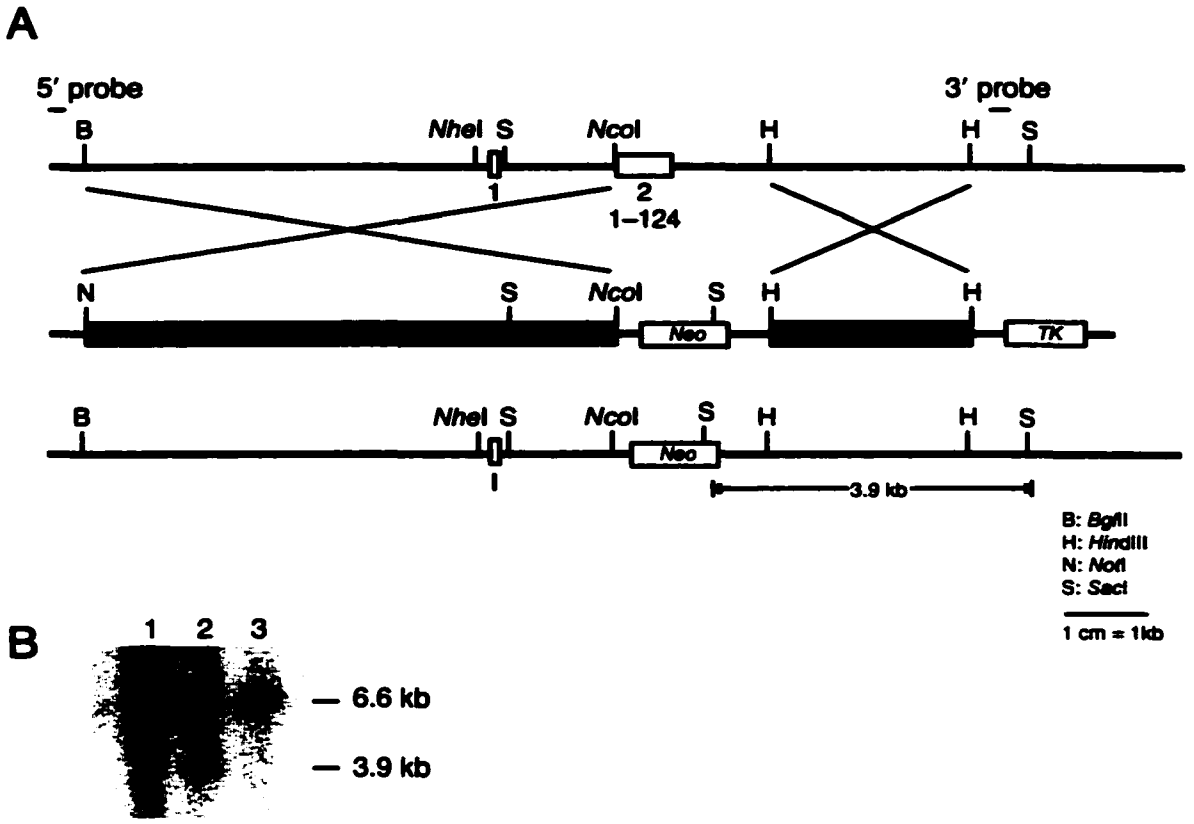
A
5′ probe
3′ probe
B
NheI S
NcoI
H
H S
1
2
1–124
N
S
NcoI
S
H
H
Neo
TK
B
NheI S
NcoI
S
H
H S
Neo
I
3.9 kb
B: BglII
H: HindIII
N: NotI
S: SacI
1 cm = 1kb
B
1 2 3
6.6 kb
3.9 kb

Figure 6.2 Fluorescent *in situ* hybridization of *Rnh*. The *Rnh* BAC clone was used as a FISH probe on metaphase karyotypes from NIH3T3 cells, which are triploid. The *D7Mit145* BAC clone was used as a positive control for chromosome 7.

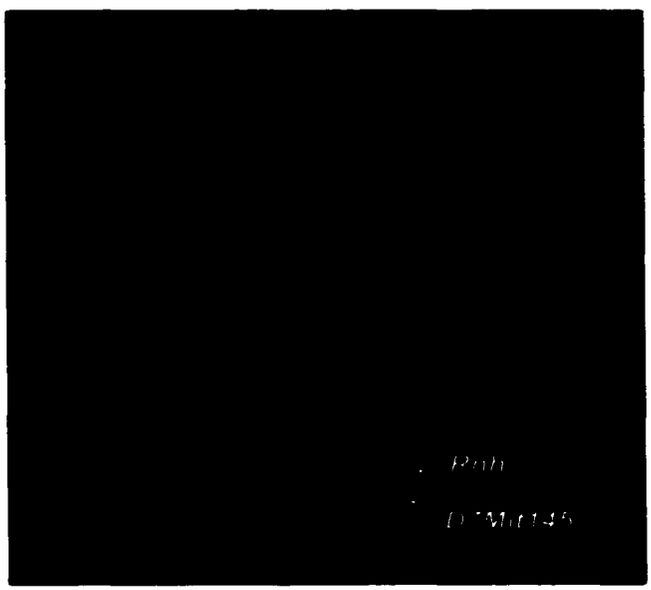

Figure 6.3 Targeted gene disruption of *Rnh*. (A) Targeting vector pRnh-TC was constructed by using the pNT-3 vector. A 3.0-kb 5′ homology unit was inserted upstream of *Neo*. A 4.4-kb 3′ homology unit was inserted downstream of *Neo*. (B) DNA from embryonic stem cell colonies was digested with *Hin*dIII and screened for homologous recombination with a 5′ probe. Colonies that were not targeted (lanes 2 and 3) had a single band at 6.4 kb. A correctly targeted allele (lane 1) was identified by its additional 3.9-kb band.

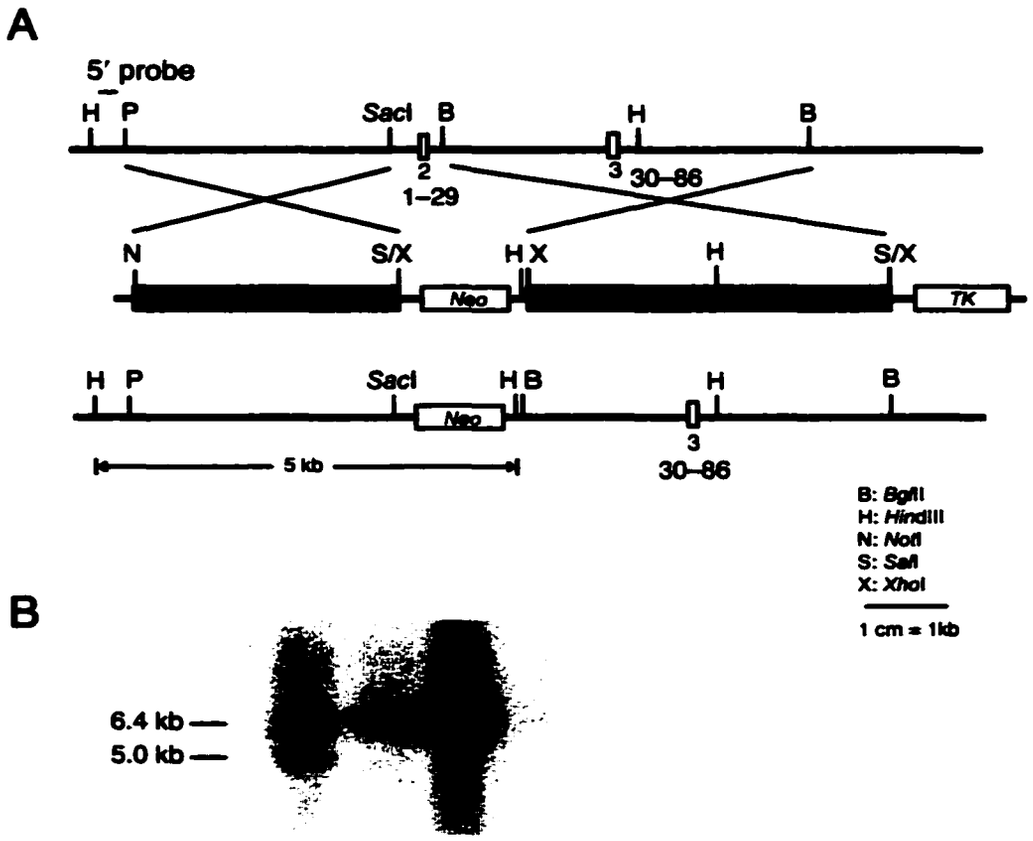
A
5′ probe
H P
SacI B
H
B
2
1–29
3
30–86
N
S/X
H X
H
S/X
Neo
TK
H P
SacI
H B
H
B
Neo
3
30–86
5 kb
B: BglII
H: HindIII
N: NotI
S: SalI
X: XhoI
1 cm = 1kb
B
6.4 kb
5.0 kb

Chapter 7

Prospectus

In the 1940's, Armour, Inc. prepared 1 kg of crystalline bovine pancreatic ribonuclease A (RNase A). In 1967, the crystalline structure of RNase A was solved (Kartha *et al.*, 1967; Wyckoff *et al.*, 1967), and Barnard wrote in response: "The [ribonuclease] field will never be the same again" (Barnard, 1969a). Indeed, the abundance of purified RNase A available in the 1940's, along with this structural information set the stage for prolific structure and function studies using RNase A. The advent of DNA technology, and the cloning and purification of recombinant RNase A marked a new era in RNase A research. RNase A is now, arguably, the most characterized enzyme. Today, scientists continue to use RNase A as a tool for understanding other fields, such as evolution, protein chemistry, and cell biology. For example, Ritter and Helenius used the structural knowledge of RNase S and S-peptide as a basis for designing elegant experiments to investigate the recognition of misfolded proteins in the endoplasmic reticulum (Ritter & Helenius, 2000).

In a 1969 review, Barnard wrote, "Bovine pancreatic RNase, on the other hand, has yielded many of its secrets...it seems inevitable that the main interest in RNase will shift to other proteins having this activity"(Barnard, 1969a). Yet, more than thirty years later, scientists are still coaxing RNase A to reveal its secrets. As discussed in Chapter 6, the biological role of pancreatic ribonuclease remains unresolved. The rediscovery of the antitumor potential of ribonucleases, has reawakened the question: what is the physiological function of ribonucleases? The biological role historically ascribed as a digestive aid is no longer satisfactory, as the experiments in Chapter 2 reveal that ribonucleases are readily internalized by cells. The physiological role of ribonuclease inhibitor (RI) is even more intriguing, as RI functions *in vitro* to regulate many ribonucleases. The experiments in

Chapter 6 describe efforts that will lead to the creation of *Rnh* and *Rib1* knockout mice. The *Rnh* nullizygous mice will hold clues to the physiological roles of the pancreatic-type ribonucleases, as well as that of RI. Likewise, *Rib1*$^{-/-}$ animals could provide insight into the role of RI.

The rich history of pancreatic-type ribonucleases will enable unprecedented structure–function studies, where function is not limited to the walls of a cuvette. In future experiments, the biochemical information of pancreatic ribonucleases can be used to probe specific enzymatic activities *in vivo*. For example, replacing Lys41 of RNase A with an alanine residue is known to reduce the k_{cat}/K_M value by 10^4(Messmore *et al.*, 1995), and this substitution can be used to create hypomorph alleles of *Rib1* which have decreased ribonucleolytic activity *in vivo*. Our understanding of RNase A conformational stability could allow scientists to create transgenic mice with a destabilized (or more stabilized) ribonuclease, of known T_m value. Cytotoxic variants of RNase A, such as K7A/G88R RNase A (Chapter 3) (Haigis *et al.*, 2002b), could be utilized to create mice with pancreatic-type ribonucleolytic activity that is not tightly regulated by RI.

Likewise, the growing wealth of information on RI will be useful in structure–function studies. As discussed in Chapter 4, RI can modulate the intracellular activity of a ribonuclease (Haigis *et al.*, 2002c). As expected from its modular gene structure (Chapter 5) (Haigis *et al.*, 2002a), truncated variants of RI can still bind ribonucleases, but perhaps with weakened affinity (Lee & Vallee, 1990; Hofsteenge *et al.*, 1991). As we predict the phenotype of RI nullizygous animals to be severe, even lethal, a truncated RI variant could be used to create viable animals that have attenuated RI function. RI uses different residues

to bind RNase A than it does to bind angiogenin (ANG) (Shapiro *et al.*, 2000). This information can be useful for understanding the biological role of ANG, as the creation of an *Ang* knockout animal has been impeded by its many pseudogenes (Brown *et al.*, 1995). Variants of RI can be made that resist oxidation (Kim *et al.*, 1999), and these substitutions could be used to create mice that have a more redox-stable RI. The characterization of the *Rib1* and *Rnh* knockout animals could lead to a new era of ribonuclease study—one that explores and exploits its *in vivo* function.

Chapter 8

References

References

Abel, R. A., Haigis, M. C., Park, C. & Raines, R. T. (2002). Fluorescence assay for the binding of ribonuclease A to its cytosolic inhibitor protein. *Submitted.*

Agarraberes, F. A., Terlecky, S. R. & Dice, J. F. (1997). An intralysosomal hsp70 is required for a selective pathway of lysosomal protein degradation. *J. Cell Biol.* **137**, 825-834.

Anfinsen, C. B. (1973). Principles that govern the folding of protein chains. *Science* **181**, 223-230.

Antignani, A., Naddeo, M., Cubellis, M. V., Russo, A. & D'Alessio, G. (2001). Antitumor action of seminal ribonuclease, its dimeric structure, and its resistance to the cytosolic ribonuclease inhibitor. *Biochemistry* **40**, 3492-3496.

Ardelt, W., Mikulski, S. M. & Shogen, K. (1991). Amino acid sequence of an anti-tumor protein from *Rana pipiens* oocytes and early embryos. *J. Biol. Chem.* **266**, 245-251.

Barnard, E. A. (1969a). Biological function of pancreatic ribonuclease. *Nature* **221**, 340-344.

Barnard, E. A. (1969b). Ribonucleases. *Annu. Rev. Biochem.* **38**, 677-732.

Beintema, J. J. (1998). The ribonuclease A superfamily. *Cell. Mol. Life Sci.* **54**, 763-765.

Beintema, J. J., Breukelman, H. J., Carsana, A. & Furia, A. (1997). Evolution of vertebrate ribonucleases: ribonuclease A superfamily. In *Ribonucleases: Structures and Functions* (D'Alessio, G. & Riordan, J. F., eds.), pp. 245-269. Academic Press, New York.

Beintema, J. J. & Kleineidam, R. G. (1998). The ribonuclease A superfamily: general discussion. *Cell. Mol. Life Sci.* **54**, 825-832.

Beintema, J. J., Schüller, C., Irie, M. & Carsana, A. (1988). Molecular evolution of the ribonuclease superfamily. *Prog. Biophys. Molec. Biol.* **51**, 165-192.

Bielawski, J. P., Dunn, K. A. & Yang, Z. (2000). Rates of nucleotide substitution and mammalian nuclear gene evolution. Approximate and maximum-likelihood methods lead to different conclusions. *Genetics* **156**, 1299-1308.

Blackburn, P. & Moore, S. (1982). Pancreatic ribonuclease. *The Enzymes* **XV**, 317-433.

Blackburn, P., Wilson, G. & Moore, S. (1977). Ribonuclease inhibitor from human placenta. Purification and properties. *J. Biol. Chem.* **252**, 5904-5910.

Blake, J. A., Richardson, J. E., Davisson, M. T. & Eppig, J. T. (1997). The Mouse Genome Database (MGD). A comprehensive public resource of genetic, phenotypic and genomic data. The Mouse Genome Informatics Group. *Nucleic Acids Res.* **25**, 85-91.

Blázquez, M., Fominaya, J. M. & Hofsteenge, J. (1996). Oxidation of sulfhydryl groups of ribonuclease inhibitor in epithelial cells is sufficient for its intracellular degradation. *J. Biol. Chem.* **271**, 18638-18642.

Boix, E., Nogués, M. V., Schein, C. H., Benner, S. A. & Cuchillo, C. M. (1994). Reverse transphosphorylation by ribonuclease A needs an intact p_2-binding site. *J. Biol. Chem.* **269**, 2529-2534.

Boix, E., Wu, Y., Vasandani, V. M., Saxena, S. K., Ardelt, W., Ladner, J. & Youle, R. J. (1996). Role of the N terminus in RNase A homologues: differences in catalytic activity, ribonuclease inhibitor interaction and cytotoxicity. *J. Mol. Biol.* **257**, 992-1007.

Bond, M. D., Strydom, D. J. & Vallee, B. L. (1993). Characterization and sequencing of rabbit, pig and mouse angiogenins: discernment of functionally important residues and regions. *Biochim. Biophys. Acta* **1162**, 177-186.

Botella-Estrada, R., Malet, G., Revert, F., Dasi, F., Crespo, A., Sanmartin, O., Guillen, C. & Alino, S. F. (2001). Antitumor effect of B16 melanoma cells genetically modified with the angiogenesis inhibitor rnasin. *Cancer Gene Ther.* **8**, 278-284.

Bradford, M. M. (1976). A rapid an sensitive method for the quantitation of micrograms quantities of protein utilizing the principle of protein-dye binding. *Anal. Biochem.* **72**, 248-252.

Bradley, A., Zheng, B. & Liu, P. (1998). Thirteen years of manipulating the mouse genome: a personal history. *Int. J. Dev. Biol.* **42**, 943-950.

Bretscher, L. E., Abel, R. L. & Raines, R. T. (2000). A ribonuclease A variant with low catalytic activity but high cytotoxicity. *J. Biol. Chem.* **275**, 9893-9896.

Brown, W. E., Nobile, V., Subramanian, V. & Shapiro, R. (1995). The mouse angiogenin gene family: structures of an angiogenin-related protein gene and two pseudogenes. *Genomics* **29**, 200-206.

Cao, H., Thompson, H. M., Krueger, E. W. & McNiven, M. A. (2000). Disruption of Golgi structure and function in mammalian cells expressing a mutant dynamin. *J. Cell Sci.* **113**, 1993-2002.

Capecchi, M. R. (1989). Altering the genome by homologous recombination. *Science* **244**, 1288-1292.

Chen, C. Z. & Shapiro, R. (1999). Superadditive and subadditive effects of "hot spot" mutations within the interfaces of placental ribonuclease inhibitor with angiogenin and ribonuclease A. *Biochemistry* **38**, 9273-9285.

Collier, R. J. (2001). Understanding the mode of action of diphtheria toxin: a perspective on progress during the 20th century. *Toxicon* **39**, 1793-1803.

Crawford, D., Hagerty, K. & Beutler, B. (1989). Multiple splice forms of ribonuclease-inhibitor mRNA differ in the 5'- untranslated region. *Gene* **85**, 525-531.

Cubitt, A. B., Heim, R., Adams, S. R., Boyd, A. E., Gross, L. A. & Tsien, R. Y. (1995). Understanding, improving and using green fluorescent proteins. *Trends Biochem. Sci.* **20**, 448-455.

Cuchillo, C. M., Vilanova, M. & Nogues, M. V. (1997). Pancreatic Ribonucleases. In *Ribonucleases: Structures and Functions* (D'Alessio, G. & Riordan, J. F., eds.), pp. 271-304. Academic Press, New York.

Cuervo, A. M. & Dice, J. F. (1998). Lysosomes, a meeting point of proteins, chaperones, and proteases. *J. Mol. Med.* **76**, 6-12.

D'Alessio, G. (1993). New and cryptic biological messages from RNases. *Trends Cell Biol.* **3**, 106-109.

D'Alessio, G., Di Donato, A., Mazzarella, L. & Piccoli, R. (1997). Seminal ribonuclease: the importance of diversity. In *Ribonucleases: Structures and Functions* (D'Alessio, G. & Riordan, J. F., eds.), pp. 383-423. Academic Press, New York.

D'Alessio, G., Di Donato, A., Parente, A. & Piccoli, R. (1991). Seminal RNase: a unique member of the ribonuclease superfamily. *Trends Biochem. Sci.* **16**, 106-108.

D'Alessio, G. & Riordan, J. F., Eds. (1997). *Ribonucleases: Structures and Functions*. New York: Academic Press.

Damke, H., Baba, T., van der Bliek, A. M. & Schmid, S. L. (1995). Clathrin-independent pinocytosis is induced in cells overexpressing a temperature-sensitive mutant of dynamin. *J. Cell. Biol.* **131**, 69-80.

Damke, H., Baba, T., Warnock, D. E. & Schmid, S. L. (1994). Induction of mutant dynamin specifically blocks endocytic coated vesicle formation. *J. Cell. Biol.* **127**, 915-934.

Darzynkiewicz, Z., Carter, S. P., Mikulski, S. M., Ardelt, W. J. & Shogen, K. (1988). Cytostatic and cytotoxic effect of Pannon (P-30 Protein), a novel anticancer agent. *Cell Tissue Kinet.* **21**, 169-182.

delCardayré, S. B. & Raines, R. T. (1995). The extent to which ribonucleases cleave ribonucleic acid. *Anal. Biochem.* **225**, 176-178.

delCardayré, S. B., Ribó, M., Yokel, E. M., Quirk, D. J., Rutter, W. J. & Raines, R. T. (1995). Engineering ribonuclease A: production, purification, and characterization of wild-type enzyme and mutants at Gln11. *Protein Engng.* **8**, 261-273.

Deng, C. & Capecchi, M. R. (1992). Reexamination of gene targeting frequency as a function of the extent of homology between the targeting vector and the target locus. *Mol. Cell. Biol.* **12**, 3365-3371.

De Prisco, R., Sorrentino, S., Leone, E. & Libonati, M. (1984). A ribonuclease from human seminal plasma active on double-stranded RNA. *Biochim. Biophys. Acta* **788**, 356-363.

de Souza, S. J., Long, M., Schoenbach, L., Roy, S. W. & Gilbert, W. (1997). The correlation between introns and the three-dimensional structure of proteins. *Gene* **205**, 141-144.

Dice, J. F. (1987). Molecular determinants of protein half-lives in eukaryotic cells. *FASEB J.* **1**, 349-357.

Dice, J. F. (1988). Microinjected ribonuclease A as a probe for lysosomal pathways of intracellular protein degradation. *J. Protein Chem.* **7**, 115-127.

Dice, J. F. (1990). Peptide sequences that target cytosolic proteins for lysosomal proteolysis. *Trends Biochem. Sci.* **15**, 305-309.

Dice, J. F., Chiang, H. L., Spencer, E. P. & Backer, J. M. (1986). Regulation of catabolism of microinjected ribonuclease A. Identification of residues 7-11 as the essential pentapeptide. *J. Biol. Chem.* **261**, 6853-6859.

Dinter, A. & Berger, E. G. (1998). Golgi-disturbing agents. *Histochem. Cell Biol.* **109**, 571-590.

Dixon, M. S., Hatzixanthis, K., Jones, D. A., Harrison, K. & Jones, J. D. (1998). The tomato Cf-5 disease resistance gene and six homologs show pronounced allelic variation in leucine-rich repeat copy number. *Plant Cell* **10**, 1915-1925.

Dostál, J. & Matousek, J. (1972). Purification of aspermatogenic substance (BS) from the bull seminal vesicle fluid. *J. Reprod. Fert.* **31**, 273-275.

Draper, R. K. & Simon, M. I. (1980). The entry of diphtheria toxin into the mammalian cell cytoplasm: evidence for lysosomal involvement. *J. Cell Biol.* **87**, 849-854.

Dunn, B. M. & Chaiken, I. M. (1975). Relationship between alpha-helical propensity and formation of the ribonuclease-S complex. *J. Mol. Biol.* **95**, 497-511.

Eberhardt, E. S., Wittmayer, P. K., Templer, B. M. & Raines, R. T. (1996). Contribution of a tyrosine side chain to ribonuclease A catalysis and stability. *Protein Sci.* **5**, 1697-1703.

Fett, J. W., Strydom, D. J., Lobb, R. R., Alderman, E. M., Bethune, J. L., Riordan, J. F. & Vallee, B. L. (1985). Isolation and characterization of angiogenin, an angiogenic protein from human carcinoma cells. *Biochemistry* **24**, 5480-5486.

Fedorov, A., Fedorova, L., Starshenko, V., Filatov, V. & Grigor'ev, E. (1998). Influence of exon duplication on intron and exon phase distribution. *J. Mol. Evol.* **46**, 263-271.

Findlay, D., Herries, D. G., Mathias, A. P., Rabin, B. R. & Ross, C. A. (1961). The active site and mechanism of action of bovine pancreatic ribonuclease. *Nature* **190**, 781-784.

Fisher, B. M., Ha, J.-H. & Raines, R. T. (1998). Coulombic forces in protein-RNA interactions: binding and cleavage by ribonuclease A and variants at Lys7, Arg10 and Lys66. *Biochemistry* **37**, 12121-12132.

Futami, J., Maeda, T., Kitazoe, M., Nukui, E., Tada, H., Seno, M., Kosaka, M. & Yamada, H. (2001). Preparation of potent cytotoxic ribonucleases by cationization: enhanced cellular uptake and decreased interaction with ribonuclease inhibitor by chemical modification of carboxyl groups. *Biochemistry* **40**, 7518-7524.

Futami, J., Tsushima, Y., Murato, Y., Tada, H., Sasaki, J., Seno, M. & Yamada, H. (1997). Tissue-specific expression of pancreatic-type RNases and RNase inhibitor in humans. *DNA Cell. Biol.* **16**, 413-419.

Gilbert, W., de Souza, S. J. & Long, M. (1997). Origin of genes. *Proc. Natl. Acad. Sci. U.S.A.* **94**, 7698-7703.

Green, M. & Loewenstein, P. M. (1988). Autonomous functional domains of chemically synthesized human immunodeficiency virus tat trans-activator protein. *Cell* **55**, 1179-1188.

Gribnau, A. A., Schoenmakers, J. G., van Kraaikamp, M., Hilak, M. & Bloemendal, H. (1970). Further studies on the ribonuclease inhibitor from rat liver: stability and other properties. *Biochim. Biophys. Acta* **224**, 55-62.

Griffiths, S. J., Adams, D. J. & Talbot, S. J. (1997). Ribonuclease inhibits Kaposi's sarcoma. *Nature* **390**, 568.

Haigis, M. C., Haag, E. S. & Raines, R. T. (2002a). Evolution of ribonuclease inhibitor by exon duplication. *Mol. Biol. Evol.*, In press.

Haigis, M. C., Kurten, E. L. & Raines, R. T. (2002b). KFERQ sequence in ribonuclease A-mediated cytotoxicity. *J. Biol. Chem.*, In press.

Haigis, M. C., Kurten, E. L. & Raines, R. T. (2002c). Ribonuclease inhibitor is an intracellular sentry., Submitted.

Hayano, K., Iwama, M., Sakamoto, H., Watanabe, H., Sanda, A., Ohgi, K. & Irie, M. (1993). Characterization of poly C preferential ribonuclease from chicken liver. *J. Biochem. (Tokyo)* **114**, 156-162.

Hasty, P., Rivera-Perez, J. & Bradley, A. (1991). The length of homology required for gene targeting in embryonic stem cells. *Mol. Cell. Biol.* **11**, 5586-5591.

Heim, R., Prasher, D. C. & Tsien, R. Y. (1994). Wavelength mutations and posttranslational autoxidation of green fluorescent protein. *Proc. Natl. Acad. Sci. U.S.A.* **91**, 12501-12504.

Heim, R. & Tsien, R. Y. (1996). Engineering green fluorescent protein for improved brightness, longer wavelengths and fluorescence resonance energy transfer. *Curr. Biol.* **6**, 178-182.

Henley, J. R., Krueger, E. W., Oswald, B. J. & McNiven, M. A. (1998). Dynamin-mediated internalization of caveolae. *J. Cell. Biol.* **141**, 85-99.

Hillig, R. C., Renault, L., Vetter, I. R., Drell, T. t., Wittinghofer, A. & Becker, J. (1999). The crystal structure of rna1p: a new fold for a GTPase-activating protein. *Mol. Cell* **3**, 781-791.

Hofsteenge, J. (1997). Ribonuclease inhibitor. In *Ribonucleases: Structures and Functions* (D'Alessio, G. & Riordan, J. F., eds.), pp. 621-658. Academic Press, New York.

Hofsteenge, J., Kieffer, B., Matthies, R., Hemmings, B. A. & Stone, S. R. (1988). Amino acid sequence of the ribonuclease inhibitor from porcine liver reveals the presence of leucine-rich repeats. *Biochemistry* **27**, 8537-8544.

Hofsteenge, J., Vincentini, A. & Stone, S. R. (1991). Purification and characterization of truncated ribonuclease inhibitor. *Biochem. J.* **275**, 541-543.

Hofsteenge, J., Vicentini, A. & Zelenko, O. (1998). Ribonuclease 4, an evolutionarily highly conserved member of the superfamily. *Cell. Mol. Life Sci.* **54**, 804-810.

Hudson, T. H. & Grillo, F. G. (1991). Brefeldin-A enhancement of ricin A-chain immunotoxins and blockade of intact ricin, modeccin, and abrin. *J. Biol. Chem.* **266**, 18586-18592.

Ilyin, G. P., Rialland, M., Glaise, D. & Guguen-Guillouzo, C. (1999). Identification of a novel Skp2-like mammalian protein containing F-box and leucine-rich repeats. *FEBS Lett.* **459**, 75-79.

Irie, M., Nitta, K. & Nonaka, T. (1998). Biochemistry of frog ribonucleases. *Cell. Mol. Life Sci.* **54**, 775-784.

Iwama, M., Kunihiro, M., Ohgi, K. & Irie, M. (1981). Purification and properties of human urine ribonucleases. *J. Biochem. (Tokyo)* **89**, 1005-1016.

Jinno, H., Ueda, M., Ozawa, S., Ikeda, T., Enomoto, K., Psarras, K., Kitajima, M., Yamada, H. & Seno, M. (1996). Epidermal growth factor receptor-dependent cytotoxicity for human squamous carcinoma cell lines of a conjugate composed of human EGF and RNase 1. *Life Sci.* **58**, 1901-1908.

Jones, S. M., Howell, K. E., Henley, J. R., Cao, H. & McNiven, M. A. (1998). Role of dynamin in the formation of transport vesicles from the trans- Golgi network. *Science* **279**, 573-577.

Juan, G., Ardelt, B., Li, X., Mikulski, S. M., Shogen, K., Ardelt, W., Mittelman, A. & Darzynkiewicz, Z. (1998). G1 arrest of U937 cells by onconase is associated with suppression of cyclin D3 expression, induction of p16INK4A, p21WAF1/CIP1 and p27KIP and decreased pRb phosphorylation. *Leukemia* **12**, 1241-1248.

Kajava, A. V. (1998). Structural diversity of leucine-rich repeat proteins. *J. Mol. Biol.* **277**, 519-527.

Kartha, G., Bello, J. & Harker, D. (1967). Tertiary structure of ribonuclease. *Nature* **213**, 862-865.

Kawanomoto, M., Motojima, K., Sasaki, M., Hattori, H. & Goto, S. (1992). cDNA cloning and sequence of rat ribonuclease inhibitor, and tissue distribution of mRNA. *Biochim. Biophys. Acta* **1129**, 335-338.

Kelemen, B. R., Klink, T. A., Behlke, M. A., Eubanks, S. R., Leland, P. A. & Raines, R. T. (1999). Hypersensitive substrate for ribonucleases. *Nucleic Acids Res.* **27**, 3696-3701.

Kim, B. M., Schultz, L. W. & Raines, R. T. (1999). Variants of ribonuclease inhibitor that resist oxidation. *Protein Sci.* **8**, 430-434.

Kim, J.-S., Soucek, J., Matousek, J. & Raines, R. T. (1995a). Catalytic activity of bovine seminal ribonuclease is essential for its immunosuppressive and other biological activities. *Biochem. J.* **308**, 547-550.

Kim, J.-S., Soucek, J., Matousek, J. & Raines, R. T. (1995b). Mechanism of ribonuclease cytotoxicity. *J. Biol. Chem.* **270**, 31097-31102.

Kim, J.-S., Soucek, J., Matousek, J. & Raines, R. T. (1995c). Structural basis for the biological activities of bovine seminal ribonuclease. *J. Biol. Chem.* **270**, 10525-10530.

Klink, T. A. & Raines, R. T. (2000). Conformational stability is a determinant of ribonuclease A cytotoxicity. *J. Biol. Chem.* **275**, 17463-17467.

Klink, T. A., Vicentini, A. M., Hofsteenge, J. & Raines, R. T. (2001). High-level soluble production and characterization of porcine ribonuclease inhibitor. *Protein Expr. Purif.* **22**, 174-179.

Klink, T. A., Woycechowsky, K. J., Taylor, K. M. & Raines, R. T. (2000). Contribution of disulfide bonds to the conformational stability and catalytic activity of ribonuclease A. *Eur. J. Biochem.* **267**, 566-572.

Kobayashi, T. & Kawakubo, T. (1994). Prospective investigation of tumor markers and risk assessment in early cancer screening. *Cancer* **73**, 1946-1953.

Kobe, B. & Deisenhofer, J. (1993). Crystal structure of porcine ribonuclease inhibitor, a protein with leucine-rich repeats. *Nature* **366**, 751-756.

Kobe, B. & Deisenhofer, J. (1994). The leucine-rich repeat: a versatile binding motif. *Trends Biochem. Sci.* **19**, 415-421.

Kobe, B. & Deisenhofer, J. (1995a). Proteins with leucine-rich repeats. *Curr. Opin. Struct. Biol.* **5**, 409-416.

Kobe, B. & Deisenhofer, J. (1995b). A structural basis of the interactions between leucine-rich repeats and protein ligands. *Nature* **374**, 183-186.

Kobe, B. & Deisenhofer, J. (1996). Mechanism of ribonuclease inhibition by ribonuclease inhibitor protein based on the crystal structure of its complex with ribonuclease A. *J. Mol. Biol.* **264**, 1028-1043.

Kobe, B. & Kajava, A. V. (2001). The leucine-rich repeat as a protein recognition motif. *Curr. Opin. Struct. Biol.* **11**, 725-732.

Kojima, K. (1993). Molecular aspects of the plasma membrane in tumor cells. *Nagoya J. Med. Sci.* **56**, 1-18.

Kothandaraman, S., Hebert, M. C., Raines, R. T. & Nibert, M. L. (1998). No role for pepstatin-A-sensitive acidic proteinases in reovirus infections of L or MDCK cells. *Virology* **251**, 264-272.

Kraulis, P. J. (1991). MOLSCRIPT: a program to produce both detailed and schematic plots of protein structures. *J. Appl. Crystallogr.* **24**, 946-950.

Kunkel, T. A., Roberts, J. D. & Zakour, R. A. (1987). Rapid and efficient site-specific mutagenesis without phenotypic selection. *Methods Enzymol.* **154**, 367-382.

Kyner, D., Christman, J. K. & Acs, G. (1979). The effect of 12-O-tetradecanoyl-phorbol 13-acetate on the ribonuclease activity of circulating human lymphocytes. *Eur. J. Biochem.* **99**, 395-399.

Laemmli, U. K. (1970). Cleavage of structural proteins during the assembly of the head of bacteriophage T4. *Nature* **227**, 680-685.

Lang, D., Thoma, R., Henn-Sax, M., Sterner, R. & Wilmanns, M. (2000). Structural evidence for evolution of the beta/alpha barrel scaffold by gene duplication and fusion [see comments]. *Science* **289**, 1546-1550.

Leamon, C. P. & Low, P. S. (1993). Membrane folate-binding proteins are responsible for folate-protein conjugate endocytosis into cultured cells. *Biochem. J.* **291**, 855-860.

Ledoux, L. (1955a). Action of ribonuclease on certain ascites tumours. *Nature* **175**, 258-259.

Ledoux, L. (1955b). Action of ribonuclease on two solid tumours *in vivo*. *Nature* **176**, 36-37.

Lee, F. S., Fox, E. A., Zhou, H.-M., Strydom, D. J. & Vallee, B. L. (1988). Primary structure of human placental ribonuclease inhibitor. *Biochemistry* **27**, 8545-8553.

Lee, F. S., Shapiro, R. & Vallee, B. L. (1989). Tight-binding inhibition of angiogenin and ribonuclease A by placental ribonuclease inhibitor. *Biochemistry* **28**, 225-230.

Lee, F. S. & Vallee, B. L. (1990). Modular mutagenesis of human placental ribonuclease inhibitor, a protein with leucine-rich repeats. *Proc. Natl. Acad. Sci. U.S.A.* **87**, 1879-1883.

Lee, F. S. & Vallee, B. L. (1993). Structure and action of mammalian ribonuclease (angiogenin) inhibitor. *Progress Nucl. Acid Res. Molec. Biol.* **44**, 1-30.

Leland, P. A. & Raines, R. T. (2001). Cancer chemotherapy--ribonucleases to the rescue. *Chem. Biol.* **8**, 405-413.

Leland, P. A., Schultz, L. W., Kim, B.-M. & Raines, R. T. (1998). Ribonuclease A variants with potent cytotoxic activity. *Proc. Natl. Acad. Sci. U.S.A.* **98**, 10407-10412.

Leland, P. A., Staniszewski, K. E., Kim, B. & Raines, R. T. (2000). A synapomorphic disulfide bond is critical for the conformational stability and cytotoxicity of an amphibian ribonuclease. *FEBS Lett.* **477**, 203-207.

Lin, J. J., Newton, D. L., Mikulski, S. M., Kung, H. F., Youle, R. J. & Rybak, S. M. (1994). Characterization of the mechanism of cellular and cell free protein synthesis inhibition by an anti-tumor ribonuclease. *Biochem. Biophys. Res. Commun.* **204**, 156-162.

Llorente, A., Rapak, A., Schmid, S. L., van Deurs, B. & Sandvig, K. (1998). Expression of mutant dynamin inhibits toxicity and transport of endocytosed ricin to the Golgi apparatus. *J. Cell Biol.* **140**, 553-563.

Lord, J. M. & Roberts, L. M. (1998). Toxin entry: retrograde transport through the secretory pathway. *J. Cell. Biol.* **140**, 733-736.

Mallard, F., Antony, C., Tenza, D., Salamero, J., Goud, B. & Johannes, L. (1998). Direct pathway from early/recycling endosomes to the Golgi apparatus revealed through the study of shiga toxin B-fragment transport. *J. Cell Biol.* **143**, 973-990.

Mancheño, J. M., Gasset, M., Onaderra, M., Gavilanes, J. G. & D'Alessio, G. (1994). Bovine seminal ribonuclease destabilizes negatively charged membranes. *Biochem. Biophys. Res. Commun.* **199**, 119-124.

Marsh, M., Ed. (2001). *Endocytosis*. Frontiers in Molecular Biology. Edited by Hames, B. D. & Glover, D. M. Oxford: Oxford University Press.

Matousek, J. (1973). The effect of bovine seminal ribonuclease (AS RNase) on cells of crocker tumour in mice. *Experientia* **29**, 858-859.

Matousek, J. (1975). Embryotoxic effect of bull seminal ribonuclease and tissue absorption studies in rats. *J. Reprod. Fertil.* **43**, 171-174.

Matousek, J. (1994). Aspermatogenic effect of the bull seminal ribonuclease (BS RNase) in the presence of anti BS RNase antibodies in mice. *Animal Genet.* **25**, Suppl. 1, 45-50.

Matousek, J. (2001). Ribonucleases and their antitumor activity. *Comp. Biochem. Physiol. C Toxicol. Pharmacol.* **129**, 175-191.

Matousek, J., Soucek, J., Rfha, J., Zankel, T. R. & Benner, S. A. (1995). Immunosuppressive activity of angiogenin in comparison with bovine seminal ribonuclease and pancreatic ribonuclease. *Comp. Biochem. Physiol.* **112**, 235-241.

McElligott, M. A., Miao, P. & Dice, J. F. (1985a). Lysosomal degradation of ribonuclease A and ribonuclease S-protein microinjected into the cytosol of human fibroblasts. *J. Biol. Chem.* **260**, 11986-11993.

McElligott, M. A., Miao, P. & Dice, J. F. (1985b). Lysosomal degradation of ribonuclease A and ribonuclease S-protein microinjected into the cytosol of human fibroblasts. *J. Biol. Chem.* **260**, 11986-11993.

McNiven, M. A. (1998). Dynamin: a molecular motor with pinchase action. *Cell* **94**, 151-154.

McNiven, M. A., Cao, H., Pitts, K. R. & Yoon, Y. (2000). The dynamin family of mechanoenzymes: pinching in new places. *Trends Biochem. Sci.* **25**, 115-120.

Melton, D. W. (1994). Gene targeting in the mouse. *Bioessays* **16**(9), 633-638.

Merrifield, B. (1985). Solid phase synthesis. Nobel lecture, 8 December 1984. *Biosci. Rep.* **5**, 353-376.

Merrifield, B. (1986). Solid phase synthesis. *Science* **232**, 341-347.

Messmore, J. M., Fuchs, D. N. & Raines, R. T. (1995). Ribonuclease A: revealing structure – function relationships with semisynthesis. *J. Am. Chem. Soc.* **117**, 8057-8060.

Mikulski, S. M., Chun, H. G., Mittelman, A., Panella, T., Puccio, C. A., Shogen, K. & Constanzi, J. J. (1995). Relationship between response rate and median survival in patients with advanced non-small cell lung cancer: comparison of ONCONASE® with other anticancer agents. *Int. J. Oncol.* **6**, 889-897.

Mikulski, S. M., Costanzi, J. J., Vogelzang, N. J., McCachren, S., Taub, R. N., Chun, H., Mittelman, A., Panella, T., Puccio, C., Fine, R. & Shogen, K. (2002). Phase II Trial of a Single Weekly Intravenous Dose of Ranpirnase in Patients With Unresectable Malignant Mesothelioma. *J. Clin. Oncol.* **20**, 274-281.

Mikulski, S. M., Grossman, A. M., Carter, P. W., Shogen, K. & Costanzi, J. J. (1993). Phase I human clinical trial of ONCONASE (P-30 Protein) administered intravenously on a weekly schedule in cancer patients with solid tumors. *Int. J. Oncol.* **3**, 57-64.

Mikulski, S. M., Viera, A., Deptala, A. & Darzynkiewicz, Z. (1998). Enhanced in vitro cytotoxicity and cytostasis of the combination of onconase with a proteasome inhibitor. *Int. J. Oncol.* **13**, 633-644.

Miles, E. W. & Davies, D. R. (2000). Protein evolution. On the ancestry of barrels [comment]. *Science* **289**, 1490.

Moore, S. & Stein, W. H. (1973). Chemical structures of pancreatic ribonuclease and deoxyribonuclease. *Science* **180**, 458-464.

Moriyama, E. N. & Gojobori, T. (1992). Rates of synonymous substitution and base composition of nuclear genes in Drosophila. *Genetics* **130**, 855-864.

Mosimann, S. C., Ardelt, W. & James, M. N. G. (1994). Refined 1.7 Å X-ray crystallographic structure of P-30 protein, an amphibian ribonuclease with anti-tumor activity. *J. Mol. Biol.* **236**, 1141-1153.

Nadano, D., Yasuda, T., Takeshita, H., Uchide, K. & Kishi, K. (1994). Purification and characterization of human brain ribonuclease inhibitor. *Arch. Biochem. Biophys.* **312**, 421-428.

Nagano, H., Kiuchi, H., Abe, Y. & Shukuya, R. (1976). Purification and properties of an alkaline ribonuclease from the hepatic cytosol fraction of bullfrog, Rana catesbeiana. *J. Biochem. (Tokyo)* **80**, 19-26.

Nei, M. & Gojobori, T. (1986). Simple methods for estimating the numbers of synonymous and nonsynonymous nucleotide substitutions. *Mol. Biol. Evol.* **3**, 418-426.

Neumann, U. & Hofsteenge, J. (1994). Interaction of semisynthetic variants of RNase A with ribonuclease inhibitor. *Protein Sci.* **3**, 248-256.

Newton, D. L., Boque, L., Wlodawer, A., Huang, C. Y. & Rybak, S. M. (1998). Single amino acid substitutions at the N-terminus of a recombinant cytotoxic ribonuclease markedly influence biochemical and biological properties. *Biochemistry* **37**, 5173-5183.

Newton, D. L., Ilercil, O., Laske, D. W., Oldfield, E., Rybak, S. M. & Youle, R. J. (1992). Cytotoxic ribonuclease chimeras. Targeted tumoricidal activity in vitro and in vivo. *J. Biol. Chem.* **267**, 19572-19578.

Newton, D. L., Walbridge, S., Mikulski, S. M., Ardelt, W., Shogen, K., Ackerman, S. J., Rybak, S. M. & Youle, R. J. (1994). Toxicity of an antitumor ribonuclease to Purkinje neurons. *J. Neurosci.* **14**, 538-544.

Newton, D. L., Xue, Y., Boque, L., Wlodawer, A., Kung, H. F. & Rybak, S. M. (1997). Expression and characterization of a cytotoxic human-frog chimeric ribonuclease: potential for cancer therapy. *Protein Eng.* **10**, 463-470.

Nitta, K., Ozaki, K., Ishikawa, M., Furusawa, S., Hosono, M., Kawauchi, H., Sasaki, K., Takayanagi, Y., Tsuiki, S. & Hakomori, S. (1994). Inhibition of cell proliferation by *Rana catesbeiana* and *Rana japonica* lectins belonging to the ribonuclease superfamily. *Cancer Res.* **54**, 920-927.

Nitta, K., Takayanagi, G., Kawauchi, H. & Hakomori, S. (1987). Isolation and characterization of Rana catesbeiana lectin and demonstration of the lectin-binding glycoprotein of rodent and human tumor cell membranes. *Cancer Res.* **47**, 4877-4883.

Nogués, M. V., Vilanova, M. & Cuchillo, C. M. (1995). Bovine pancreatic ribonuclease A as a model of an enzyme with multiple substrate binding sites. *Biochim. Biophys. Acta* **1253**, 16-24.

Nonaka, T., Hirayama, E., Iwama, M., Ohgi, K., Irie, M. & Mitsui, Y. (1996). *International Union of Crystallography XVII Congress and General Assembly, Seattle, WA, USA.*

Notomista, E., Catanzano, F., Graziano, G., Dal Piaz, F., Barone, G., D'Alessio, G. & Di Donato, A. (2000). Onconase: an unusually stable protein. *Biochemistry* **39**, 8711-8718.

Notomista, E., Catanzano, F., Graziano, G., Di Gaetano, S., Barone, G. & Di Donato, A. (2001). Contribution of chain termini to the conformational stability and biological activity of onconase. *Biochemistry* **40**, 9097-9103.

Olsnes, S. & Kozlov, J. V. (2001). Ricin. *Toxicon* **39**, 1723-1728.

Orlandi, P. A. & Fishman, P. H. (1998). Filipin-dependent inhibition of cholera toxin: evidence for toxin internalization and activation through caveolae-like domains. *J. Cell Biol.* **141**, 905-915.

Pace, C. N., Vajdos, F., Fee, L., Grimsley, G. & Gray, T. (1995). How to measure and predict the molar absorption coefficient of a protein. *Protein Sci.* **4**, 2411-2423.

Papageorgiou, A., Shapiro, R. & Acharya, K. (1997). Molecular recognition of human angiogenin by placental ribonuclease inhibitor—an X-ray crystallographic study at 2.0 Å resolution. *EMBO J.* **16**, 5162-5177.

Parés, X., Nogués, M. V., de Llorens, R. & Cuchillo, C. M. (1991). Structure and function of ribonuclease A binding subsites. *Essays Biochem.* **26**, 89-103.

Park, C. & Raines, R. T. (2001). Quantitative analysis of the effect of salt concentration on enzymatic catalysis. *J. Am. Chem. Soc.* **123**, 11472-11479.

Pelham, H. R. B. (1991). Multiple targets for brefeldin A. *Cell* **67**, 449-451.

Peracaula, R., Cleary, K. R., Lorenzo, J., de Llorens, R. & Frazier, M. L. (2000). Human pancreatic ribonuclease 1: expression and distribution in pancreatic adenocarcinoma. *Cancer* **89**, 1252-1258.

Pirotte, M. & Desreux, V. (1952). *Bull. Soc. Chim. Belg.* **61**, 167.

Price, S. R., Evans, P. R. & Nagai, K. (1998). Crystal structure of the spliceosomal U2B"-U2A' protein complex bound to a fragment of U2 small nuclear RNA. *Nature* **394**, 645-650.

Prochiantz, A. (2000). Messenger proteins: homeoproteins, TAT and others. *Curr. Opin. Cell Biol.* **12**, 400-406.

Quirk, D. J., Park, C., Thompson, J. E. & Raines, R. T. (1998). His···Asp catalytic dyad of ribonuclease A: conformational stability of the wild-type, D121N, D121A, and H119A enzymes. *Biochemistry* **37**, 17985-17964.

Radhakrishnan, A., Anderson, T. G. & McConnell, H. M. (2000). Condensed complexes, rafts, and the chemical activity of cholesterol in membranes. *Proc. Natl. Acad. Sci. U.S.A.* **97**, 12422-12427.

Raines, R. T. (1998). Ribonuclease A. *Chem. Rev.* **98**, 1045-1065.

Raines, R. T. (1999). Ribonuclease A: from model system to cancer chemotherapeutic. In *Enzymatic Mechanisms* (Frey, P. A. & Northrop, D. B., eds.), pp. 235-249. IOS Press, Washington, DC.

Rapak, A., Falnes, P. O. & Olsnes, S. (1997). Retrograde transport of mutant ricin to the endoplasmic reticulum with subsequent translocation to cytosol. *Proc. Natl. Acad. Sci. U.S.A.* **94**, 3783-3788.

Reardon, D. & Farber, G. K. (1995). The structure and evolution of alpha/beta barrel proteins. *FASEB J.* **9**, 497-503.

Ritter, C. & Helenius, A. (2000). Recognition of local glycoprotein misfolding by the ER folding sensor UDP-glucose:glycoprotein glucosyltransferase. *Nat. Struct. Biol.* **7**, 278-280.

Rosenberg, H. F. & Dyer, K. D. (1995). Eosinophil cationic protein and eosinophil-derived neurotoxin. *J. Biol. Chem.* **270**, 21539-21544.

Roth, J. S. (1962). Ribonuclease IX. Further studies on ribonuclease inhibitor. *Biochim. Biophys. Acta* **61**, 903-915.

Roth, J. S. (1963). Ribonuclease activity and cancer: a review. *Cancer Res.* **23**, 657-666.

Rutter, J., Reick, M., Wu, L. C. & McKnight, S. L. (2001). Regulation of clock and NPAS2 DNA binding by the redox state of NAD cofactors. *Science* **293**, 510-514.

Rybak, S. M. & Newton, D. L. (1999). Natural and engineered cytotoxic ribonucleases: therapeutic potential. *Exp. Cell Res.* **253**, 325-335.

Sakakibara, F., Kawauchi, H., Takayanagi, G. & Ise, H. (1979). Egg lectin of Rana japonica and its receptor glycoprotein of Ehrlich tumor cells. *Cancer Res.* **39**, 1347-1352.

Sakakibara, F., Takayanagi, G., Ise, H. & Kawauchi, H. (1977). Isolation of two agglutinins with different biological properties from the eggs of Rana catesbeiana. *Yakugaku Zasshi* **97**, 855-862.

Samuelson, L. C., Wiebauer, K., Howard, G., Schmid, R. M., Koeplin, D. & Meisler, M. H. (1991). Isolation of the murine ribonuclease gene Rib-1: structure and tissue specific expression in pancreas and parotid gland. *Nucleic Acids Res.* **19**, 6935-6941.

Sandvig, K., Garred, O., Prydz, K., Kozlov, J. V., Hansen, S. H. & van Deurs, B. (1992). Retrograde transport of endocytosed Shiga toxin to the endoplasmic reticulum. *Nature* **358**, 510-512.

Sandvig, K. & Olsnes, S. (1980). Diphtheria toxin entry into cells is facilitated by low pH. *J. Cell Biol.* **87**, 828-832.

Sandvig, K. & Olsnes, S. (1981). Rapid entry of nicked diphtheria toxin into cells at low pH. Characterization of the entry process and effects of low pH on the toxin molecule. *J. Biol. Chem.* **256**, 9068-9076.

Sandvig, K. & Olsnes, S. (1982). Entry of the toxic proteins abrin, modeccin, ricin, and diphtheria toxin into cells. II. Effect of pH, metabolic inhibitors, and ionophores and evidence for toxin penetration from endocytotic vesicles. *J. Biol. Chem.* **257**, 7504-7513.

Sandvig, K. & van Deurs, B. (2000). Entry of ricin and Shiga toxin into cells: molecular mechanisms and medical perspectives. *EMBO J.* **19**, 5943-5950.

Sasso, M. P., Lombardi, M., Confalone, E., Carsana, A., Palmieri, M. & Furia, A. (1999). The differential pattern of tissue-specific expression of ruminant pancreatic type ribonucleases may help to understand the evolutionary history of their genes. *Gene* **227**, 205-212.

Saxena, S. K., Gravell, M., Wu, Y. N., Mikulski, S. M., Shogen, K., Ardelt, W. & Youle, R. J. (1996). Inhibition of HIV-1 production and selective degradation of viral RNA by an amphibian ribonuclease. *J. Biol. Chem.* **271**, 20783-20788.

Saxena, S. K., Rybak, S. M., Winkler, G., Meade, H. M., McGray, P., Youle, R. J. & Ackerman, E. J. (1991). Comparison of RNases and toxins upon injection into *Xenopus* oocytes. *J. Biol. Chem.* **266**, 21208-21214.

Schein, C. H. (1997). From housekeeper to microsurgeon: the diagnostic and therapeutic potential of ribonucleases. *Nature Biotechnol.* **15**, 529-536.

Schmid, S. L., McNiven, M. A. & De Camilli, P. (1998). Dynamin and its partners: a progress report. *Curr. Opin. Cell Biol.* **10**, 504-512.

Schneider, R., Schneider-Scherzer, E., Thurnher, M., Auer, B. & Schweiger, M. (1988). The primary structure of human ribonuclease/angiogenin inhibitor (RAI) discloses a novel highly diversified protein superfamily with a common repetitive module. *EMBO J.* **7**, 4151-4156.

Schulman, B. A., Carrano, A. C., Jeffrey, P. D., Bowen, Z., Kinnucan, E. R., Finnin, M. S., Elledge, S. J., Harper, J. W., Pagano, M. & Pavletich, N. P. (2000). Insights into SCF ubiquitin ligases from the structure of the Skp1-Skp2 complex. *Nature* **408**, 381-386.

Sciaky, N., Presley, J., Smith, C., Zaal, K. J., Cole, N., Moreira, J. E., Terasaki, M., Siggia, E. & Lippincott-Schwartz, J. (1997). Golgi tubule traffic and the effects of brefeldin A visualized in living cells. *J. Cell Biol.* **139**, 1137-1155.

Scoffone, E., Rocchi, R., Marchiori, F., Moroder, L., Marzotto, A. & Tamburro, A. M. (1967). Synthesis of peptide analogs of the N-terminal eicosapeptide sequence of ribonuclease A. VII. Synthesis of ile, orn -and ala, orn - eicosapeptides. *J. Am. Chem. Soc.* **89**, 5450-5455.

Segel, L. A. (1980). *Mathematical models in molecular and cellular biology*, Cambridge University, London.

Sela, M., Anfinsen, C. B. & Harrington, W. F. (1957). The correlation of ribonuclease activity with specific aspects of tertiary structure. *Biochim. Biophys. Acta* **26**, 502-512.

Shapiro, R. (2001). Cytoplasmic ribonuclease inhibitor. *Methods Enzymol.* **341**, 611-628.

Shapiro, R., Fox, E. A. & Riordan, J. F. (1989). Role of lysines in human angiogenin: chemical modification and site-directed mutagenesis. *Biochemistry* **28**, 1726-1732.

Shapiro, R., Ruiz-Gutierrez, M. & Chen, C. Z. (2000). Analysis of the interactions of human ribonuclease inhibitor with angiogenin and ribonuclease A by mutagenesis: importance of inhibitor residues inside versus outside the C-terminal "hot spot". *J. Mol. Biol.* **302**, 497-519.

Shapiro, R., Strydom, D. J., Olson, K. A. & Vallee, B. L. (1987). Isolation of angiogenin from normal human plasma. *Biochemistry* **26**, 5141-5146.

Shapiro, R. & Vallee, B. L. (1991). Interaction of human placental ribonuclease with placental ribonuclese inhibitor. *Biochemistry* **30**, 2246-2255.

Shimotakahara, S., Rios, C. B., Laity, J. H., Zimmerman, D. E., Scheraga, H. A. & Montelione, G. T. (1997). NMR structural analysis of an analog of an intermediate formed in the rate-determining step of one pathway in the oxidative folding of bovine pancreatic ribonuclease A: automated analysis of 1H, 13C, and 15N resonance assignments for wild-type and [C65S, C72S] mutant forms. *Biochemistry* **36**, 6915-6929.

Simpson, E. M., Linder, C. C., Sargent, E. E., Davisson, M. T., Mobraaten, L. E. & Sharp, J. J. (1997). Genetic variation among 129 substrains and its importance for targeted mutagenesis in mice. *Nat. Genet.* **16**, 19-27.

Simpson, J. C., Smith, D. C., Roberts, L. M. & Lord, J. M. (1998). Expression of mutant dynamin protects cells against diphtheria toxin but not against ricin. *Exp. Cell. Res.* **239**, 293-300.

Slavik, T., Matousek, J., Fulka, J. & Raines, R. T. (2000). Effect of bovine seminal ribonuclease and bovine pancreatic ribonuclease A on bovine oocyte maturation. *J. Exp. Zool.* **287**, 394-399.

Smith, M. R., Newton, D. L., Mikulski, S. M. & Rybak, S. M. (1999). Cell cycle-related differences in susceptibility of NIH/3T3 cells to ribonucleases. *Exp. Cell Res.* **247**, 220-232.

Snook, J. T. (1965). Dietary regulation of pancreatic enzyme synthesis, secretion and inactivation in the rat. *J. Nutr.* **87**, 297-305.

Soriano, P., Montgomery, C., Geske, R. & Bradley, A. (1991). Targeted disruption of the c-src proto-oncogene leads to osteopetrosis in mice. *Cell* **64**, 693-702.

Sorrentino, S., De Prisco, R. & Libonati, M. (1989). Human seminal ribonuclease. Immunological quantitation of cross- reactive enzymes in serum, urine and seminal plasma. *Biochim. Biophys. Acta* **998**, 97-101.

Strydom, D. J. (1998). The angiogenins. *Cell. Mol. Life Sci.* **54**, 811-824.

Suzuki, M., Saxena, S. K., Boix, E., Prill, R. J., Vasandani, V. M., Ladner, J. E., Sung, C. & Youle, R. J. (1999). Engineering receptor-mediated cytotoxicity into human ribonucleases by steric blockade of inhibitor interaction [see comments]. *Nat. Biotechnol.* **17**, 265-270.

Suzuki, Y. & Takahashi, Y. (1970). Developmental and regional variations in ribonuclease inhibitor activity in brain. *J. Neurochem.* **17**, 1521-1524.

Swofford, D. L. (1998). *PAUP* Phylogenetic analysis using parsimony (*and other methods)*. 4 edit, Sinauer Associates, Sunderland.

Tagge, E., Chandler, J., Tang, B. L., Hong, W., Willingham, M. C. & Frankel, A. (1996). Cytotoxicity of KDEL-terminated ricin toxins correlates with distribution of the KDEL receptor in the Golgi. *J. Histochem. Cytochem.* **44**, 159-165.

te Riele, H., Maandag, E. R. & Berns, A. (1992). Highly efficient gene targeting in embryonic stem cells through homologous recombination with isogenic DNA constructs. *Proc. Natl. Acad. Sci. U.S.A.* **89**, 5128-5132.

Tomita, Y., Goto, Y., Okazaki, T. & Shukuya, R. (1979). Liver ribonucleases from bullfrog, *Rana catesbeiana*. Purification, properties and changes in activity during metamorphosis. *Biochim. Biophys. Acta* **562**, 504-514.

Tong, Z. B., Nelson, L. M. & Dean, J. (2000). Mater encodes a maternal protein in mice with a leucine-rich repeat domain homologous to porcine ribonuclease inhibitor. *Mamm. Genome* **11**, 281-287.

Tsien, R. Y. (1998). The green fluorescent protein. *Annu. Rev. Biochem.* **67**, 509-544.

Urrutia, R., Henley, J. R., Cook, T. & McNiven, M. A. (1997). The dynamins: redundant or distinct functions for an expanding family of related GTPases? *Proc. Natl. Acad. Sci. U.S.A.* **94**, 377-384.

van Dam, E. M. & Stoorvogel, W. (2002). Dynamin-dependent transferrin receptor recycling by endosome-derived clathrin-coated vesicles. *Mol. Biol. Cell.* **13**, 169-182.

van der Bliek, A. M., Redelmeier, T. E., Damke, H., Tisdale, E. J., Meyerowitz, E. M. & Schmid, S. L. (1993). Mutations in human dynamin block an intermediate stage in coated vesicle formation. *J. Cell Biol.* **122**, 553-563.

van Deursen, J. & Wieringa, B. (1992). Targeting of the creatine kinase M gene in embryonic stem cells using isogenic and nonisogenic vectors. *Nucleic Acids Res.* **20**, 3815-3820.

Vasandani, V. M., Wu, Y.-N., Mikulski, S. M., Youle, R. J. & Sung, C. (1996). Molecular determinants in the plasma clearance and tissue distribution of ribonucleases of the ribonuclease A superfamily. *Cancer Res.* **56**, 4180-4186.

Vicentini, A. M., Kieffer, B., Mathies, R., Meyhack, B., Hemmings, B. A., Stone, S. R. & Hofsteenge, J. (1990). Protein chemical and kinetic characterization of recombinant porcine ribonuclease inhibitor expressed in *Saccharomyces cerevisiae*. *Biochemistry* **29**, 8827-8834.

Volles, M. J., Xu, X. & Scheraga, H. A. (1999). Distribution of disulfide bonds in the two-disulfide intermediates in the regeneration of bovine pancreatic ribonuclease A: further insights into the folding process. *Biochemistry* **38**, 7284-7293.

Wales, R., Roberts, L. M. & Lord, J. M. (1993). Addition of an endoplasmic reticulum retrieval sequence to ricin A chain significantly increases its cytotoxicity to mammalian cells. *J. Biol. Chem.* **268**, 23986-23990.

Warnock, D. E. & Schmid, S. L. (1996). Dynamin GTPase, a force-generating molecular switch. *Bioessays* **18**, 885-893.

Wedemeyer, W. J., Welker, E., Narayan, M. & Scheraga, H. A. (2000). Disulfide bonds and protein folding. *Biochemistry* **39**, 4207-4216.

Weickmann, J. L. & Glitz, D. G. (1982). Human ribonucleases. Quantitation of pancreatic-like enzymes in serum, urine, and organ preparations. *J. Biol. Chem.* **257**, 8705-8710.

Weickmann, J. L., Olson, E. M. & Glitz, D. G. (1984). Immunological assay of pancreatic ribonuclease in serum as an indicator of pancreatic cancer. *Cancer Res.* **44**, 1682-1687.

Weremowicz, S., Fox, E. A., Morton, C. C. & Vallee, B. L. (1990). The placental ribonuclease inhibitor (RNH) gene is located on chromosome subband 11p15.5. *Genomics* **8**, 717-721.

Wlodawer, A. (1985). Structure of bovine pancreatic ribonuclease by X-ray and neutron diffraction. In *Biological Macromolecules and Assemblies, Vol. II, Nucleic Acids and Interactive Proteins* (Jurnak, F. A. & McPherson, A., eds.), pp. 395-439. Wiley, New York.

Wlodawer, A., Anders, L. A., Sjölin, L. & Gilliland, G. L. (1988). Structure of phosphate-free ribonuclease A refined at 1.26 Å. *Biochemistry* **27**, 2705-2717.

Wojnar, R. J. & Roth, J. S. (1965). Ribonuclease inhibitor and latent ribonuclease in rat liver during feeding of 2-acetamidofluorene. *Cancer Res.* **25**, 1913-1918.

Wu, Y., Mikulski, S. M., Ardelt, W., Rybak, S. M. & Youle, R. J. (1993). A cytotoxic ribonuclease. *J. Biol. Chem.* **268**, 10686-10693.

Wu, Y., Saxena, S. K., Ardelt, W., Gadina, M., Mikulski, S. M., De Lorenzo, V., D'Alessio, G. & Youle, R. J. (1995). A study of the intracellular routing of cytotoxic ribonucleases. *J. Biol. Chem.* **270**, 17476-17481.

Wyckoff, H. W., Hardman, K. D., Allewell, N. M., Inagami, T., Johnson, L. N. & Richards, F. M. (1967). The structure of ribonuclease-S at 3.5 Å resolution. *J. Biol. Chem.* **242**, 3984-3988.

Wyckoff, G. J., Wang, W. & Wu, C. I. (2000). Rapid evolution of male reproductive genes in the descent of man. *Nature* **403**, 304-309.

Yang, F., Moss, L. G. & Phillips, G. N., Jr. (1996). The molecular structure of green fluorescent protein. *Nat. Biotechnol.* **14**, 1246-1251.

Yoshida, T., Chen, C. C., Zhang, M. S. & Wu, H. C. (1991). Disruption of the Golgi apparatus by brefeldin A inhibits the cytotoxicity of ricin, modeccin, and Pseudomonas toxin. *Exp. Cell Res.* **192**, 389-395.

Youle, R. J. & D'Alessio, G. (1997). Antitumor RNases. In *Ribonucleases: Structures and Functions* (D'Alessio, G. & Riordan, J. F., eds.), pp. 491-514. Academic Press, New York.

Zhou, A., Paranjape, J., Brown, T. L., Nie, H., Naik, S., Dong, B., Chang, A., Trapp, B., Fairchild, R., Colmeenares, C. & Silverman, R. H. (1997). Interferon action and apoptosis are defective in mice devoid of 2',5'-oligoadenylate-dependent RNase L. *EMBO J.* **16**, 6355-6363.

Zneimer, S. M., Crawford, D., Schneider, N. R. & Beutler, B. (1990). Mapping of the human ribonuclease inhibitor gene (RNH) to chromosome 11p15 by in situ hybridization. *Genomics* **8**, 175-178.